THE EFFECT OF FLUID PROPERTIES ON THE PHYSICAL BEHAVIOR OF ADIABATIC ANNULAR TWO-PHASE FLOW

By

Patricia Lynn Blankenberger

A thesis submitted in partial fulfillment of

the requirements for the degree of

Master of Science

(Mechanical Engineering)

at the

UNIVERSITY OF WISCONSIN-MADISON

2003

The Effect of Fluid Properties on the Physical Behavior of Adiabatic Annular Two-Phase Flow

Patricia Lynn Blankenberger, M.S.
Department of Mechanical Engineering
University of Wisconsin-Madison, 2003
Professor Timothy A. Shedd, Advisor

Three separate experimental facilities were used to explore the mechanics of both vertical and horizontal annular flow. The first facility described was a low-pressure two-phase refrigerant facility with a horizontal, adiabatic test section. The second apparatus described was an air/water facility with an identical horizontal, adiabatic test section to the refrigerant facility. The final test set-up described was an air/oil facility with a vertical, adiabatic test section.

Air/water mixtures have been studied extensively in the present study as a vehicle for developing an understanding of two-phase flow behavior. In order to make use of air/water data to better understand the two-phase flow of refrigerants, it has been hypothesized that the best method to relate the pressure drop and behavior of the air/water and refrigerant data was to equate the kinetic energy of the refrigerant vapor to the kinetic energy of the air.

The research effort summarized here directly compared the behavior of adiabatic air/water and R-123 vapor/liquid flows in identical test sections. The air/water and refrigerant flows were compared using pressure drop measurements, film thickness measurements, and qualitative visual observations including wave behavior. The pressure drop measurements were well correlated using vapor kinetic energy; however, the R-123 pressure drop was higher overall. The different fluids exhibited similar trends in film thickness, but the air/water film thickness was generally more circumferentially uniform. At similar vapor kinetic energies, each fluid pair appeared to be in similar flow regimes. However, the wave structure and behavior of R-123 was quite different than that of the air/water mixture. The R-123 liquid appeared to wet the inside tube surface better than the water.

An important design problem in large refrigeration and air-conditioning systems is sizing of large diameter vertical vapor lines optimized to carry liquid up the pipe walls while attempting to minimize overall pressure loss. Of particular concern is the ability of refrigerant vapor flow to drive a liquid oil film through a refrigerant circuit so that oil does not accumulate outside the compressor under normal operation. Thus, this work also described a study aimed at characterizing the dynamic behavior of an annular oil film layer driven upward by air through a 50.8 mm I.D. pipe and a 25.4 mm I.D. pipe. The film thickness and gas mass flow at which flow reversal occurred were presented. Flow reversal in the oil film layer was identified both qualitatively (visually) and quantitatively by particle streak tracking. These results were compared and discussed with previously published experimental data and modeling work for air/water experiments.

The significance of this work can be seen by applying the results of each study to the practical design of vertical risers. The refrigerant vapor kinetic energy required for flow reversal to occur was found using the method of equating the vapor kinetic energies.

Acknowledgements

I appreciate the financial support for this project provided by the University of Wisconsin-Madison and the National Science Foundation under award number CTS-0134510.

I would like to thank my advisor, Dr. Tim Shedd, for all of his help, guidance, encouragement, counseling, and concern throughout this project. He made a point of making himself available with assistance and advice for this project and anything else on my mind. I owe him many hours of work for the construction and leak testing, as well as data analysis that he has done. This project was his brainchild and I am proud to have been a part of bringing it into existence.

I would like to thank my second advisor, Dr. Doug Reindl, for his helpful suggestions and guidance throughout the course of this project. He has helped to keep me focused and grounded in real world applications.

A big thank you to Dr. Greg Nellis for the use of his machine shop for the construction of much of my test facility.

Thanks to all of my office mates that I have had throughout my two years, including Daniel Rodriguez, Diego Arias, Frank Burkholder, Charlie Kopplin, Adam Pautsch, Sebastian Freund, and Greg Schlegel. These gentlemen have put up with a lot of my stress and venting and always made me laugh when I needed it most. I have also gotten quite a bit of good advice from many of them.

Special thanks to two individuals for their help in the lab. Audrey Miller helped me to build a large portion of the air/oil loop and to take preliminary data. She was a good sport about constantly getting covered in oil and kept me entertained with her great company. Katie Plzak worked long hours on the film thickness measurement program, without which I would not have been able to finish my project. She was also willing to lend a hand whenever possible during the construction stages of my test facility. She has been a great friend throughout my two years here and I am grateful to her for her friendship.

Thanks to both my advisors and my office and lab mates for making this project a very rewarding experience. Each one these people have contributed in some way to making this a great learning experience, and just a great experience in general.

I would also like to thank all those people who have inspired me to pursue my dream of becoming an engineer and work in the field of fluids and energy, including Dr. Berndt, Dr. Robert Hurt, Dr. Marty Morris, Dr. Tim Shedd, and Dr. Richard Shaten.

On a more personal note, I would like to thank my roommates, Brooke Swanson and Rebecca Tedford, for all of their support throughout my two years here. They have always been there for me with a shoulder to lean on, an ear for my complaining, and a word of great advice or comfort. They could always make me feel better and get me laughing. I could not have done this without them. (Also a big thank you to the two cats of the house, Bo-bert and Audrey, for the hours of entertainment they provided.)

My family has been a constant source of support and love. They have always encouraged me to do my best and be whatever I wanted to be, and I thank them for getting me to where I am today. I would not have achieved what I have without them. I would not be the person I am today without the influence of my zany, wonderful family.

Finally, I cannot thank my boyfriend, Brad Drews, enough for all of his support and love over the past years. He has been a shoulder to cry on and someone to laugh with whenever I needed it. He had to make sacrifices and put up with my stress and lack of time and energy. I could not have done as good of a job without his help and understanding. Thank you, my love.

Contents

Definitions of Symbols Used

C	Wallis' empirical constant (Eqn 4.3)	[--]
C_1	Kutateladze's empirical constant (Eqn 4.4)	[--]
C_2	Kutateladze's empirical constant (Eqn 4.4)	[--]
D	inside pipe diameter	[m]
dP/dz	pressure drop across test section per unit length	[Pa/m]
e	wall roughness	[--]
f	smooth tube friction factor	[--]
f_i	interfacial friction factor	[--]
f_{moody}	single phase friction factor	[--]
Fr_{GO}	gas only Froude number given by $Fr_{GO} = j_g / ((g\ D)^{1/2})$	[--]
f_{TP}	two-phase friction factor	[--]
g	gravitational acceleration constant	[m/s^2]
G_f	liquid mass flux	[kg/s-m^2]
G_g	vapor mass flux	[kg/s-m^2]
G_{tot}	liquid and vapor mass flux	[kg/s-m^2]
j_{air}	superficial air velocity	[m/s]
j_f	liquid superficial velocity	[m/s]
j_f*	dimensionless liquid superficial velocity (Eqn 4.2)	[--]
j_g	superficial gas velocity	[m/s]
j_g*	dimensionless gas superficial velocity (Eqn 4.1)	[--]
KE_{air}	kinetic energy of air	[J/m^3]
KE_{vapor}	vapor kinetic energy	[J/m^3]
Ku_f*	Kutateladze dimensionless liquid superficial velocity (Eqn 4.5)	[--]
Ku_g*	Kutateladze dimensionless gas superficial velocity (Eqn 4.5)	[--]
L	length of pipe	[m]
m	Wallis' empirical constant (Eqn 4.3)	[--]
Q_{air}	volume flow rate of air	[l/min]
Q_{liquid}	volume flow rate of R-123 liquid	[l/min]
Q_{vopor}	volume flow rate of R-123 vapor	[l/min]

Q_{water}	volume flow rate of water	[l/min]
Re	Reynolds number based on pipe diameter (general)	[--]
Re_g	vapor Reynolds number given by $Re_g = j_g D / \nu_g$	[--]
Re_{LF}	liquid film Reynolds number given by $Re_{LF} = (4 W_f) / (\pi D \mu_f)$	[--]
U	velocity (general)	[m/s]
u_g	velocity of gas	[m/s]
u_f	velocity of liquid	[m/s]
u_τ	shear velocity (used for non-dimensionalization) (Eqn 4.9)	[m/s]
W_f	liquid film mass flow rate	[kg/s]
W_g	gas mass flow rate	[kg/s]
x	mass quality given by $x=W_g/(W_g+W_f)$	[--]
X_{tt}	dimensionless two-phase Lockhart-Martinelli parameter (Eqn 4.10)	[--]
δ	optically measured film thickness	[mm]
δ_τ^+	non-dimensional film thickness (Eqn 4.9)	[--]
ΔP	pressure drop (general)	[Pa]
μ_f	liquid viscosity	[kg/m-s]
ν_f	liquid kinematic viscosity	[m^2/s]
ν_g	gas kinematic viscosity	[m^2/s]
ν_w	kinematic viscosity of water at 20^{o}C	[m^2/s]
ρ	density (general)	[kg/m^3]
ρ_{air}	air density	[kg/m^3]
ρ_f	liquid density	[kg/m^3]
ρ_g	gas density	[kg/m^3]
σ	surface tension	[N/m]
$\tau_{i,P}$	interfacial shear stress (Eqn 4.8)	[Pa]

1. Introduction

Background

The simultaneous flow of liquid and vapor is a regular occurrence in many applications. This two-phase flow can occur with single component fluid systems such as water-steam or refrigerant liquid-vapor as well as multi-component fluid systems such as refrigerant vapor-oil mixtures. This type of flow is important in applications that range from domestic refrigerators and air-conditioners to heat exchangers found in nuclear power and chemical process plants. Two-phase flow can be found in piping systems, valves, separators, and heat exchangers. The performance of many systems and plants is highly dependent on the nature of the two-phase flow found in these components; therefore, a better understanding of two-phase flow will contribute to improvements in the design, operation, efficiency, and safety of a wide range of applications.

For instance, a design concern of large refrigeration systems is the sizing of the vertical pipe runs (commonly referred to as "risers"). Although, it is desirable to minimize the pressure drop in refrigeration system piping, sizing piping for low velocities can minimize pressure drop. Unfortunately, low vapor velocities will not have flow characteristics capable of entraining and returning oil within the system. As a result, designers are faced with the challenge of balancing pressure drop while maintaining sufficiently high vapor velocities to maintain oil circulation in the system.

Considering that refrigeration and air-conditioning for transportation, domestic, and commercial uses account for up to 15% of the world's electricity use (IIR News, 2002), a better understanding of the two-phase flow is needed to facilitate in the design of efficient systems. Improved sizing of two-phase equipment used in these refrigeration

and air-conditioning systems might allow for a 10% increase in efficiency and, therefore, would have a significant effect on the electricity used world-wide.

Overview of Two-Phase Flow Regimes

There are several different regimes that arise in adiabatic two-phase flow. There are differences in the types of flow that occur in both vertical and horizontal flow. The regimes pertinent to vertical flow situations are shown in Figure 1.1 and include bubbly, slug, churn, wispy-annular, and annular. *Bubbly flow* consists of discrete bubbles of the vapor phase distributed throughout a continuous liquid phase. The main characteristics of *slug flow* are large vapor bubbles (with sizes up to the diameter of the tube) separated by a small liquid film between the wall and adjacent bubbles. In this flow regime, most of the liquid mass in slugs is found between the large bubbles. With further increases in vapor velocity, the large vapor bubbles will break down and transition into *churn flow*. *Churn flow* is characterized by a chaotic flow of vapor with a majority of the liquid thrown outward toward the wall surface. *Wispy-annular* flow is characterized by a thick liquid film along the tube walls with large amounts of entrained liquid (in the form of droplets) in the vapor core. The liquid droplets in the core tend to conglomerate into long irregular filaments or wisps. The main characteristics of annular flow are the liquid film that forms along the tube wall and the continuous vapor core down the center of the tube. In *annular flow*, the core may or may not include entrained droplets. The liquid-vapor interface will often have coherent waves. The focus of this research project is aimed at the *annular flow* regime.

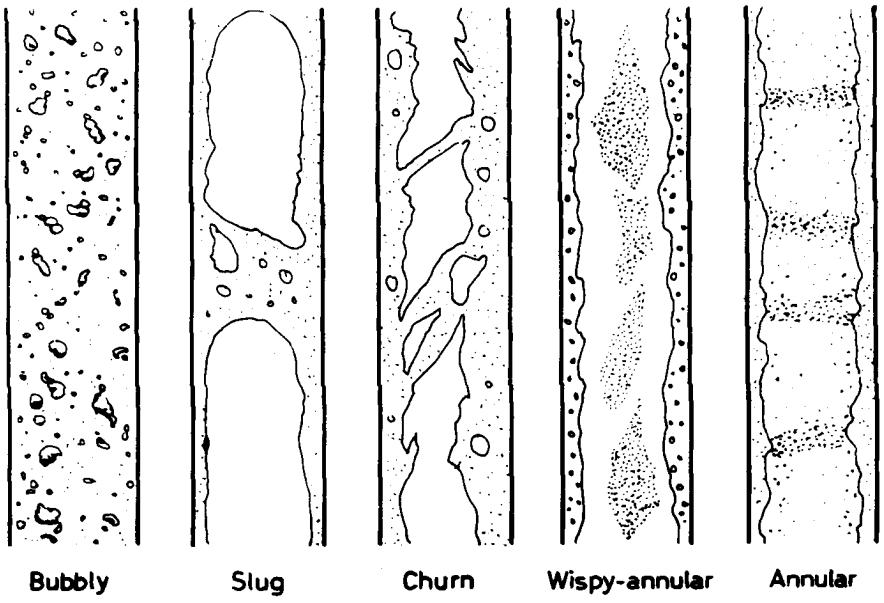

Figure 1.1: Vertical flow regimes (Collier and Thome, 1996).

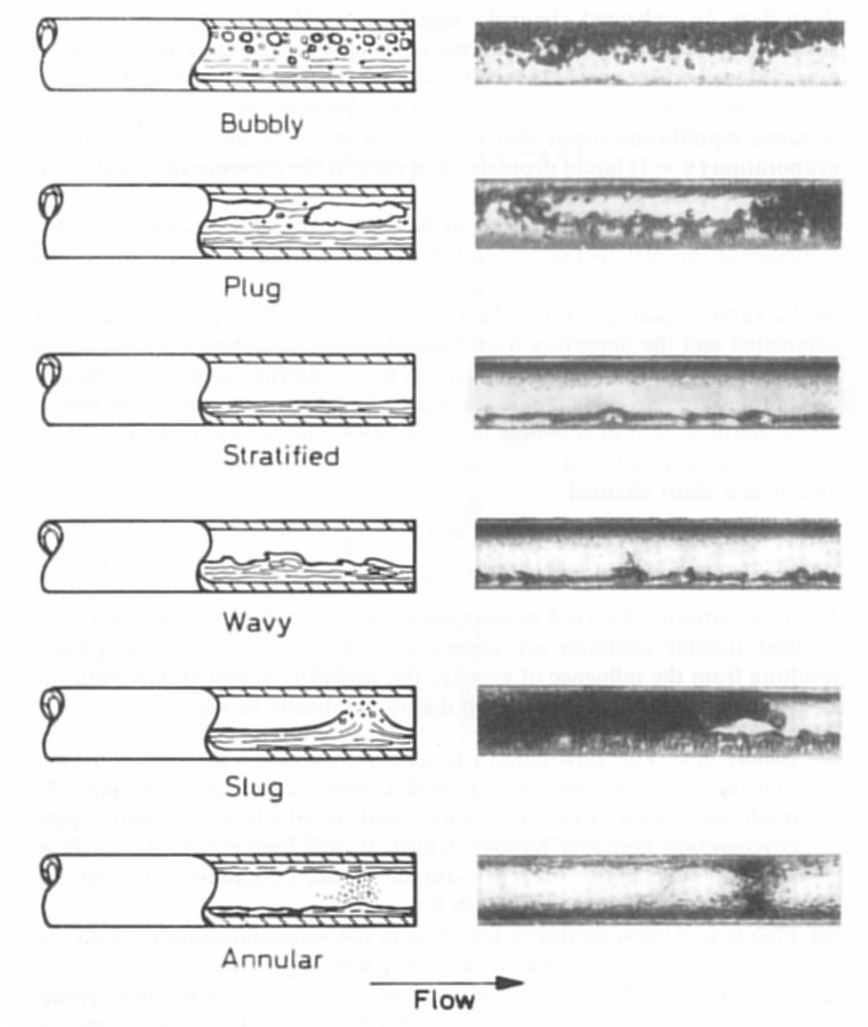

Figure 1.2: Horizontal flow regimes (Collier and Thome, 1996)

The influence of gravity causes the flow regimes in horizontal tubes to be somewhat different than vertical orientations. Figure 1.2 shows horizontal flow regimes that include bubbly, plug, stratified, wavy, slug, and annular flow. The *bubbly flow* pattern is similar to the vertical *bubbly flow* but with the difference that gravity effects cause most of the bubbles to stratify to the upper half of the tube. *Plug flow* is similar to vertical *slug flow*, again with the large vapor bubbles appearing in the upper half of the tube. Only at very low liquid and vapor flow rates can *stratified flow* be observed. This flow pattern has a

liquid flow along the bottom and a continuous vapor flow in the upper portion of the pipe with a smooth interface. At higher vapor velocities, the quiescence at the liquid-vapor interface disappears leading to the *wavy flow* regime. By further increasing the vapor velocity, large waves are formed that fill the tube and are pushed down the tube in the direction of flow leading to *slug flow*. *Annular flow* is seen at even higher vapor velocities. The main characteristics of *annular flow* include a liquid film that may or may not entirely cover the tube walls and a vapor core down the center of the tube, which may or may not contain liquid droplets (entrained liquid). In horizontal flow, the liquid film is often not the same thickness circumferentially. The surface of the liquid film may exhibit ring-like (disturbance) waves, roll waves like those on a lake, and/or ripples. These waves can move at different velocities and frequencies. The understanding of the behavior of the liquid film is important in heat transfer applications, which is why this type of flow is of interest in this experimental study.

Overview of Annular Flow

A number of theories have been forwarded that attempt to explain the spreading of the liquid film in horizontal annular flow (Butterworth, 1972, Fukano and Ousaka, 1989) including:

1) the spreading of the film by wave action,
2) the transfer of liquid by entrainment and deposition of droplets,
3) the spreading of the liquid by circumferential shear forces due to secondary gas flows, and
4) the spreading of the liquid by surface tension forces.

Several models of liquid film distribution have been constructed based on one or more of these theories. Laurinat et al. (1985) produced a rather comprehensive liquid distribution model for annular flow. They take into account all effects listed above except surface tension forces in their model. In their conclusions, they state that secondary gas flows are the most important effect in the formation of the liquid film; however, they state that their model has several constants that are not based on any physical aspects, which questions the applicability of their findings when applied to other fluids (not air and water) or different geometries.

Fukano and Ousaka (1989) created a model with much emphasis on the spreading of the film through wave action (or pumping action of disturbance waves). However, their work shows that secondary gas flows also play an important role in maintaining the film. In support of Fukano and Ousaka's model, Jayanti and Hewitt (1991) observed that the waves are at least partially responsible for wetting the top of the tube. However, except for Darling and McManus' work (1968), there has been little experimental evidence that the secondary gas flows even exist. With all of the theories advanced and models proposed for characterizing liquid film spreading, there is still considerable disagreement on the importance of each of the possible theories (i.e. waves, deposition, etc.) on the spreading of the liquid film. A need exists to develop a more concrete understanding of the fluid mechanics of annular flow including the interactions between the liquid and vapor phases.

Much of the work aimed at developing an understanding of the mechanics of annular flow (under adiabatic conditions) has relied on air/water experiments. These experiments are relatively easy to build and operate; however, many systems of interest

do not rely on the use of air and water as working fluids. As a result, the applicability of air/water results to pure component systems and other working fluid pairs is questionable. In order to understand the behavior of fluids used in actual systems, some experiments have been done to study the effects of varying fluid properties.

Several experiments have been done to study the effect of altering the viscosity, density, and/or surface tension from those of air and water as the working fluid pair. The experiments attempted to determine the property effects on wave behavior, droplet entrainment, and/or liquid film behavior in vertical flow. Fukano and Furukawa (1998) studied the effects of changing the liquid kinematic viscosity on the behavior of the liquid film and waves in equal flow conditions. They found that higher liquid viscosities tended to dampen out the waves causing smaller waves with lower frequencies when compared to less viscous fluids. They also found that the mean film thickness increased strongly with an increase in liquid viscosity under the same flow conditions. Other studies focused on changing liquid viscosity were conducted by Mori, Kondo, Kaji, and Yagashita (1999), who increased the liquid viscosity from that of the base fluid, water. They also found that as the viscosity increased, the appearance of huge waves and disturbance waves persisted but the frequency of these waves decreased (especially at lower liquid velocities). Jepson et al. (1990) varied both the gas density and the surface tension in their experiments. They found that as the gas density (or the shear stress on the liquid film) is decreased there is less liquid entrainment at a constant gas velocity. They also discovered that as the surface tension (stabilizing force) decreased more entrainment would result at a constant gas velocity, with reductions in the drop size and deposition of droplets. Whalley and Jepson (1994) confirmed these findings in their work. Bousman

et al. (1996) performed a set of microgravity experiments in which they varied the tube diameter, liquid viscosity (higher than water), and surface tension (lower than water) to determine the effect on flow regime transitions and flow mapping. Although these experiments added to the knowledge of how the fluid properties can affect annular flow, they do not provide a method of relating results between different experimental works and the working fluids more commonly found in applications.

A few groups have performed experiments in order to directly relate different fluids or to create models that are not dependent on the type of fluid used. Fukano and Furukawa (1998) predict the two-phase pressure drop in a vertical tube using an interfacial friction factor calculated from density and viscosity and a correlation for film thickness. They use this correlation to compare with the experimental pressure drop found for several fluids with different viscosities and densities (and a fairly constant surface tension). This correlation is referenced to the properties of water at 20^{o}C and the comparison fluids chosen all had higher kinematic viscosities than water (and higher densities). These last two points could have affected their finding that this correlation had good success in the fluids studied. Hashizume and Ogawa (1985, 1987) created a model to predict the horizontal two-phase pressure drop between fluid flows having different liquid viscosities. This correlation worked well for their data.

Motivation for Study

In this work, two different adiabatic experiments were performed in order to compare the results with air/water data taken both from other works and obtained in this study. The chosen fluids for these experiments are R-123 (HCFC-123) and air/oil. The low-pressure refrigerant, R-123, was chosen to compare with air/water data in order to

have a method of relating the multitude of air/water data available in the literature to the design of refrigeration and air conditioning systems, and, in a broader sense, to find a method of relating between any fluid pairs. The air/oil fluid pair was selected to study a specific case of a problem faced in the design of refrigeration facility, i.e. the design of a vertical riser for the return of the viscous oil flow. The selection of R-123 also allowed for the general study of changing the vapor properties, while the selection of oil allowed for the study of changing the liquid properties.

Thesis Organization

Chapter 2 discusses the experimental setups for the horizontal refrigerant test facility, the horizontal air/water test facility, and the vertical air/oil test facility. As part of this work the refrigerant test facility and the air/oil test facility were designed and constructed. The air/water test facility used in this investigation was already operational.

Chapter 3 discusses an experiment done to compare fluid behavior of different fluids in identical, horizontal, adiabatic test sections using a refrigerant and air/water as the different fluids. The refrigerant (R-123) has a higher gas and liquid density and a lower gas and liquid viscosity and surface tension than that of air and water. The air/water and refrigerant flows are compared using pressure drop measurements, film thickness measurements, and qualitative visual observations including wave behavior. This experiment attempted to match liquid film behavior, flow regime, and pressure drop of the different fluid pairs by equating the kinetic energy of the vapor flow. If successful, this technique would allow for a direct comparison between different experiments and different fluids in the future; thus being able to do experiments in simple to use fluids, such as air and water and design a system using a refrigerant or other fluid.

Chapter 4 of this work describes findings relating to changing the viscosity, density, and surface tension of the liquid (compared with water) in a vertical annular flow experiment. This experiment uses air and soybean oil to study a significant increase in liquid viscosity and a slight decrease in liquid density (viscosity=0.04 kg/m-s, density=920 kg/m^3) from that of water. This work discusses the measured pressure drop and film thickness, the types of waves observed and the behavior of the liquid film between points of definite up-flow and definite down flow. This work also tries to identify the point of flow reversal, an important design concern for vertical risers. These findings are compared with other published works dealing with commonly used experimental fluids (i.e. air/water).

References

Bousman W. S., J. B. McQuillen, and L. C. Witte, "Gas-liquid flow patterns in microgravity: effects of tube diameter, liquid viscosity, and surface tension." *International Journal of Multiphase Flow*, **22**(6): 1035-1053, 1996.

Butterworth, D., "Air-water annular flow in a horizontal tube." *Progress in Heat and Mass Transfer*, **6**: 235-251, 1972.

Collier, J. G. and J. R. Thome, *Convective Boiling and Condensation*. Clarendon Press, Oxford, Third Edition, 11 and 16, 1996.

Darling, R. S. and H. N. McManus, "Flow patterns in circular ducts with circumferential variation of roughness: a two-phase flow analog." *Proceedings of the 11th Mid-Western Mechanics Conference (Developments in Mechanics)*, **5**:153-170, 1968.

Fukano, T. and T. Furukawa, "Prediction of the effects of liquid viscosity on interfacial shear stress and frictional pressure drop in vertical upward gas-liquid annular flow." *International Journal of Multiphase Flow*, **24**(4): 587-603, 1998.

Fukano, T. and A. Ousaka, "Prediction of the circumferential distribution of film thickness in horizontal and near-horizontal gas-liquid annular flows." *International Journal of Multiphase Flow,* **24**(4): 587-603, 1989.

Hashizume, K. and N. Ogawa, “Flow pattern, void fraction and pressure drop of refrigerant two-phase flow in a horizontal pipe (II): analysis of frictional pressure drop.” *International Journal of Multiphase Flow*, **11**(5): 643-658, 1985.

Hashizume, K. and N. Ogawa, “Flow pattern, void fraction and pressure drop of refrigerant two-phase flow in a horizontal pipe (III).” *International Journal of Multiphase Flow*, **13**(2): 261-267, 1987.

IIR News, “A word from the Director.” *International Journal of Refrigeration*, 25: 1-2, 2002.

Jayanti, S. and G. F. Hewitt, “Structure of interfacial waves in air-water horizontal annular flow.” *Phase-Interface Phenomena in Multiphase Flow*, Hemisphere Publishing Corporation, New York, 95-104, 1991.

Jepson, D. M., B. J. Azzopardi, and P. B. Whalley, “The effect of physical properties on drop size in annular flow.” *Heat Transfer 1990: Proceedings of the Ninth International Heat Transfer Conference,* **6**:95-100, 1990.

Laurinat, J. E., T. J. Hanratty, and W. P. Jepson, “Film thickness distribution for gas-liquid annular flow in a horizontal pipe.” *PhysicoChemical Hydrodynamics Journal*, **6**(1,2): 179-195, 1985.

Mori K., Y. Kondo, M. Kaji, and T. Yagashita, “Effects of liquid viscosity on characteristics of waves in gas-liquid two-phase flow (Characteristics of huge waves and disturbance waves).” JSME International Journal Series B-Fluids and Thermal Engineering, **42**(4):658-666, 1999.

Whalley, P. B. and D. M. Jepson, “Entrainment and deposition in annular gas-liquid flow: the effect of fluid physical properties.” *Heat Transfer 1994: Proceedings of the Tenth International Heat Transfer Conference*, **6**:289-294, 1994.

2. Experimental Set-up

Introduction

Three separate experimental facilities used to explore the mechanics of both vertical and horizontal annular flow are described in detail in this chapter. The first facility described is a low-pressure two-phase refrigerant facility with a horizontal, adiabatic test section. The second set-up described is an air/water facility with an identical horizontal, adiabatic test section to the refrigerant facility. The final test set-up described is an air/oil facility with a vertical, adiabatic test section.

R-123 Test Facility

The purpose of the horizontal adiabatic R-123 (dichlorotrifluoroethane, HCFC-123) experimental facility was to allow the collection of data to better understand the mechanics of the two-phase flow of a low-pressure refrigerant. One of the goals of this facility was to compare data obtained from this facility to data taken from an identical test section that uses the most commonly studied binary fluid pair in two-phase flow, air and water. The R-123 test apparatus included a 5.7-meter long, insulated, horizontal test section made of clear PVC (schedule 40) with an inside diameter of 15.1 mm. The test apparatus had the capability of controlling mixture (mass) quality at the test section inlet by managing the proportion of liquid and vapor flow through two separate circulating paths. A separator was placed at the end of the test section to insure that the vapor and liquid phases remained within their individual paths outside of the test section (see Figure 2.1). Vapor was generated in the evaporator tank by boiling liquid refrigerant from heat addition provided by three 5 kW heaters. The vapor generation was controlled with a software-based PID controller using the measured vapor flow rate as the feedback for the

controller. The liquid flow rate was controlled using a variable-speed peristaltic pump and measured with a Coriolis flow meter. Using separate flow paths for liquid and vapor allowed the quality and mass flux to be controlled at any desired value within the operating range of the loop. The R-123 facility was capable of operating at volumetric vapor flow rates of 40-220 LPM with liquid flows ranging from 0-1.1 LPM at approximate pressures and temperatures of 90 kPa and 24ºC in the test section with two-phase flow running. The properties of R-123 at these conditions are listed in Table 2.1. A schematic of the test facility is shown in Figure 2.1 and a photo of the facility in Figure 2.2.

Table 2.1: Properties of R-123 at saturation conditions used in experiment.

Properties of R-123 at saturation conditions of 88.1 kPa and 24^{O}C		
Liquid Density	1466	kg/m3
Vapor Density	5.7	kg/m3
Density Ratio	257	
Liquid Viscosity	$4.2*10^{-4}$	kg/m-s
Vapor Viscosity	$4.2*10^{-6}$	kg/m-s
Surface Tension	0.015	N/m

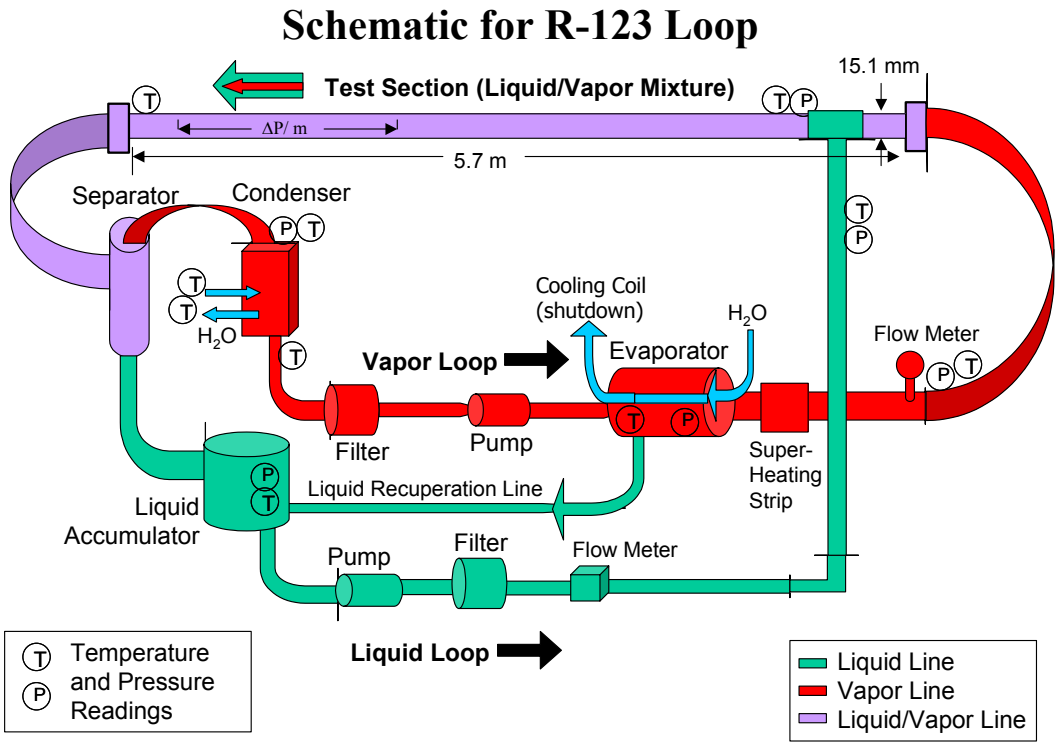

Figure 2.1: Schematic for R-123 test facility.

Figure 2.2: Photograph of R-123 test facility.

A requirement in the design and construction of this facility was that all materials had to be compatible with R-123. Appendix A shows a list of compatible and incompatible materials. Each part discussed below was chosen partially for the compatibility of the wetted materials. Table 2.2(a,b) has a full list of the parts used, with accuracies (where applicable), part numbers, and vendors. The following sections have a short description of the part and, where applicable, a description of the construction methodology and/or the calibration techniques. However, one portion of the facility is not listed below, that being the metal framework used to support the entire facility. This framework was bolted to the concrete floor for greater stability and can be seen in Figure 2.2.

Table 2.2 (a, b): List of parts (a) and sensors (b) used in the construction of the R-123 test facility.

Parts	Manufacturer	Part Number(s)
Brazed Plate Heat Exchanger	Alfa Laval	CB26-34H S52
Heaters (5 kW)	Omega Engineering	TMW-250A/240V
Vapor Tank	Grainger (Speedaire)	5Z359
Liquid Tank	Grainger (Amtrol)	3GD23 (941-1141)
Liquid Pump	Cole-Parmer (Masterflex)	U-77201-60, EW-07553-70, EW-07596-20
Tygon 2075 Pump Tubing	Cole-Parmer (Masterflex)	00052BY (#15), 00052CB (#36)
Condensed Vapor Pump	Cole-Parmer (Micropump)	75211-22
Flexible Polyethelyne Tubing	McMaster-Carr	5181K25
Filter-Drier Installation	Sporlan	(Catch-All) C-163-S-HH
Compression Fittings	Swagelok (Badger Valve and Fitting Corp.)	Assorted
Replacement Viton O-rings	McMaster-Carr	Assorted sizes
Manifold Gauge Set	Grainger	6X639
Vacuum Pump	Fast-Vac	DV-85N (C55JXHJW-4084)
Data Acquisition Parts	**Manufacturer**	**Part Number(s)**
Data Acquisition Unit	Agilent Technologies	34970A, 34901A
Data Acquisition Unit	National Instruments	SC-2345, SCC-CI20, SCC-FT01, SCC-TC01
Heater Control Circuit Parts	**Manufacturer**	**Part Number(s)**
Single-phase Control Module	Omega Engineering	PCM1
Finned Heat Sink	Omega Engineering	FHS-1
Solid State Relay	Omega Engineering	SSR240DC45
Fast Blow Fuse for SSR	Omega Engineering	KAX-45

Sensors	Manufacturer	Part Number(s)	Range	Accuracies
Thermocouple (T-type)	Omega Engineering	TMQSS-125G-6	220^{O}C	±1.0^{O}C
Absolute Pressure Transducer	Omega Engineering	PX303-050A5V	0-3.45 bar	±0.25% FS
Differential Pressure Transducer	Omega Engineering	PX2300-2DI	0-2 psig	±0.25% FS
Heat Exchanger Pressure Transducer	Cole-Parmer	PN# 68075-34	-14.7-30 psig	±0.25% FS
Pressure Release Valve	Swagelok (Badger Valve and Fitting Corp.)	SS-RL4S8	10-225 psig (adjustable set point)	N/A
Liquid Volumetric/Mass Flow Meter	Emerson (Micromotions, Inc.)	ELITE CM025 Sensor, 2700R Transmitter	0-10 LPM	±0.1% FS
Vapor Volumetric Flow Meter	Thermal Instrument Co.	62-9/9500, S/N:2001387	0-1000 LPM	±0.5% FS
Pressure Gauge (Bourdon tube for refrigerant tanks)	Grainger	2C783, 4ZG17, 2C772	VAC-30 psig, 0-15 psig, 0-30 psig	±3-2-3%
Current Transformer	Omega Engineering	CTL-094020	200:5	N/A
Ultrasonic Leak Detector	Superior Signal Company, Inc.	AccuTrak VPE (2501-V14037)	N/A	N/A
Refrigerant Leak Detector	Inficon	D-TEK	Indoor/Outdoor	7 g/yr
Liquid Leak Detector	Swagelok (Badger Valve and Fitting Corp.)	Snoop	N/A	N/A

The vapor tank (evaporator shown in Figure 2.1) served two functions. First it was used as a reservoir to store the system's refrigerant charge. Second, it served as the vapor generator; thereby, providing a motive force for vapor flow. The construction of the vapor tank involved a series of iterations. First, the upper metal protective cover was cut off. Four 1-inch FNPT fittings were welded into the four holes cut for the heaters. A 2-inch FNPT fitting was welded onto the top of the tank to be used as the vapor outlet. The welding was done by an outside contractor. Because of the difficulty in welding curved surfaces, much J/B Kwik® was used to fill any holes that were left. The vapor tank houses three 5 kW resistance heaters that were used to generate vapor flow. The heaters were fitted into the 1-inch fittings mounted on each end of the vapor tank and were screwed into place. The fourth of these fittings was used for a thermocouple placed in the liquid inside the tank and a thermocouple attached to one heater that are both fed into the data acquisition system. The vapor tank had three ½-inch FNPT fittings to start with that were used for a sight glass, a pressure reading, a safety pressure release valve, an outlet for draining the tank, and the liquid inlet to the vapor tank by using tee connections. The safety pressure release valve was connected to an exhaust vented outside of the building. The vapor tank came with a ¾-inch FNPT fitting in the center of each end. This fitting was used to thread a coil of ½-inch copper tubing around the inside of the tank. The copper tubing was connected to the water inlet and outlet of the heat exchanger, which comes from the building city water supply. The coil of copper tubing was used to cool the tank quickly after running experiments and to cool the tank to the lowest temperature in the experimental set-up in order to collect all refrigerant in one location.

Each heater was controlled by an electrical circuit that used a pulse control modulator and solid state relay to send a controlled pulse of current through the heater (essentially turning it off and on with varying pulses of current). The pulse width modulator was controlled by a voltage-to-current circuit that converts voltage signals sent from the PID controller to a 4-20 mA signal. This control circuit was designed by a colleague. The PID controller used the vapor flow as the feedback. The PID controller will be explained in detail in a later section. The schematic for the electrical circuit is shown in Figure 2.3.

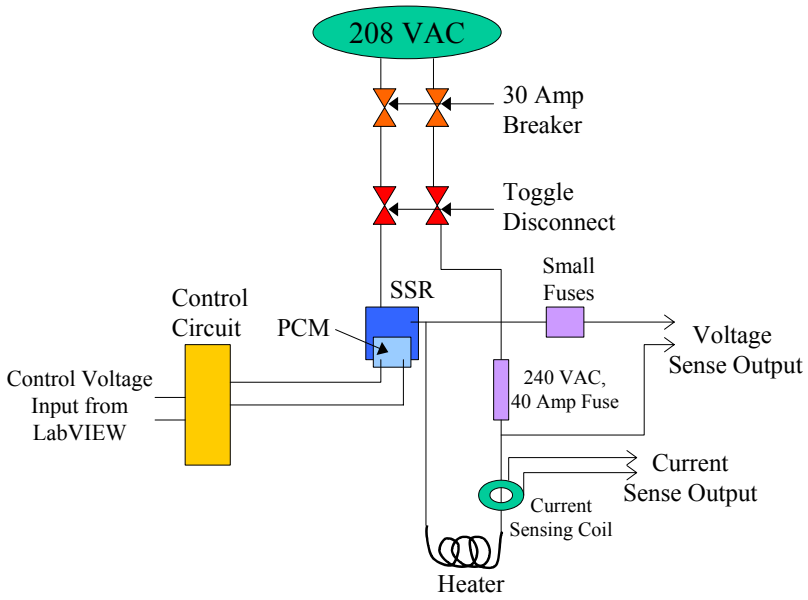

Figure 2.3: Schematic of circuit used to control heaters for vapor production.

The heat exchanger (condenser) was used to condense the vapor leaving the test section for ease in pumping of the refrigerant and to provide the low pressure in the set-up to force the refrigerant vapor flow. The heat exchanger was chosen based on the amount of heat that would be used to evaporate the refrigerant in the vapor tank, and

therefore the amount of heat that would need to be removed. Male 1-inch copper fittings were soldered onto the ends of the heat exchanger with PVC unions attached to these fittings. The cold side inlet was attached to the building water supply with the outlet leading to a drain. The building water was at an average temperature of 10ºC upon entry to the test facility. The hot side inlet was attached to the vapor outlet from the separator and connected back to the vapor tank. Thermocouples were attached at each inlet and outlet and a pressure transducer was placed at the refrigerant inlet, all of these were read by the data acquisition system.

The liquid tank was used as storage and a liquid accumulation point while running experiments. The tank had three ½-inch FNPT fittings welded to the tank to be used for a sight glass (used 2 fittings) and the liquid outlet point (located on bottom of tank). The tank had two fittings already installed that were used for pressure and temperature readings (using a tee section) and the liquid inlet from the separator.

The liquid flow rate was measured by a Coriolis flow meter. This type of flow meter was chosen because of the very low pressure drop, the accuracy, and all the different options of measurements it can yield. The Coriolis flow meter can report the mass flow rate, the volume flow rate, the density, and temperature of the liquid flow. Some instructions for use of this flow meter are found in the *Running Liquid* section of Appendix E under step 2(d). For a more detailed description of all functions see the Micromotion users manual for the Coriolis flow meter.

The vapor flow was measured by a NIST-traceable thermal probe-type flow meter. The flow meter was calibrated for use with R-123 by the manufacturer. The calibration is simply 1.4 times an air flow. This flow meter will not work below 40 LPM

and also has a slight delay when starting up. The flow meter must be mounted in a 3-inch diameter tube in a vertically upright position 10 tube diameters from the entrance and 5 tube diameters from the exit. The reason for choosing this type of flow meter was the low-pressure drop and the accuracy in measuring vapor flow, which was a difficult combination to find.

The purpose of the separator was to separate the liquid and the vapor at the test section exit. As seen in Figure 2.4, the two-phase flow entered through the separator inlet and then passed through an elbow that imparted a tangential velocity to aid in separation. This caused the heavier liquid to get thrown to the walls and drop out the bottom of the separator and into the liquid tank. The lighter vapor flowed through a screen/demister and out the top of the separator to the heat exchanger. The fitting containing the turning elbow was machined down to slide through the opening in the side of the separator to make a smooth transition point and was then secured. The vapor outlet was also machined in order to slide the tube holding the screen into the center of the separator and secured. The liquid outlet was simply a compression fitting screwed into the PVC to transition to copper tubing.

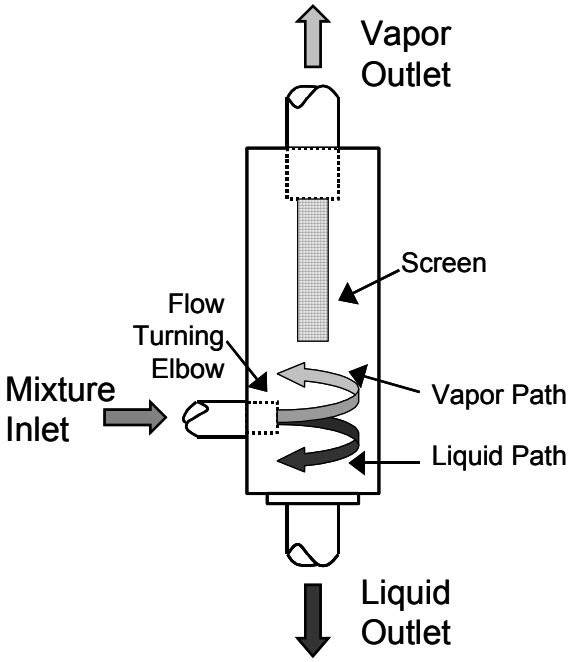

Figure 2.4: Schematic of liquid and vapor separator.

The test section itself was made of clear ½-inch Schedule 40 PVC with I.D. of 15.1 mm. The three sections of PVC were connected using one union and one coupling. Each of these was machined to achieve a seamless connection to reduce disturbance of the flow. The end of the test section was attached with a union for the flexibility of putting in a different test section. The original section that was installed became coated on the inside with a white powdery residue due to a contamination problem. This section was equipped with pressure taps in order to obtain the pressure drop data. An identical, but clean, section was constructed for the purpose of taking film thickness data. The entire test section was designed to be interchangeable with different sized test sections using the unions on each end. The vapor entered the test section from one end of the test section (Figure 2.1). The liquid inlet at the far right end of the schematic was constructed by drilling many small holes in the test section and then sliding a slightly larger clear PVC tee over these holes and sealing each end of the tee around the test section. (See

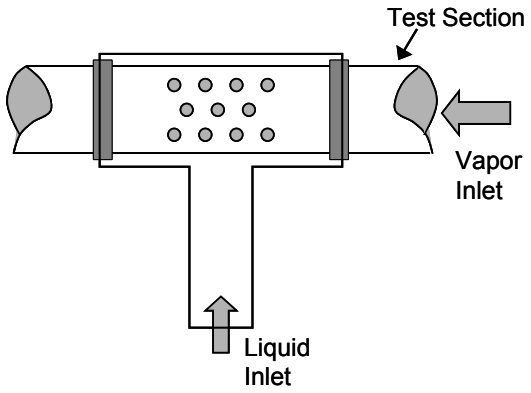

Figure 2.5: Schematic of liquid inlet to the test section

Figure 2.5.) The liquid was then pumped into the tee section of the PVC tee and through the holes for a uniform distribution of liquid around the tube.

The pump in the vapor loop was a Micropump variable speed gear pump. This pump returned the condensed vapor from the heat exchanger to the vapor tank. It also, effectively, kept the pressure lower at the end of the test section causing the vapor to flow from a higher pressure to a lower pressure.

The pump in the liquid loop was a Masterflex peristaltic pump with two adjustable occlusion pump heads for greater range. This pump controlled the flow of liquid entering the test section from the liquid tank.

The pressure sensors were placed in strategic positions for monitoring the flow as seen in Figure 2.1. The output from the pressure sensors was fed into the data acquisition system. A pressure gauge was placed on each tank as a safety check.

The T-type thermocouple probes were used in any location where a bored-through fitting would fit. The T-type thermocouple wires that were used had to be made from bulk thermocouple wire and were used in any location where the probes could not be used. The procedure for making these wires into thermocouples can be seen in Appendix B. The thermocouple wires were attached using either a conducting metal epoxy (on the heat exchanger) or by soldering to the surface (of the heater). The thermocouple probes were installed using 1/8" bored-through compression fittings and tapped holes for the fittings. The approximate placement of each thermocouple can be seen in Figure 2.1. All thermocouples and thermocouple probes were calibrated using an ice slurry bath to within ±0.1ºC of 0ºC.

The filters used were standard refrigerant system filter/driers. A type typically used on systems that are being cleaned or purged was used to achieve a more thorough filtering of the fluid. The connecting ends of each filter were solder ends, however, for

ease of replacement and assembly, ½ inch compression fittings were used over the solder-end. The excess paint on the solder-end had to be carefully scraped off for the fitting to fit.

The vacuum pump was a Fast Vac deep vacuum pump with a capacity of three cubic feet per minute This pump was used to remove air from the system prior to start-up.

Several different types of leak detectors were used. In the initial building stage, a liquid leak detector was mainly used called Snoop® by Swagelok. The liquid was applied over the surface being tested and would bubble in the presence of a leak of any kind of vapor/gas. Each section, after construction, was pressurized with air to test for leaks in this manner.

The ultrasonic leak detector also detected any type of vapor/gas leak by amplifying the sound made by the escaping gas. This method was also used in conjunction with the above method. However, it was very susceptible to background noise; and therefore, it was difficult to discriminate leaks.

The refrigerant leak detector detected only refrigerant vapor (not pure air). Therefore, in order to do preliminary leak tests of the entire system, the system was slightly pressurized with air and a small amount of refrigerant vapor released into the system. This method was used a great deal both after the assembly of the entire system and in the testing stage (because this leak detector was more sensitive than the other leak detectors listed).

Several different methods were used to fix any leaks that were found. If the fitting was of the type that could be tightened (screw fitting), this was attempted, or the fitting was removed and rewrapped in Teflon tape and reinstalled. If this did not fix the

leak, the fitting was glued in using only J/B Kwik® epoxy (or J/B Weld® for slower drying times). If the fitting being fixed did not need to be removed, the epoxy was applied to the threads of the fitting for best results. All other leaks (non-screw fittings) were filled using J/B Kwik® epoxy. The epoxy was applied on clean surfaces (roughened if necessary with sand paper) and only when the system was **not** pressurized.

The data acquisition system used the LabVIEW software for recording data and for controlling the heaters. The interface of the LabVIEW program can be seen in Figure 2.6. The channel assignments and program code can be found in Appendix C and D, respectively. All pressure sensor and thermocouple read outs can be seen on the front panel of the program (Figure 2.6), as well as the volume flow for vapor and liquid, and the liquid density read out. The program included the option to sample the power (voltage and current) of each heater if desired; however, this significantly slowed the sampling process. When this feature was activated, the control of the heaters became ineffective due to the sampling being slowed while the system averaged the AC voltage and current for each sample. The heater temperature and the LabVIEW voltage output that was sent to the heaters for control were monitored. When the program was sending an *ON* signal (above 0.89 volts) to the heaters, the indicator light turned orange, if the program was not sending a signal, the indicator light turned blue. The program included a safety shutdown mechanism in the instance that the heater temperature exceeded 100ºC (which can be adjusted). If the program were shut down in this manner, the heater control output would be 0.8 volts (or no signal) so that the heaters would begin to cool immediately.

There were two ways in which to control the heaters, manual and automatic. In manual control, the voltage output can be set using the horizontal slide. It was recommended to set this conservatively (~2 volts at high end) and to monitor the heater temperature and vapor tank temperature and pressure closely, because this control can easily be left on unwatched. In automatic mode, the program used the vapor flow signal as the feedback in a PID controlling subprogram. The ultimate goal of the heater control system was to control the vapor flow rate. The desired vapor flow rate was set (in LPM) in the given slot, and the mode switch was set to *automatic* for the program to control the flow. It was recommended to step the desired flow rate up slowly (increments of ~25 LPM) to avoid over-heating.

The program had the option to write all data taken from the time the program was started by turning on the '*Write to File?*' option at any time during the sampling process. All data from the start of the program would be recorded and the '*Write to File?*' option had to be on (lit up) when the program was stopped to have the option to write the data to a file.

The program should be stopped using the large, red *STOP* button. This was also an added safety feature. If the program were aborted using the stop button on the menu bar the program would continue to send the last voltage signal output to the heaters. **This could be very dangerous!** The program would no longer be activated and therefore the heater temperature safety cutoff would no longer be activated. The system would then have the potential to run wild and would have only one safety mechanism left on the vapor tank, the pressure release valve. If the program's *STOP* button were used, the program would send a voltage signal of 0.8 volts (no signal) to the heaters and

immediately start the cooling process. Also, of less importance would be the fact that the data being taken would not be written to a file if the program were aborted using the stop button on the menu bar. The *STOP* button must be 'up' or bright red in order for the program to run.

To access the other pages of the program interface, click on the tabs above the front panel. These should not be needed during normal use. When sampling power from the heaters, the heater voltage and current can be viewed on the second page. If the data acquisition channels must be changed or viewed, check the third page. To change or view the PID parameters, see page four. All pages can be viewed while the program is running without harming the heater control or data taking processes.

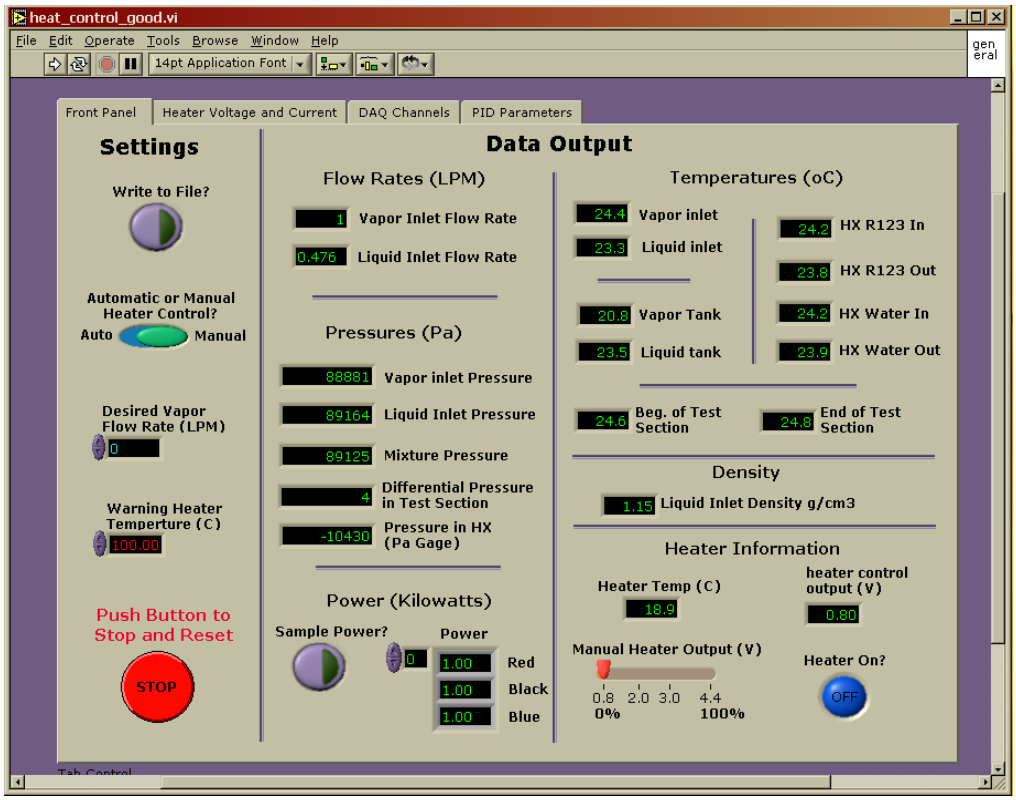

Figure 2.6: LabVIEW program interface used for data acquisition and for control of vapor production through control of heaters.

As was stated earlier, the pressures and temperatures were recorded by the data acquisition system and LabVIEW program. This included the differential pressure in the test section as well. This pressure drop had the option of being measured over a one meter section or a two meter section using a three way valve.

The film thickness measurements were recorded using a separate LabVIEW program. Film thickness measurements were obtained using an optical method (Shedd and Newell, 1998). This optical measurement method involved illuminating the pipe wall and liquid film with a small circular light source (such as a light emitting diode, or LED). The light was refracted and reflected by the liquid film, creating a ring of light on the pipe wall. The diameter of the reflected light ring was proportional to the thickness of the liquid film. Using geometry and the indices of refraction for the pipe wall and the liquid, the film thickness was determined. Uncertainties typically ranged from 9% for very wavy films to less than 0.1% for smoother conditions.

Each flow was illuminated by a flashing strobe light and videotaped. The flow was then analyzed on a frame-by-frame basis to study the wave, bubble, and droplet behavior in a purely qualitative analysis.

The flow conditions used in the R-123 experiment are shown in Table 2.3. To see detailed instructions on how to operate the R-123 facility to achieve these flow conditions, see Appendix E.

Table 2.3: Flow conditions run in R-123 experiments.

Flow Conditions for R123				
x	G_{tot}	KE_{vapor}	Q_{liquid}	Q_{vapor}
	kg/m^2-s	J/m^3	lpm	lpm
0.23	100.00	48.38	0.56	46
0.21	145.00	85.23	0.84	61
0.45	90.72	150.50	0.37	80
0.21	190.50	152.10	1.09	81
0.71	84.14	329.80	0.18	120
0.45	135.20	335.00	0.54	119
0.46	182.80	626.10	0.72	160
0.72	132.30	789.30	0.27	179
0.73	184.70	1509.00	0.36	240

Air/water Test Facility

The air/water test apparatus included a 5.7-meter long, clear PVC (schedule 40), horizontal test section with an inside diameter of 15.1 mm. The tubing materials and methods of construction were identical to that used in the R-123 test section, although the test facility was not designed as part of this project. This test apparatus consisted of two separate paths for the water and the air. The water was circulated from the test section through the liquid path using a peristaltic pump (similar combination as the refrigerant facility) and variable area flow meter. The water flowed through the test section into a separator and was pumped back through the test section. The air was supplied through a compressed air line, ran through a set of variable area flow meters into the test section, and was then vented to the room from the separator. The water and air were mixed in the same type of tee connection described in the refrigerant set-up and shown in Figure 2.5. The separator in the air-water test facility used the centrifugal effects described in the refrigerant separator and the action of gravity to separate the flow. However, unlike the refrigerant separator, no screen/demister was used and the air was vented to the room. In an unrelated, previous experiment, a pink-colored dye was used in the water and therefore showed up in the pictures taken of this flow. This dye did not measurably affect the properties of the water.

Pressure and temperature measurements were obtained for each flow condition at the points indicated in Figure 2.7. The digital differential pressure gauge was verified using a U-tube manometer. Temperatures were measured with T-type thermocouples calibrated in the same manner as in the R-123 experiment. A list of the sensors used and their accuracies can be seen in Table 2.4.

Table 2.4: List of sensors used in the air/water experiments for data taking.

Sensors	Manufacturer	Part Number(s)	Range	Accuracies
Thermocouple (T-type)	Omega Engineering	TMQSS-125G-6	220^{O}C	±1.0^{O}C
Absolute Pressure Transducer	Omega Engineering	PX303-050A5V	0-3.45 bar	±0.25% FS
Differential Pressure Gauge (Digital Manometer)	Grainger (Dwyer)	1W435 (475-2)	0-40 in H_2O	±0.5% FS
Water Volumetric Flow Meter	Cole-Parmer	EW-32458-42	200-3000 ccm	±3% FS
Air Volumetric Flow Meter	Cole-Parmer	EW-32461-64, EW-32466-68	30-280 LPM, 100-1400 LPM	±3% FS, ±2% FS
Pressure Gauge	Grainger	4ZG17, 2C772	0-15 psig, 0-30 psig	±3-2-3%

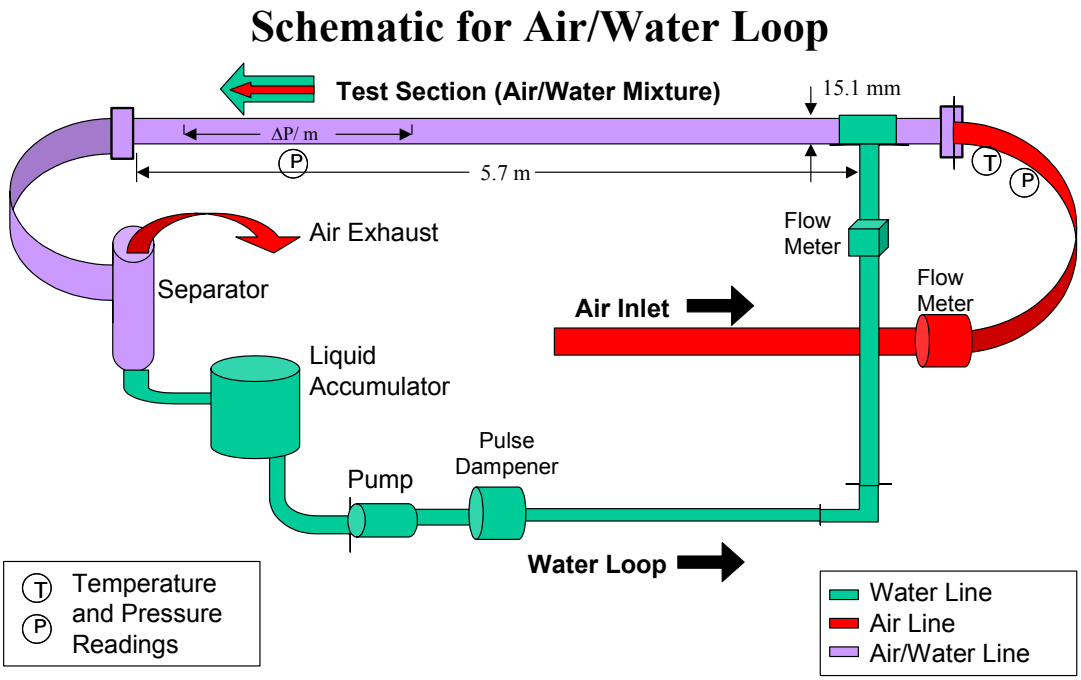

Figure 2.7: Schematic for air/water test facility.

Operation of Air/Water Facility

The air/water loop requires less explanation to use than the refrigerant test facility. Simply turn on the air by turning the valve located on the flow meter and set the flow rate by adjusting this valve. The water flow is activated and adjusted by turning on

the pump (be sure the pump tubing is clamped in the pump head) and adjusting the speed of the pump to adjust the flow rate. The air flow may need to be adjusted after the water begins to flow (just as in the refrigerant flow). Be sure that the liquid level in the liquid tank is high enough to prevent air bubbles being pumped through with the liquid. Add water if necessary. Also check that the pulse dampener is full of liquid after the liquid pump is turned on to prevent bubbles entering the liquid in this manner. Briefly turn the pulse dampener upside down to rid it of air bubbles. The tubing for the pump should be regularly changed, first by moving the pump to a different section, then by replacing the used tubing. The system should be allowed to run for a short time to achieve thermal equilibrium of the water and avoid evaporation. When shutting down the system, the liquid flow should always be shut down first and run in reverse to clear the liquid lines. The air flow should be left on till any liquid is dragged down and out of the test section. The air flow can then be shut off and any instrumentation can be turned off (i.e. differential pressure gauge).

The pressure differential across the test section could be measured over a one meter section or a two meter section. As in the refrigerant test facility valves controlled which measurement was taken. The pressure in the test section was measured at the location shown in Figure 2.7. The pressure of the incoming compressed air was also measured in order to adjust the density of the inlet air flow. The film thickness measurements and videos were taken in the same manner as the refrigerant data.

The flow conditions used in the air/water study can be seen in Table 2.5.

Table 2.5: Flow conditions used in air/water experiment.

Flow Conditions for Air-Water				
x	G_{tot}	KE_{air}	Q_{water}	Q_{air}
	kg/m^2-s	J/m^3	lpm	lpm
0.17	61.84	45.12	0.55	90
0.16	93.90	85.64	0.85	123
0.37	54.72	156.50	0.37	165
0.17	122.60	156.70	1.10	165
0.66	49.23	380.50	0.18	252
0.39	84.16	392.30	0.55	255
0.40	113.70	677.30	0.73	317
0.66	73.54	798.60	0.27	354
0.69	112.70	1752.00	0.37	481

Air/Oil Test Facility

In this work, a flow of dry air and soybean oil (density=920 kg/m^3, viscosity=0.047 kg/m-s) were used to study the behavior of immiscible vapor/liquid vertical annular systems. One of the purposes of studying this particular type of flow was to study the point of flow reversal that can occur in large vertical refrigerant risers. These systems can include oil that has escaped the compressor and therefore needs to be returned to the compressor. In this experiment, the air was used to simulate refrigerant vapor, and the soybean oil was used to simulate the liquid refrigerant mixed with oil.

The experimental apparatus featured a clear acrylic vertical 1.8-meter long test section (50.8 mm I.D. or 25.4 mm I.D.), as shown in Figure 2.8. Dry compressed air entered the test section at the lower end and flows upward. The oil inlet was also at the lower end; thereby, allowing the oil to mix with the air before entering the test section through a similar tee section as was described in the refrigerant experiment. The oil was pumped by a peristaltic pump into the perforated length of tubing inside the tee section (Figure 2.5) at the riser base. The oil flow was measured with a volumetric floating-ball flow meter. After exiting the test section, the air/oil mixture flowed into a separator of the same design as for the refrigerant system after which the air was vented to the lab

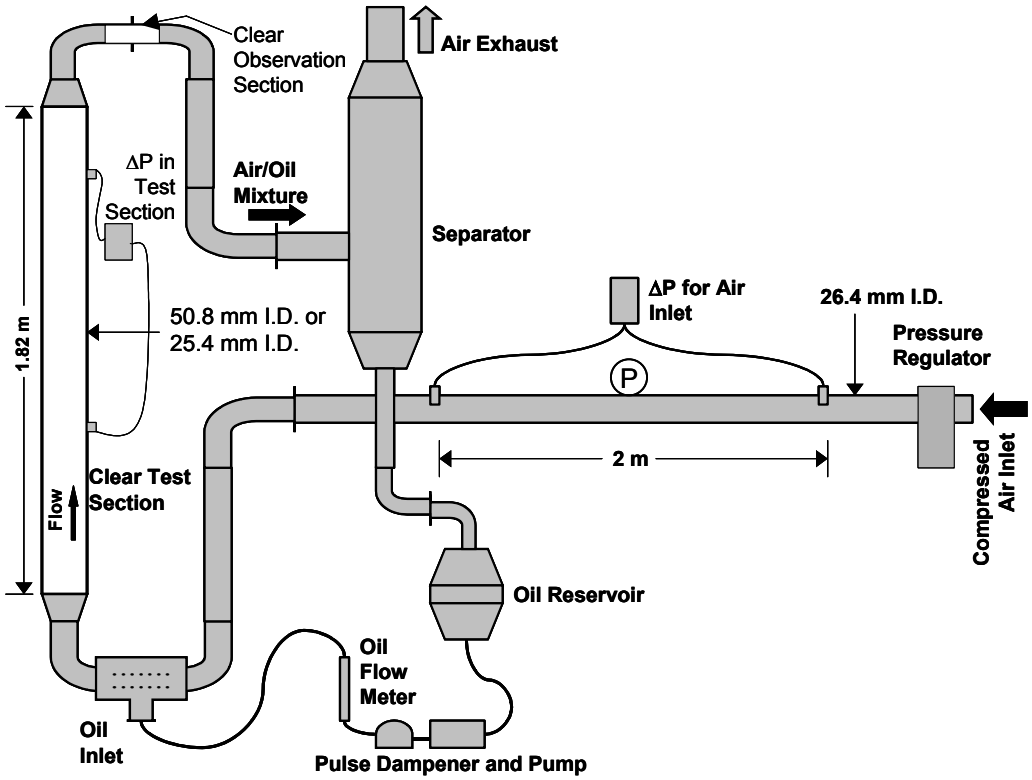

Figure 2.8: Schematic of air/oil test facility.

exhaust and the recovered oil fell by gravity into an oil reservoir. The separator was designed to use gravity, centrifugal effects, and a coalescing filter (or demister) to separate the oil from the air. The part numbers, accuracies (where applicable), and vendors of the parts and sensors used in this set up can be seen in Table 2.6a,b.

Table 2.6 (a, b): List of sensors (a) and parts (b) used in the air/oil test facility.

Sensors	Manufacturer	Part Number(s)	Range	Accuracies
Thermocouple (T-type)	Omega	TMQSS-125G-6	220^{O}C	±1.0^{O}C
Differential Pressure Transducer	Omega	PX2300-2DI	0-2 psig	±0.25% FS
Liquid Volumetric Flow Meter	Cole-Parmer (Gilmont)	A-03204-00	10-850 mL/min (water)	±2% FS
Digital Manometer (Air flow meter)	Grainger (Dwyer)	1W435 (475-2)	0-40 in H2O	±0.5% FS
Pressure Gauge	Grainger	4ZG17, 2C772	0-15 psig, 0-30 psig	±3-2-3%

Parts	Manufacturer	Part Number(s)
Liquid Pump	Cole-Parmer (Masterflex)	U-77200-62, EW-07553-70, EW-07596-20
Tygon LFL Pump Tubing	Cole-Parmer (Masterflex)	6430-24

The connections at either end of the test section were designed to accommodate different sized test sections and to attempt to have smooth transition regions. At the top of the test section, before the separator, a clear observation section was added to observe the amount of liquid flow that was being returned to the separator for each flow condition.

The volumetric flow rate of the inlet air was determined by measuring the pressure drop across a 2 m length of the entrance pipe. The Colebrook relation for turbulent friction factor is (Colebrook, 1938-39),

$$\frac{1}{f^{0.5}} = -2.0\log\left(\frac{e/D}{3.7} + \frac{2.51}{\mathrm{Re}\, f^{0.5}}\right), \tag{2.1}$$

where e is the wall roughness and D is the pipe diameter. The relation between pressure drop and friction factor is given by,

$$\Delta P = f\left(\frac{\rho U^2}{2}\right)\left(\frac{L}{D}\right), \tag{2.2}$$

where ΔP is the pressure drop and L is the distance between pressure taps. Equations 2.1 and 2.2, together with the definition of the Reynolds number, were solved simultaneously to provide the volume flow rate of air in the loop. The solving of these equations was simplified and automated by using the EES equation solver software package (F-Chart Software, 2002). The theoretical uncertainties in this method were estimated to be 3.1% (Rush et al., 1999); uncertainty analysis of the current experiment predicted an average uncertainty of ±0.00045 kg/s. Calibration to a NIST-traceable thermal volumetric flow meter (Thermal Systems Incorporated, used in R-123 facility) gave experimental agreement to within 5%.

The oil flow was regulated using a peristaltic pump and a pulse dampener. The oil volumetric flow meter was calibrated by measuring the time to fill a graduated cylinder with 160 ml of oil.

Pressure drop measurements were taken over a distance of one meter in the test section and were obtained with some difficulty. The difficulty in taking these measurements was due to the low surface tension of the oil and a pumping action that occurs with the flow of waves over the holes for the pressure taps. These two different effects sabotaged the first attempts at taking the pressure measurements. These included using regular pressure taps and air lines, using oil drains in these lines, using pressure snubbers, and using needles inserted into the pressure tap holes. These two effects combined caused oil to seep or be pushed into the pressure tap lines in all cases and effectively disrupt reliable pressure measurements. As the final solution, using methods described in Hewitt and Hall-Taylor (1970), the pressure tap lines were filled with oil and pressurized to maintain a constant, extremely slow flow rate to ensure that the lines did

not have any air pockets. The measurements were taken using the factory calibrated pressure transducer shown in Table 2.6a.

Film thickness measurements were taken using the optical method described in the refrigerant facility set-up. The average uncertainty of the film thickness measurement is ±0.034 mm.

Particle streak tracking was also used to investigate the flow patterns. Video clips were taken with the aid of a flashing a strobe light and a set of three different colored LED lights. The three different colors indicated flow direction, and the strobe light indicated the size of bubbles and waves. Individual frames of the video were analyzed for flow behavior and to obtain particle velocities.

Operation of Air/Oil Facility

The procedure for running the air/oil facility is very similar to that of the air/water facility. Before beginning, the desired air flows should be converted to a pressure drop using the aforementioned equations and EES program. First, turn on the air flow by turning on the pressure regulator and adjusting it to achieve the desired pressure drop reading (air flow) on the digital manometer. Now, the liquid flow can be activated. Check to be sure the pump tubing is clamped in the pump head. After turning on the pump, get most of the air out of the pulse dampener by turning it upside down for a short time. The oil flow should have very few bubbles in it. If the flow seems to be intermittent, check the oil level in the oil reservoir tank, add oil if necessary. The air flow may need to be adjusted slightly to reach the set point after turning on the oil flow. The oil flow rate is controlled using the pump speed adjustment. At each oil flow, the air flow was stepped down until flow reversal occurred. Flow reversal being the point at

which the majority of liquid is no longer flowing upward and appears to be stationary at the top of the tube. Pressure drop measurements, flow rates and film thickness data were taken at each flow setting. Videos of the flow using strobe lights and LED arrays were taken at several characteristic flow settings (shown in Table 2.7).

Table 2.7 (a, b): Flow conditions used in air/oil experiments in 25.4 mm tube (a) and 50.8 mm tube (b).

Flow Conditions for 25.4 mm Tube	
Oil Flow kg/s	Range of Air Flow kg/s
0.0003	0.004 - 0.017
0.0012	0.0038 - 0.021
0.0027	0.0041 - 0.021
0.0047	0.0036 - 0.022

Flow Conditions for 50.8 mm Tube	
Oil Flow kg/s	Range of Air Flow kg/s
0.00077	0.0233 - 0.0337
0.00188	0.02196 - 0.0340
0.0036	0.0208 - 0.03198
0.0058	0.01845 - 0.0323

After running the desired experiments, the system needs to be shut down. The liquid pump should be turned on in reverse to get as much oil into the oil storage tank. Shut off the pump when the oil is sufficiently drained. The air flow should be left on until all oil is out of the test section, then the pressure regulator can be shut off as well.

Conclusions/Recommendations

There were three facilities used in this study of the effect of altering the fluid properties from those of air and water. For the first experiment, a low-pressure refrigerant facility was constructed to have an identical test section to an already existing air/water facility. After operating the R-123 test facility in the current configuration, several improvements became obvious.

- The liquid tank needs a system to cool it during shut down and during experiments. The ability to cool the tank during experiments allows the liquid tank to draw liquid into it to make up for any lost liquid that gets drawn into

the heat exchanger (coldest point) and sent to the vapor tank. The cooling system would also be useful during a vacuuming down of the system.

- A vacuum port should be added to the top of the liquid tank for purging and filling of the tank.
- The welding done on the vapor tank caused several large leaks to occur. The vapor tank will need to be re-designed and re-made to eliminate these leaks entirely. A smaller sized tank would be more efficient as well (less refrigerant charge needed).

For the second experiment, an air/oil vertical facility was constructed to investigate the effect of changing the liquid properties on the flow reversal point. Suggested improvements to this facility include:

- Using a liquid flow meter more suited to use with a viscous flow
- Adding a pressure tap in the test section to obtain the actual pressure in the test section
- Making the inlet and outlet of the test section smoother transitions.

Nomenclature

D – inner pipe diameter	[m]
e – wall roughness	[m]
f – smooth tube friction factor	[--]
L – length of pipe (general)	[m]
Re – Reynolds number based on pipe diameter (general)	[--]
U – velocity (general)	[m/s]

Greek Variables

ΔP – pressure drop (general)	[Pa]
ρ – density (general)	[kg/m^3]

References

Dupont, Inc.: R-123 MSDS, http://www.dupont.com/suva/na/usa/literature/pdf/h42443_4.pdf, 2003.

F-Chart Software: Engineering Equation Solver (EES). *www.fchart.com*, 2002.

Hewitt, G. F. and N. S. Hall-Taylor, *Annular Two-phase Flow*. Pergamon Press, Oxford, 274-276, 1970.

Shedd, T. A. and T.A. Newell, "Automated optical liquid film thickness measurement method." *Review of Scientific Instruments,* **69**(12): 4205-4213, 1998.

3. Comparison of R-123 Flow Behavior to Air/Water Flow Behavior for Horizontal Flow

Introduction

In the current literature, there is a large amount of data on air/water mixtures in horizontal flow that collectively contributes to the understanding of horizontal two-phase flow. However, the flow behavior of refrigerants and other pure two-phase mixtures is of much greater interest in many applications. Currently, there is very little detailed data in the literature about pure refrigerant adiabatic two-phase flow behavior. In most cases, the refrigerant data obtained were not directly compared to a similar test set-up for air/water. Thus, uncertainty exists in the validity of air/water data as a basis for drawing conclusions about expected two-phase flow behavior in refrigeration system applications.

In order to utilize air/water data in other two-phase flows, it has been hypothesized that equating the kinetic energy of the refrigerant vapor to the kinetic energy of the air can effectively relate those results to pure component refrigerant data. The work of Zietlow and Peterson (1998) equates the kinetic energies of the air and refrigerant vapor to determine the equivalent velocity of air that will produce a similar type of flow behavior (regime) using Equation 3.1.

$$j_{air} = \left(\frac{\rho_g}{\rho_{air}} \right)^{0.5} j_g \tag{3.1}$$

The vapor kinetic energy is defined using the superficial gas velocity. This equation was used in this work to find the air flows with vapor kinetic energies equivalent to those in the refrigerant flows. The model used in this work agreed well with other experimental results, but they did not experimentally validate the concept of equating the vapor kinetic energies.

The pressure drop is related to kinetic energy through consideration of fundamental flow physics. The fundamental relation for two-phase annular flow pressure gradient according to Wallis (1969) (Equation 3.2) indicates that the kinetic energy of the vapor dominates the mechanics of annular flow.

$$-dP/dz = f_{TP}\left(\frac{\rho_g j_g^{\,2}}{2}\right)\left(1+\left(\frac{G_f}{G_g}\right)\right)\frac{4}{D} \tag{3.2}$$

The first term in parenthesis is the vapor kinetic energy term, and G_f and G_g are the liquid and gas-phase mass fluxes, respectively, and f_{TP} is the two-phase coefficient of friction. Equation 3.2, derived for adiabatic two-phase flow, predicts that different fluids at equivalent vapor kinetic energies should have comparable pressure drops and flow regimes.

A primary purpose of the present experimental effort was to determine whether vapor kinetic energy can be used to relate the behavior of different fluids. This work describes experiments performed to compare air/water and refrigerant (R-123) two-phase flow at equivalent vapor kinetic energies. Both flows were run in identical, horizontal, adiabatic test sections, isolating the mechanical properties of the flows. The pressure drop across the test section was measured, as well as the flow rates, fluid pressure and temperature, and the liquid film thickness distribution. Flow regimes were documented using strobed video.

Experimental Methods

R-123 Test Set-up

The R-123 test apparatus included a 5.7-meter long, insulated, horizontal test section made of clear PVC with an inside diameter of 15.1 mm. The test apparatus had the capability of controlling mixture quality at the test section inlet by managing liquid and

vapor flow through two separate circulating paths. A separator was placed at the end of the test section to insure that the vapor and liquid phases remained within their individual paths outside of the test section (see Figure 3.1). The vapor was generated in the evaporator tank by boiling liquid refrigerant from heat addition provided by three 5 kW heaters. The vapor generation was controlled with a software-based PID controller using the measured vapor flow rate as the feedback for the controller. The liquid flow rate was controlled using a variable-speed peristaltic pump and measured with a Coriolis flow meter with an accuracy of 0.01 L/min. Using separate flow paths for liquid and vapor allowed the quality and mass flux to be controlled at any desired value within the operating range.

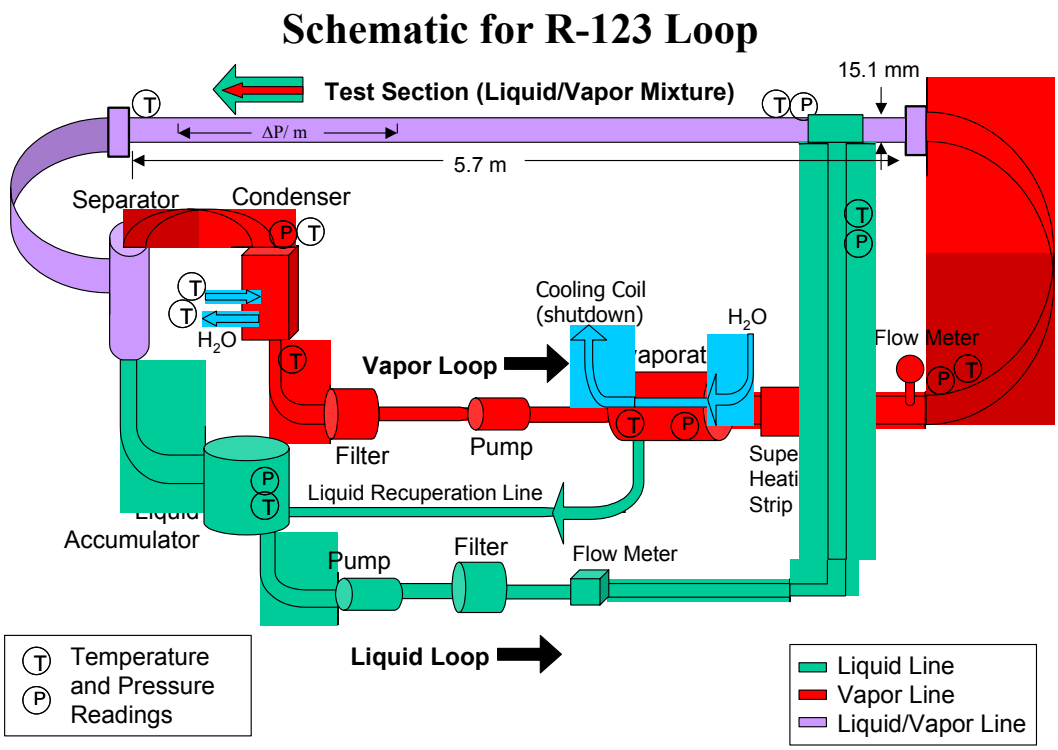

Figure 3.1: Schematic for R-123 test facility.

The nine flow conditions listed in Table 3.1 were studied in this experiment. These flow conditions were combinations of three different qualities (x) (approximately 0.20, 0.45, and 0.72) and three different total mass flux rates (G_{tot}) (approximately 90, 135, and 185 kg/s-m^2).

Table 3.1: Flow conditions used in R-123 experiment.

Flow Conditions for R123				
x	G_{tot}	KE_{vapor}	Q_{liquid}	Q_{vapor}
	kg/m^2-s	J/m^3	lpm	lpm
0.23	100.00	48.38	0.56	46
0.21	145.00	85.23	0.84	61
0.45	90.72	150.50	0.37	80
0.21	190.50	152.10	1.09	81
0.71	84.14	329.80	0.18	120
0.45	135.20	335.00	0.54	119
0.46	182.80	626.10	0.72	160
0.72	132.30	789.30	0.27	179
0.73	184.70	1509.00	0.36	240

The pressure and temperature of the refrigerant were measured at the sites indicated by T and P in Figure 3.1. The pressure was measured using absolute pressure transducers with an accuracy of 863 Pa, a gauge pressure transducer with an accuracy of 1.34 psig, and a differential pressure transducer with an accuracy of 34 Pa. Temperatures were measured with T-type thermocouples that have an accuracy of ±1^{o}C. The thermocouples have been calibrated in an ice bath to within 0.1^{o}C.

Air/water Test Set-up

The air/water test apparatus included a 5.7-meter long, clear horizontal test section with an inside diameter of 15.1 mm. The tubing materials of construction were identical to that used in the R-123 test section. This test apparatus consisted of two separate paths for the water and the air. The water was circulated from the test section through the liquid path using a peristaltic pump and variable area flow meter with an accuracy of 0.084 lpm. The air was supplied through a compressed air line and flowed into the test section and separator and then into the room. The air flow was measured by a set of variable area flow meters, with accuracies of 7.5 lpm and 24 lpm. Pressure and

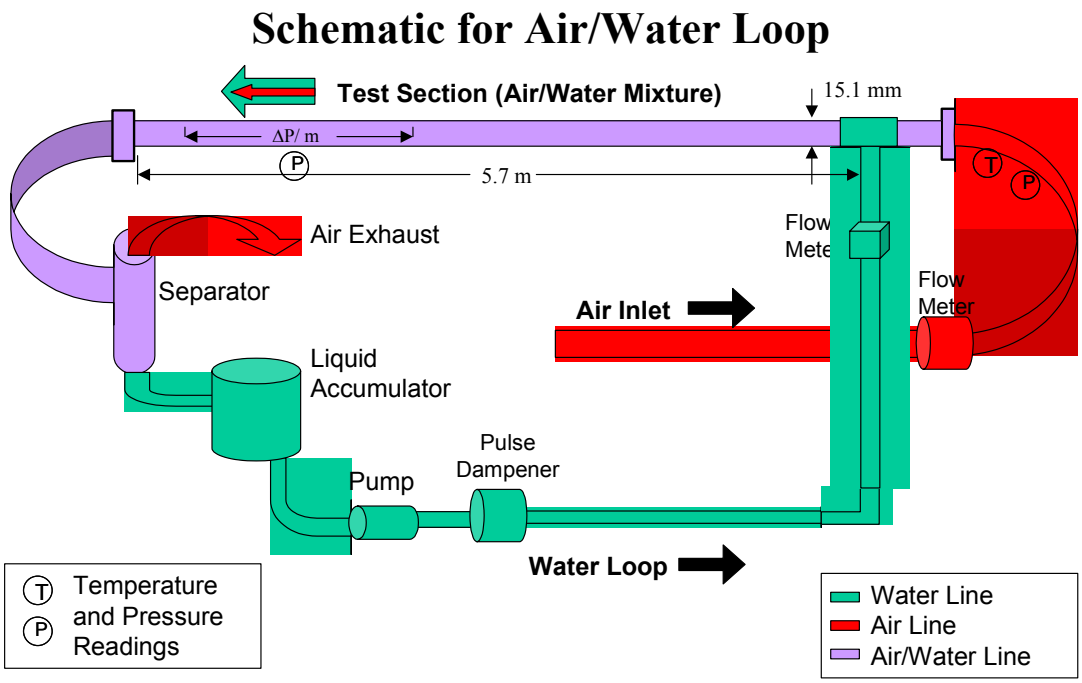

Figure 3.2: Schematic of air/water test facility.

temperature measurements were obtained for each flow condition at the points indicated in Figure 3.2. The digital differential pressure gauge, with an accuracy of 50 Pa, was verified using a U-tube manometer. Temperatures were measured with T-type thermocouples having an accuracy of ±1°C and calibrated in the same manner as in the R-123 experiment. The nine flow conditions listed in Table 3.2 were intended to match the air and refrigerant vapor kinetic energy (see Eqn 3.1) while keeping the liquid volumetric flow rates equal between the fluid pairs. This resulted in a different inlet quality for the R-123 flows. The air/water flow conditions were combinations of three

Table 3.2: Flow conditions used in air/water experiment.

Flow Conditions for Air-Water				
x	**G_{tot}**	**KE_{air}**	**Q_{water}**	**Q_{air}**
	kg/m^2-s	**J/m^3**	**lpm**	**lpm**
0.17	61.84	45.12	0.55	90
0.16	93.90	85.64	0.85	123
0.37	54.72	156.50	0.37	165
0.17	122.60	156.70	1.10	165
0.66	49.23	380.50	0.18	252
0.39	84.16	392.30	0.55	255
0.40	113.70	677.30	0.73	317
0.66	73.54	798.60	0.27	354
0.69	112.70	1752.00	0.37	481

different qualities (x) (approximately 0.16, 0.39, and 0.67) and three different total mass flux rates (G_{tot}) (approximately 55, 85, and 115 kg/s-m^2).

Verification of Test Facilities

The differential pressure transducer and the vapor flow meter were validated by running vapor only through the test section and recording pressure drop data. The single-phase friction factor was calculated using the measured volumetric flow rate and pressure drop, and the definition of friction factor given in Eqn. 3.3.

$$\Delta P = f\left(\frac{\rho U^2}{2}\right)\frac{L}{D} \tag{3.3}$$

The desired adiabatic conditions were verified by finding the thermodynamic mass quality at the inlet and outlet of the test section and comparing the two. For the largest temperature difference, the two values were within approximately 3% of one another, which was within the error of the temperature measurements.

The smooth tube friction factor for laminar and turbulent flows was calculated using the Colebrook equation (Colebrook, 1938-39) for turbulent flows. Figure 3.3 shows good agreement between the calculated friction factor and the measured friction factor, which validated the experimental set-up for both R-123 and air/water.

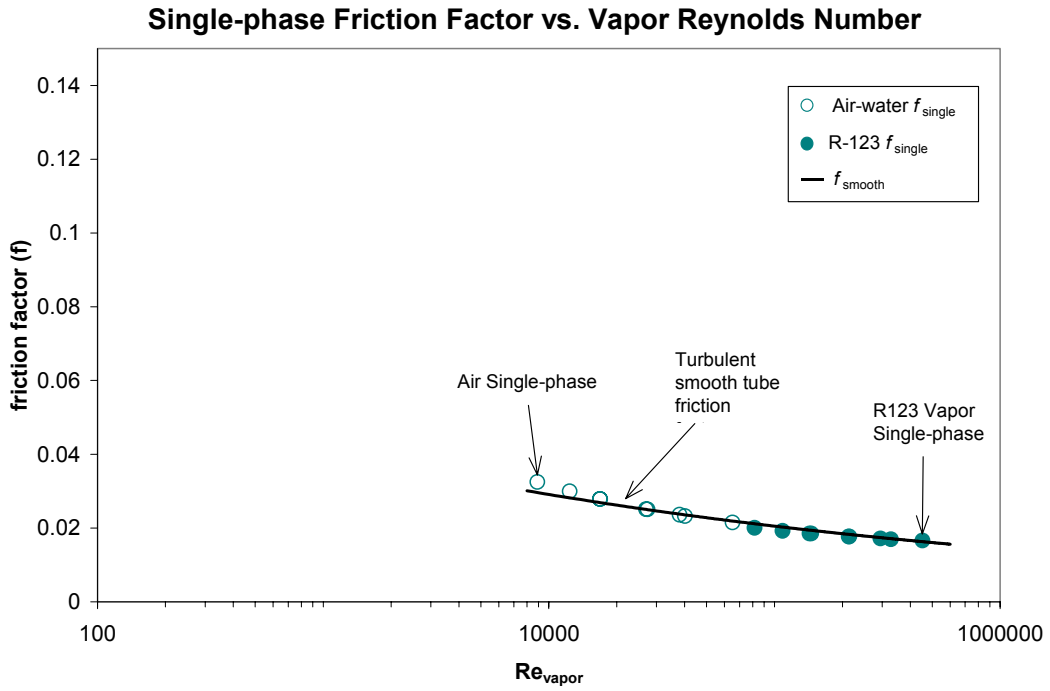

Figure 3.3: Verification of R-123 test facility by running single phase vapor and comparing against the Colebrook equation.

Film Thickness Measurement Set-Up

Film thickness measurements were obtained using an optical method (Shedd and Newell, 1998). This optical measurement method involved illuminating the pipe wall and liquid film with a small circular light source (such as a light emitting diode, or LED). The light was refracted and reflected by the liquid film, creating a ring of light on the pipe wall. The diameter of the reflected light ring was proportional to the thickness of the liquid film. Using geometry and the indices of refraction for the pipe wall and the liquid, the film thickness was determined. Uncertainties typically ranged from 9% for very wavy films to less than 0.1% for smoother conditions.

Results

Flow visualization

The images shown in Figure 3.4a-3.4f gave a comparison of the flow behavior. The air/water flows shown were for a total mass flux of approximately 85 kg/s-m^2 at each of the qualities for air/water. The R-123 flows shown were for a total mass flux of approximately 140 kg/s-m^2 at each of the three qualities. The picture of the low quality flow for air/water (Fig. 3.4a) shows a wave on the far right and basically wavy flow on the left of the picture, with no wetting at the top of the tube. The picture of the low quality flow for R-123 (Fig. 3.4d) shows a wave on the far right and wavy flow on the left of the picture with slight wetting of the top of the tube. The pictures of the mid-range quality flows (Fig. 3.4b, 3.4e) show wavy-annular flow with the surface being very rippled and wavy, where the air/water flow has much larger waves (in height and width). The high quality flows (Fig. 3.4c, 3.4f) show annular flow for both flows with a smoother surface than the mid-range quality flows that

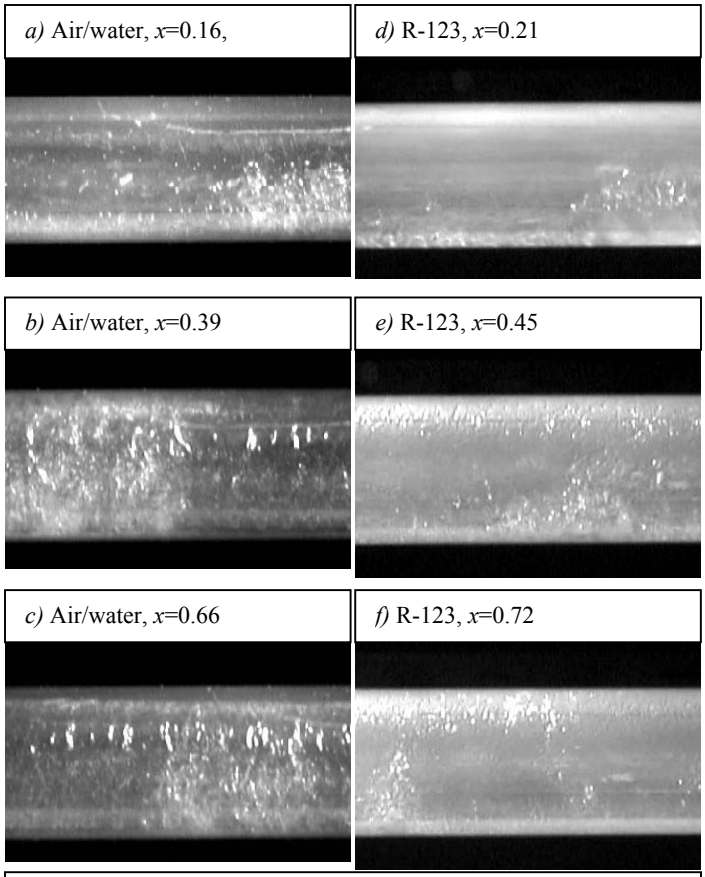

Figure 3.4: Typical appearance of flow for air/water at G~80 kg/m^2-s (a-c) and R-123 at G~135 kg/m^2-s (d-f) at different qualities.

is interrupted by intermittent disturbance waves, where the air/water flow again has larger waves.

Generally, the waves in the R-123 flows were much smaller (both in width and height) and smoother looking as can be seen in Figures 3.4a-3.4f. The waves in the air/water flows appeared to be more broken-up and choppier. The rate of entrainment of droplets appeared to be higher in the R-123 flows as evidenced by the appearance of droplets crossing a laser beam directed through the test section. Also, the walls were more easily wetted by the R-123 flows even at lower vapor flow rates.

Pressure drop

For a given vapor kinetic energy, the measured pressure drop in the R-123 flows was always slightly higher than in the air/water flows. The data points can be seen in Figure 3.5 and are grouped into similar qualities for both the R-123 flows and the air/water flows. The uncertainty in the measurements is shown in Figure 3.5 as well. As can be seen there was some overlap due to the uncertainty in the measurements, but there was a significant difference between the R-123 and air/water pressure drop, especially noticeable in the mid-range quality.

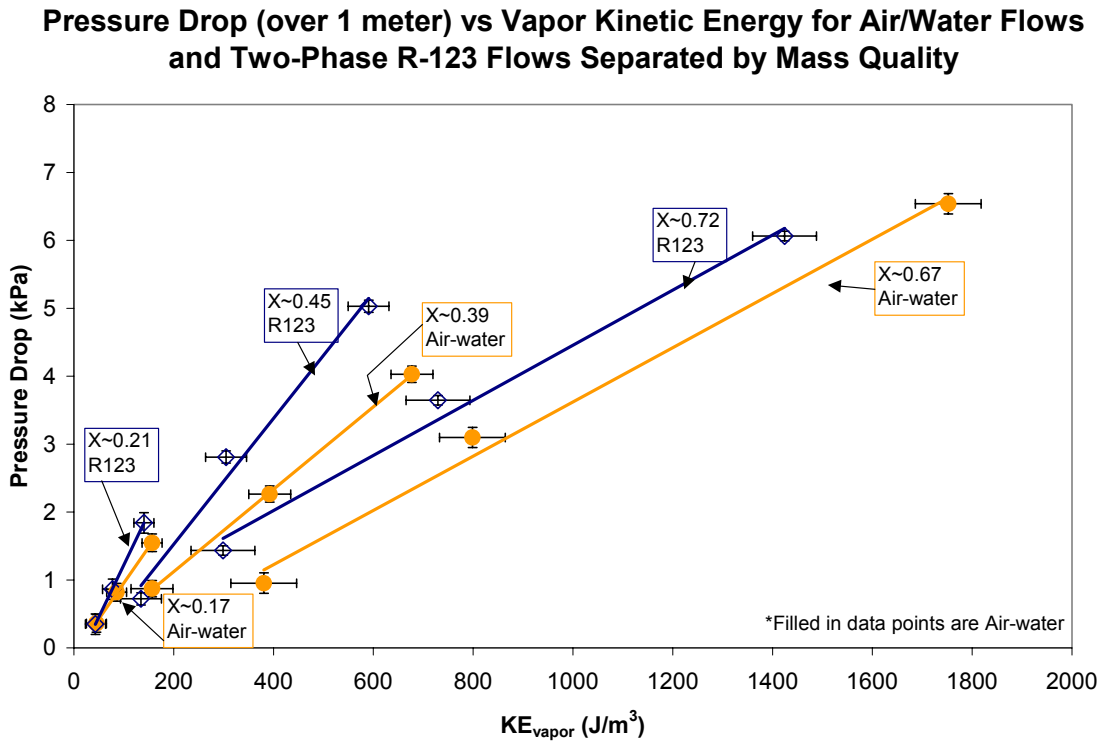

Figure 3.5: Pressure drop data for air/water and R-123 separated by quality.

Film thickness

The film thickness measurements were obtained in three different positions circumferentially around the tube: top, side, and bottom. The film thickness measurements were averaged over 30 second time intervals and can be seen in Figure 3.6. The trends for the side and bottom thicknesses were similar. The data points that fall under 0.01 mm film thickness (top thicknesses) were considered to be dry out conditions.

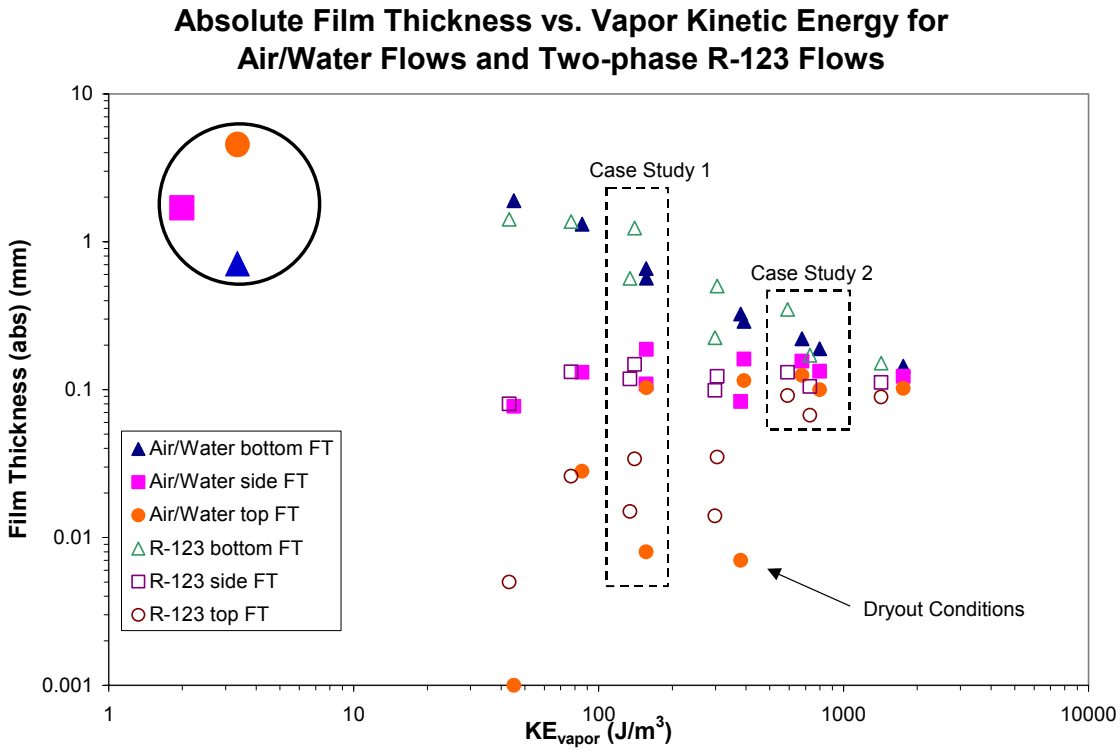

Figure 3.6: Film thickness data for air/water and R-123 flows separated into top, side, and bottom measurements.

Discussion

Flow visualization

The overall flow regimes of air/water flows and R-123 flows were approximately the same at equivalent vapor kinetic energies as shown in Figure 3.7, with increased wetting of the tube by the R-123. The increased wetting ability of the liquid R-123 compared with water could be due to several factors. The significant amount of entrainment of droplets in R-123 may have a large impact on the wetting of the tube. Other factors include the lower surface tension of R-123 as well as the different interactions between the liquid and the PVC. According to Jepson et al. (1990), as the surface tension (stabilizing force) decreases, more entrainment will result at a constant gas velocity. This would indicate that the lower surface tension aids in the wetting

process by encouraging droplet formation. Also, Williams (1990) found in air/water that entrainment does not become important/significant until the tube diameter is greater than three inches. The greater amount of entrainment observed in the R-123 flows may show a large shift in this behavior compared with air/water.

As shown in Figure 3.7, the higher kinetic energy flows were annular with disturbance waves. The annular dry out flow (at KE = 350 J/m^3) was a result of the combination of having too little liquid and not enough energy in the vapor to maintain an annular film, whereas, at the same kinetic energy and a lower quality, the flow was annular and could maintain a liquid film along the wall. At a kinetic energy of about 175 J/m^3 in Figure 3.7 there were two different flow regimes apparent, which was also due to the amount of liquid and the amount of energy required for maintaining a liquid film on the wall. The higher quality flows have less liquid but are at an equal vapor kinetic energy as the lower quality flows. This is suggestive of a minimum film thickness at each vapor kinetic energy.

The R-123 exhibited different types of waves than were seen in the air/water flows at equal vapor kinetic energies (which resulted in different vapor Reynolds numbers, see Figure 3.5). It has been observed that, in order for the air/water flows to exhibit the smoother, smaller type of waves seen in the R-123 flows, the air flow would need to be increased (resulting in even higher Reynolds numbers). This could be due to the lower viscosity and surface tension of the liquid R-123, allowing the liquid film to become turbulent at lower vapor Reynolds numbers. Fukano and Furukawa (1998) studied the effect of changing the liquid kinematic viscosity on the behavior of the liquid film and waves in equal flow conditions. The critical finding was that the higher liquid viscosity

tended to dampen out the waves causing smaller waves and lower frequencies of these waves to be more common in these fluids. In this experiment, the opposite occurred. However, R-123 has lower viscosity than water, whereas Fukano and Furukawa studied fluids with higher viscosity than water. Another possible explanation for the air/water flows having larger waves (or more mass in the waves) than the R-123 was that the air/water flows have less entrainment of liquid droplets in the vapor core than the R-123 flows.

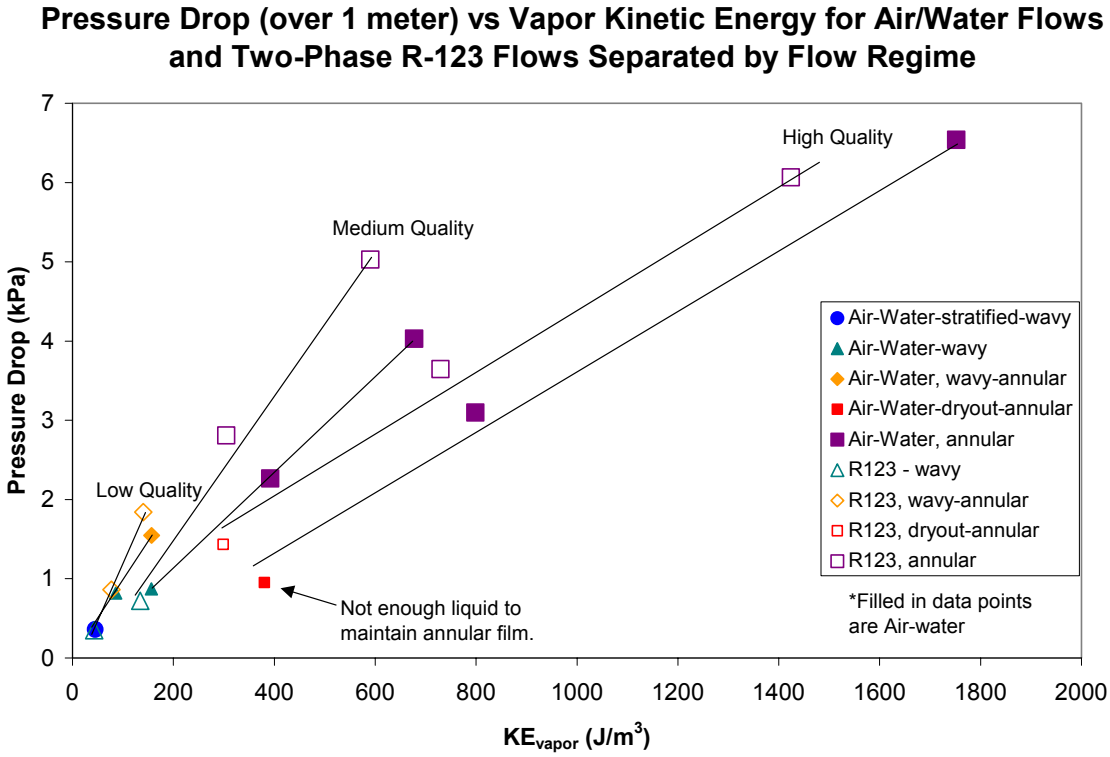

Figure 3.7: Pressure drop data for air/water and R-123 separated by quality and flow regime.

Pressure drop

As seen in Figure 3.5, using the vapor kinetic energy produced a strong correlation for both the air/water and R-123 pressure drop data. The higher pressure drop in the R-123 flows could be due to a greater amount of liquid entrainment in the vapor flow,

resulting in a vapor with a higher mean density. In addition, the liquid flow rate was kept constant between the flows, ignoring the large differences in the densities and viscosities of the two liquids.

Fukano and Furukawa (1998) predicted the two-phase pressure drop in vertical flow using an interfacial friction factor calculated from density and viscosity and using a correlation for film thickness. They used this for several fluids with different viscosity and density (and a nearly constant surface tension). This correlation was referenced to the properties of water and the fluids chosen to study all had higher kinematic viscosities than water, unlike R-123. This correlation was used on the data from the current experiments to see if the calculated pressure drop, using both the correlation for film thickness and measured film thickness, approximated the measured pressure drop. The calculated pressure drop for R-123 (using the correlation for film thickness) correlated well with the measured pressure drop. However, the calculated pressure drop for the air/water data appeared to be slightly offset from the measured pressure drop data. For both cases, the calculated pressure drop (using the measured average film thickness) over-predicted the pressure drop. The success of this correlation was surprising due to the fact that it was intended for use with vertical systems, not horizontal.

Figure 3.8 shows the friction factor plotted against the vapor Reynolds number. The square data points are found using the measured two-phase pressure drop, the measured vapor kinetic energy, and Equation 3.3 to find the two-phase friction factor (f_{TP}) for air/water and R-123. The two-phase friction factor was grouped by different qualities for both air/water and R-123 flows. The two-phase friction factor was greater than the single-phase friction factor and tended to increase with increasing Reynolds number.

This trend agreed with the behavior predicted by the Wallis two-phase friction factor shown in Equation 3.2 (Wallis, 1969). The friction factor for the air/water flows and the R-123 flows were in the same range for the low, medium, and high qualities, respectively. Also, the vapor Reynolds number was shown here to be a poor correlation factor between fluid flows.

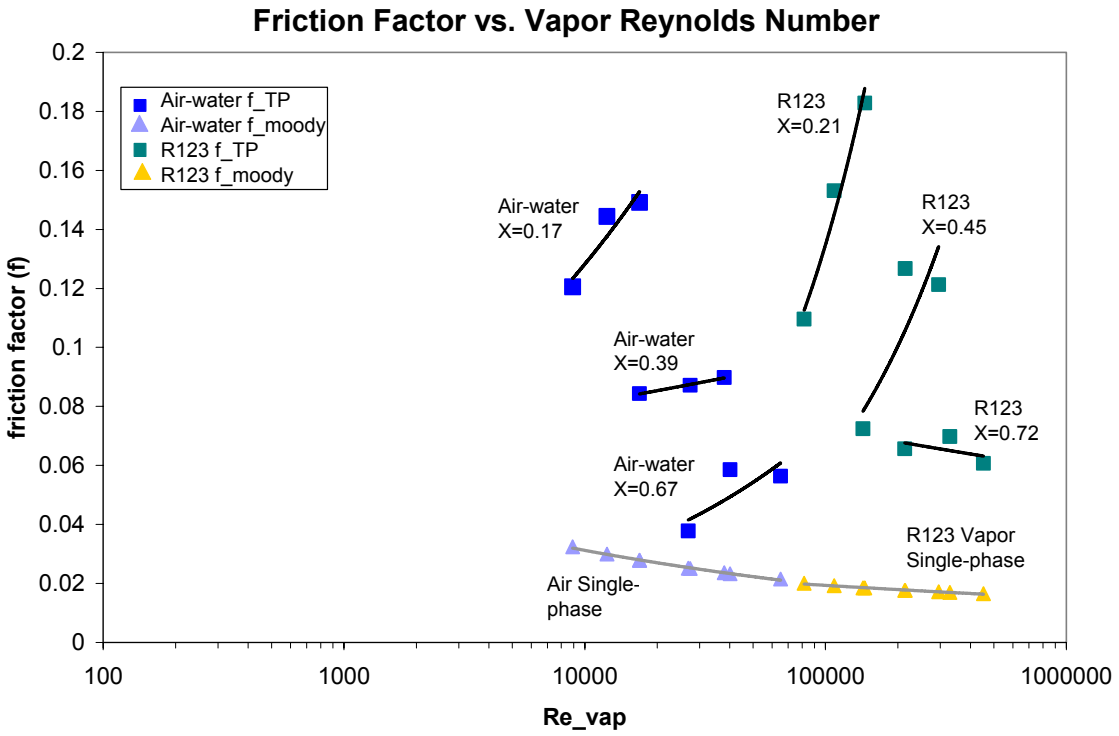

Figure 3.8: Two-phase friction factor versus the vapor Reynolds number for air/water and R-123 flows separated by quality.

As shown in Figure 3.8, there was a large spreading occurring in the friction factors for each quality set and each fluid type. In order to try to explain this, the flows were also separated by flow regime on a similar graph to compare changes in flow regime and large changes in friction factor (see Figure 3.9). There were changes in flow regime within each quality grouping, but there was not enough data to make a conclusion on the effect this would have on friction factor.

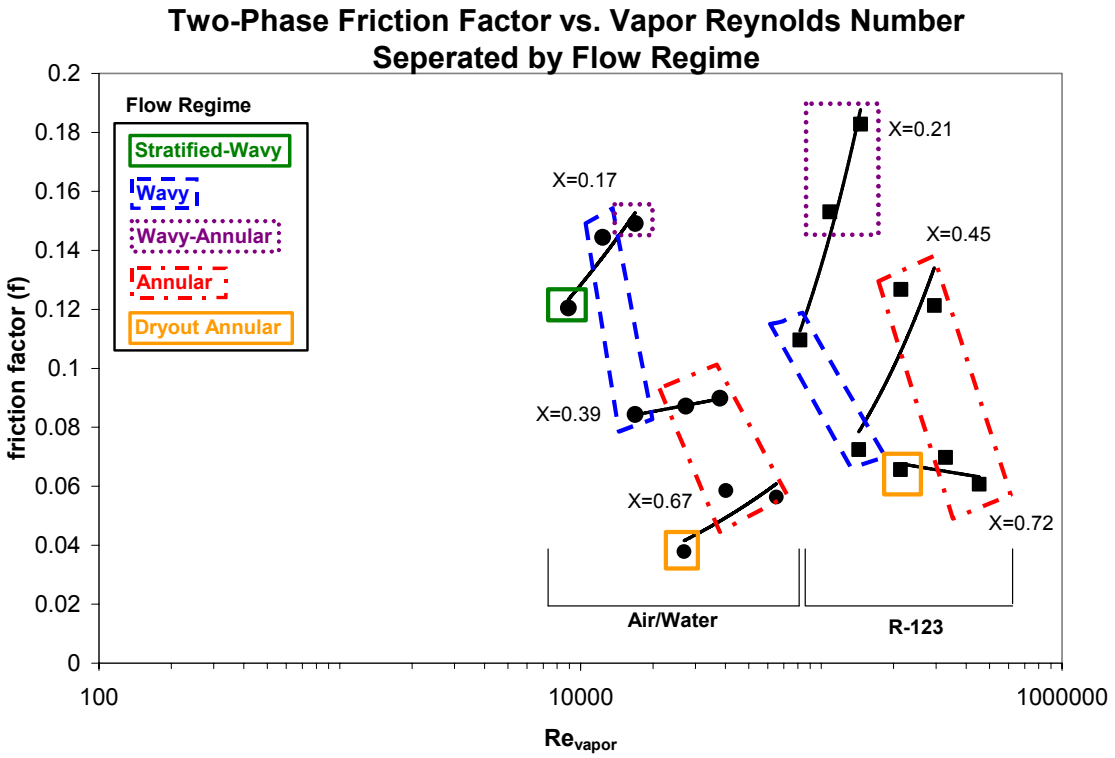

Figure 3.9: Two-phase friction factor versus the vapor Reynolds number for air/water and R-123 flows separated by quality and flow regime.

Film thickness

As shown in Figure 3.6, the film thickness measurements for the water and liquid R-123 showed good agreement at similar vapor kinetic energy outside of dryout conditions. The bottom film thickness displayed a downward trend as vapor kinetic energy increased. The side film thickness stayed relatively constant with increasing vapor kinetic energy. The top film thickness increased as vapor kinetic energy increased. This was to be expected, as the flow regime changed to annular when the vapor kinetic energy increased, causing a more uniform film around the tube.

The better wetting ability of R-123 was demonstrated by the smaller number of top film thickness data points that could be considered to be dry out conditions. Taking a closer look at the boxed data points in Figure 3.6 labeled ‘Case Study 1’ gave the

information in Figure 3.10. There were two flows with different qualities, but identical average vapor kinetic energy of 152 J/m^3. This meant that the vapor flow rate remained constant and the liquid flow rate was increased to obtain a lower quality. The flow regimes were the same for the air/water and R-123 at the similar qualities. However, as more liquid was added to each flow, it was important to note the changes in the film thicknesses at each location for each flow (see Figure 3.10).

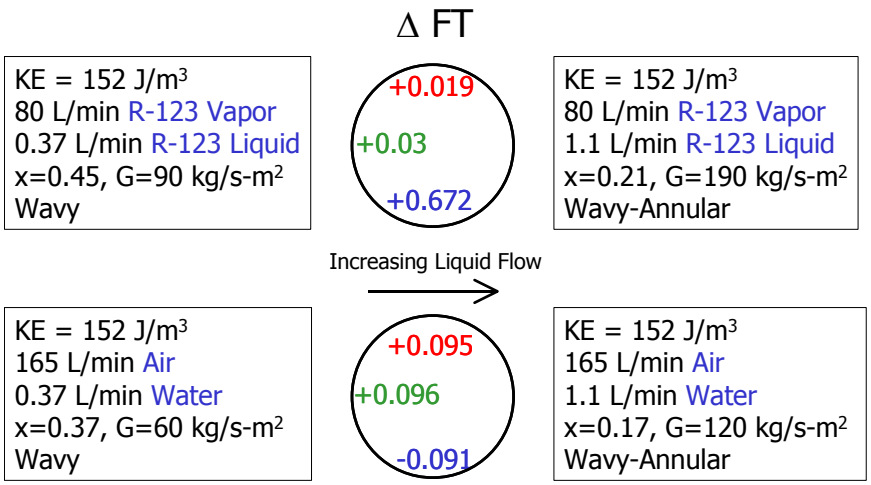

Figure 3.10: Details of four flows at approximately equal kinetic energy; increasing liquid flow in both R-123 flows and air/water.

In the case of adding liquid to the air/water flow (at equal vapor kinetic energy) the bottom film thickness actually decreased, while the side and top film thickness both increased by about 0.095 mm. In the case of adding liquid to the R-123 flow (at equal vapor kinetic energy) the bottom film thickness nearly doubled while the side and top film thickness had minimal additions. This behavior was explained by the difference in the densities of the water and the liquid R-123. Gravity acted on the denser refrigerant causing it to be harder to push up the walls of the tube. This allowed the water to form a more uniform film than the refrigerant. By looking at the boxed data points labeled 'Case Study 2' in Figure 3.6 at a higher flow rate, it could be seen that the film thickness

changed very little for both fluids when increasing the liquid flow at a nearly constant vapor kinetic energy. This suggested that there are two different behaviors occurring. It appeared that at the lower flow rates a gravity term was needed to fully describe the flow behavior along with the vapor kinetic energy term, whereas at the higher flows the vapor kinetic energy appeared to capture the behavior. This finding was supported by the work of Fukano and Ousaka (1989), who found that for a lower gas flow rate, gravity becomes the controlling term in the film thickness distribution. They also found that in the higher gas flow rates the stronger effect is due to the interfacial shear stress (or vapor kinetic energy).

Several attempts have been made to factor in the gravitational term. First, with some preliminary calculations, it appeared that a better correlation of both data sets could be obtained by including a gravitational effect in the form of the Froude rate as is done in Hurlburt and Newell (2000). However, the constants that were used in this correlation were dependent on the type of fluid used (air/water), and the correlation has, therefore, not been adjusted to many other fluids. The second attempt was to divide the measured pressure drop by the liquid density and to plot this against the vapor kinetic energy (see Figure 3.11). This appeared to capture the gravitational effect seen in the lower flow rates. And, as was expected in the range more greatly affected by the interfacial shear stress, this density term did not correlate the high kinetic energy data.

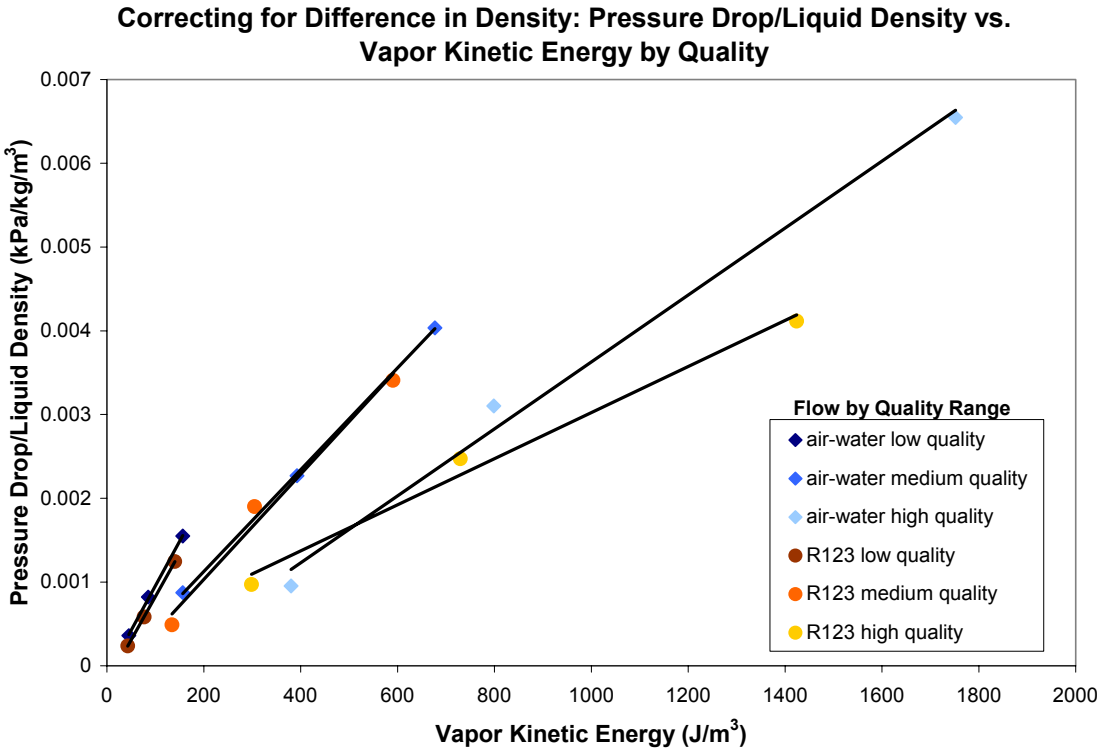

Figure 3.11: Using liquid density to include a gravity effect at low quality flows.

Conclusions

A unique experiment has been performed in which air/water and pure R-123 two-phase flows at equivalent vapor kinetic energies and in identical test sections were compared. The major findings were:

- Air/water and R-123 flows have approximately the same flow regimes at equal vapor kinetic energies, though with different wave behavior.
- Pressure drop was found to correlate well with vapor kinetic energy, though the R-123 measurements are consistently higher than the air/water data.
- There appeared to be two different behaviors for the low and high kinetic energy flows, with the low being dominated by a vapor kinetic energy term and a gravity term

and the high by an interfacial shear stress term, which was also noted by Fukano and Ousaka (1989).

- Although side film thickness measurements were nearly the same for both fluid pairs there appeared to be a delay in the transition to fully annular flow in the R-123 due to the effects of increased density.

Acknowledgments

The author appreciates the financial support for this project provided by the University of Wisconsin-Madison and the National Science Foundation under award number CTS-0134510.

Nomenclature

D	inside tube diameter	[m]
dP/dz	pressure drop per unit length	[Pa/m]
f	friction factor	[--]
f_{moody}	single phase friction factor	[--]
f_{TP}	two-phase friction factor	[--]
g	gravitational acceleration	[m/s^2]
G_f	liquid mass flux	[kg/s-m^2]
G_g	vapor mass flux	[kg/s-m^2]
G_{tot}	liquid and vapor mass flux	[kg/s-m^2]
j_{air}	superficial air velocity	[m/s]
j_g	superficial gas velocity	[m/s]
KE_{air}	kinetic energy of air	[J/m^3]
KE_{vapor}	vapor kinetic energy	[J/m^3]
L	length	[m]
Q_{air}	volume flow rate of air	[l/min]
Q_{liquid}	volume flow rate of R-123 liquid	[l/min]
Q_{vopor}	volume flow rate of R-123 vapor	[l/min]
Q_{water}	volume flow rate of water	[l/min]
U	velocity	[m/s]
x	mass quality	[--]

Greek Variables

ΔP	pressure drop	[Pa]
ρ	density	[kg/m^3]
ρ_g	vapor density	[kg/m^3]
ρ_{air}	air density	[kg/m^3]

References

Colebrook, C. F., "Turbulent Flow in pipes, with particular reference to the transition region between the smooth and the rough pipe laws." *Journal of the Institution of Civil Engineers,* **11**: 133-156, 1938-39.

F-Chart Software: Engineering Equation Solver (EES). www.fchart.com, 2002.

Fukano, T. and T. Furukawa, "Prediction of the effects of liquid viscosity on interfacial shear stress and frictional pressure drop in vertical upward gas-liquid annular flow." *International Journal of Multiphase Flow*, **24**(4): 587-603, 1998.

Fukano, T. and A. Ousaka, "Prediction of the circumferential distribution of film thickness in horizontal and near-horizontal gas-liquid annular flows." *International Journal of Multiphase Flow,* **24**(4), 587-603, 1989.

Hurlburt, E. T. and T. A. Newell, "Prediction of the circumferential film thickness distribution in horizontal annular gas-liquid flow." *ASME Transactions,* **122**: 396-402, 2000.

Jepson, D. M., B. J. Azzopardi, and P. B. Whalley, "The effect of physical properties on drop size in annular flow." *Heat Transfer 1990: Proceedings of the Ninth International Heat Transfer Conference,* **6**: 95-100, 1990.

Shedd, T. A. and T.A. Newell, "Automated optical liquid film thickness measurement method." *Review of Scientific Instruments,* **69**(12): 4205-4213, 1998.

Wallis, G.B., *One-Dimensional Two-phase Flow*. McGraw-Hill, New York, 1969.

Williams, L. R., "Effect of pipe diameter on horizontal annular two-phase flow." Ph.D. Thesis, University of Illinois at Urbana-Champaign, Urbana, Illinois, 1990.

Zietlow, D. C. and C.O. Peterson, "Flow regime mapping and analysis of R-134a in a small-channel cross-flow condenser." *ASHRAE Transactions,* **104**(2): 540-547, 1998.

The method for determining this uncertainty propagation is described in NIST Technical Note 1297 (Taylor B.N. and Kuyatt, C.E., Guidelines for Evaluating and Expressing the Uncertainty of NIST Measurement Results, National Institute of Standards and Technology Technical Note 1297, 1994). F-Chart Software

4. Oil Film Behavior Near the Onset of Flow Reversal in Immiscible Gas/liquid Vertical Annular Flow

Introduction

The study of viscous flows is important due to the oil that can be entrained in refrigerants (much less viscous fluids) during normal operation of a refrigeration system. The refrigerant will often boil off and leave behind a viscous oil film that must be transported through the system and returned to the compressor.

Oil is used in refrigeration systems primarily for lubrication and sealing within the compressor. Screw compressors are typically designed to be oil flooded as a principle means for sealing the rotors and lubricating the moving parts. As a result, oil concentrations in screw compressor discharge lines tend to be high, requiring the use of oil separators to minimize the concentration of oil carried-over to downstream system heat transfer components. Since oil separators are not 100% effective, some oil will be carried-over to the system.

Oil in reciprocating compressors is distributed by either splash or force-fed lubrication systems to provide lubrication of moving parts. The carry-over of oil in the discharge line from reciprocating compressors tends to be much lower as compared to screw compressors. As a result, systems with reciprocating compressors are oftentimes not equipped with external oil separation devices.

Regardless of the compression technology used in a system or the presence of an oil separator, oil can and will escape from the compressor and migrate out into the system. Oil carryover is particularly a problem during compressor start-up. During start-up, the refrigerant in the system undergoes a rapid expansion, throwing oil and refrigerant to the piston cylinder walls. Since the pistons cannot return the large amounts of oil on

the cylinder walls back to the compressor crankcase, a large amount of oil can be ejected out through the discharge line to the refrigeration system. The oil that now mixes with the refrigerant must be carried by the refrigerant through the entire refrigeration system and back to the compressor. If the refrigerant cannot impart enough momentum to the oil to return it to the compressor crankcase, the compressor will not have enough lubrication during operation and will be prone to unexpected shut down or low oil level. Therefore, determining the appropriate refrigerant vapor flow rate is important for keeping the system running reliably and efficiently.

A major design concern of large refrigeration systems is the sizing of the vertical risers in the system to have a minimal pressure drop for the critical refrigerant flow through these risers (critical flow meaning the vapor refrigerant flow required to bring the liquid refrigerant/oil mixture to the top of the riser). These risers can be large (on the order of 50.8 mm I.D.) and substantial refrigerant vapor flow is required to raise the oil in the system to the top of the riser and move the oil through the system. Flooding, or flow reversal, happens when the refrigerant flow is not great enough to drag the oil to the top of the riser.

Mehendale and Radermacher (2000) qualitatively determine the refrigerant mass flow rate at which reversal occurs using sight glasses in the test section. Based on their visual observations, they develop an analytical model to predict the onset of film flow reversal in annular two-phase flow, assuming the refrigerant core and the liquid film are linked by the Wallis interfacial friction factor (Wallis, 1969). Flow reversal is assumed to occur when the wall shear stress goes to zero in their model. This model predicted that as the film thickness increases, the critical refrigerant vapor mass flow rate, i.e. the vapor

mass flow rate at which flow reversal occurs, decreases. The critical vapor refrigerant flow rate increases with the pipe diameter. Their model also predicts that as the oil concentration in the circulating refrigerant increases, the oil film thickness would increase, thereby causing the critical refrigerant flow rate to decrease.

For a given pipe geometry and fluid physical properties, the flow reversal transition appears to occur at an approximately constant vapor flow rate, independent of the liquid flow rate (Hewitt, 1977). Wallis (1969) and Jacobs et al. (1976) suggest using the following parameters to determine flow reversal transitions

$$j_g^* = j_g \rho_g^{1/2} [g D (\rho_f - \rho_g)]^{-1/2} , \quad (4.1)$$

$$j_f^* = j_f \rho_f^{1/2} [g D (\rho_f - \rho_g)]^{-1/2} , \text{ and} \quad (4.2)$$

$$j_g^{*1/2} + m j_f^{*1/2} = C , \quad \text{(correlation for flooding)} \quad (4.3)$$

where j_g and j_f are the superficial velocities, ρ_g and ρ_f are the densities of the gas and liquid, respectively, and D is the diameter of the pipe (Wallis, 1969). The empirical constants m and C depend on the liquid viscosity (Jacobs et al., 1976) and have values of 1.0 and 0.88, respectively for water (Vijayan, 2001). It is thought that flooding (or flow reversal) would occur at $j_g^*=1.0$ for air/water (Hewitt, 1977) or $j_g^*=0.72$ for a refrigerant/oil mixture (Jacobs et al., 1976). However, it should be noted that, Jacobs et al. do not recommend using this criterion for pipes having an inner diameter greater than 5 cm.

Vijayan et al. (2000) note that there are several forms of liquid flow behaviors during flooding, including a ring type wave in small pipes and a churning flow behavior in larger pipes. Vijayan et al. use both the Hewitt-Wallis correlation, Eqns. (4.1-4.3), and the Kutateladze correlation, Eqns. (4.4-4.5), to analyze their data of air-water flow

through different pipes of various diameters. It is found that the Hewitt-Wallis correlation agreed well with data obtained from 25.4 mm diameter pipes or smaller, and that the Kutateladze correlation agrees well with data from the larger diameter pipes. The Kutateladze type correlation is

$$Ku^{*}_{g}{}^{1/4} + C_1 Ku^{*}_{f}{}^{1/4} = C_2, \tag{4.4}$$

where Ku^{*}_{g} and Ku^{*}_{f} are dimensionless gas and liquid superficial velocities given by

$$Ku^{*}_{g} = u_g \left[\frac{\rho_g{}^2}{g\sigma\left(\rho_f - \rho_g\right)} \right]^{1/4} \quad \text{and} \quad Ku^{*}_{f} = u_f \left[\frac{\rho_f{}^2}{g\sigma\left(\rho_f - \rho_g\right)} \right]^{1/4} \tag{4.5}$$

and C_1 and C_2 have the values 1.0 and 1.79, respectively (Vijayan et al., 2001).

A review of the previous research found that determining the point at which the vertical flow reverses is mainly done by visual observation and is based on several different criteria. According to Hewitt (1977), the methods of determining a flow regime visually are mainly subjective. Often, these qualitative methods require high speed photographic techniques to capture high speed flow patterns. The transition point, as determined by visual observation, can be very difficult to identify accurately and is subject to interpretation based on the appearance of liquid bridging, a sudden increase in pressure drop, or appearance of a chaotic flow pattern. As found by Jeong and No (1995), the point of flow reversal is also dependent on the geometry and type of liquid and vapor entrance and exit.

In this work, a flow of dry air and soybean oil (density=920 kg/m^3, viscosity=0.047 kg/m-s) was used in both 50.8 and 25.4 mm I.D. pipes to study the behavior of immiscible vapor/liquid systems. The air was used to simulate the refrigerant vapor, and the soybean oil was used to simulate the liquid refrigerant mixed with oil. The

film thickness was measured optically over a range of flows. Flow visualization techniques were used to determine the flow behavior at various flow combinations of oil and air near the onset of flow reversal. Pressure measurements across the test section were taken for the 25.4 mm I.D. pipe and the 50.8 mm I.D. pipe over a range of flow conditions. The results of this experiment were then compared to correlations found in the literature to determine the differences of the flow behavior with that of air/water and other common experimental fluids.

Experimental Setup

The experimental apparatus featured a clear, vertical 1.8-meter long test section (50.8 mm I.D. or 25.4 mm I.D.), as shown in Figure 4.1. Dry compressed air entered the test section at the lower end and flowed upward. The oil inlet was also at the lower end; thereby, allowing the oil to mix with the air before entering the test section. The oil was pumped by a peristaltic pump into a perforated length of tubing inside a tee section at the riser base. The oil flow was measured with a volumetric floating-ball flow meter. After exiting the test section, the air/oil mixture flowed into a separator after which the air was vented to the lab exhaust and the recovered oil fell by gravity into an oil reservoir. The separator was designed to use gravity, centrifugal effects, and a coalescing filter to separate the oil from the air.

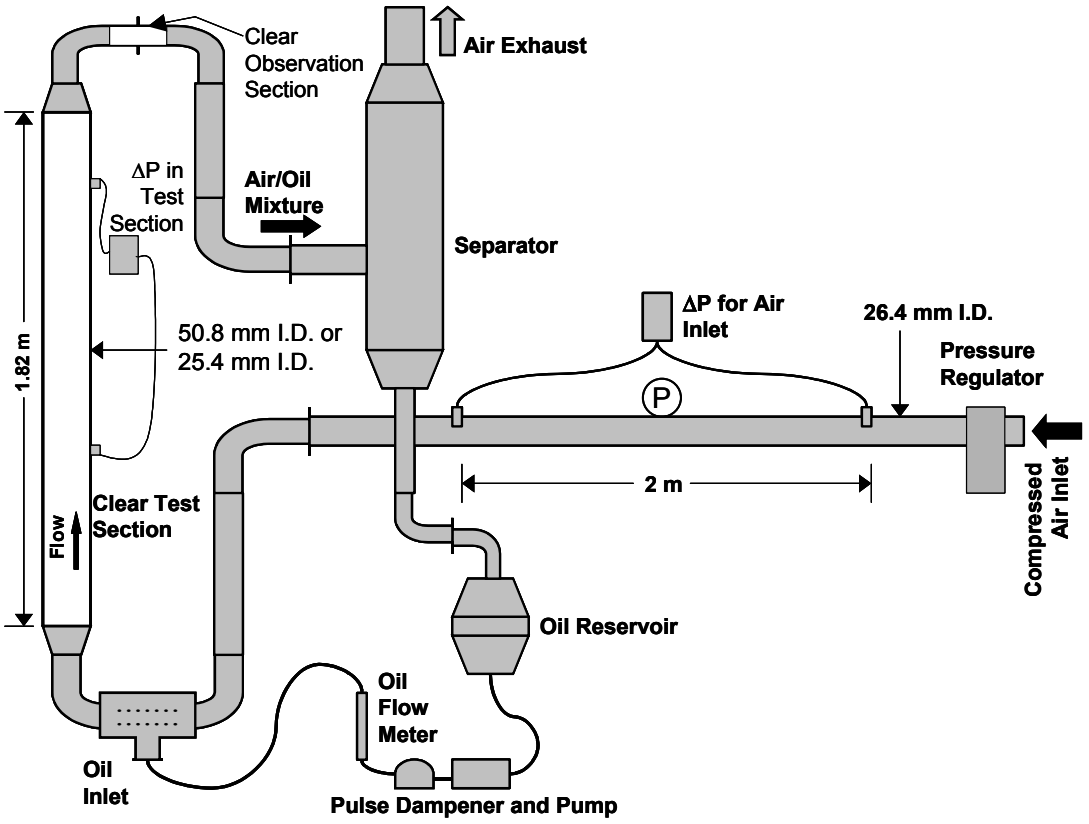

Figure 4.1: Schematic of vertical air/oil test facility.

The volumetric flow rate of the air was determined by measuring the pressure drop across a 2 m length of the entrance pipe. The Colebrook relation for turbulent friction factor is (Colebrook, 1938-39),

$$\frac{1}{f^{0.5}} = -2.0\log\left(\frac{e/D}{3.7} + \frac{2.51}{\mathrm{Re}\, f^{0.5}}\right), \tag{4.6}$$

where e is the wall roughness and D is the pipe diameter. The relation between pressure drop and friction factor is given by

$$\Delta P = f\left(\frac{\rho U^2}{2}\right)\left(\frac{L}{D}\right), \tag{4.7}$$

where ΔP is the pressure drop and L is the distance between pressure taps. Equations 4.6 and 4.7, together with the definition of the Reynolds number, were solved simultaneously to provide the volume flow rate of air in the loop. The solving of these equations was simplified and automated by using the EES equation solver software package (F-Chart Software, 2002). The theoretical uncertainties in this method were estimated to be 3.1% (Rush et al., 1999); uncertainty analysis of the current experiment predicted an average uncertainty of ±0.00045 kg/s. Calibration to a NIST-traceable thermal volumetric flow meter (Thermal Systems Incorporated) gave experimental agreement to within 5%.

Pressure drop measurements were taken over a distance of one meter in the test section and were obtained with some difficulty. Using methods described in Hewitt and Hall-Taylor (1970), the pressure tap lines were filled with oil and pressurized to maintain a constant, extremely slow flow rate to ensure that the lines did not have any air pockets. The measurements were taken using a factory calibrated pressure transducer with an accuracy of ±34 Pa.

The oil volumetric flow meter was calibrated by measuring the time to fill a graduated cylinder with 160 ml of oil. According to the manufacturer's specifications, the uncertainty of the flow meter is ±0.02 l/min at a reading of 0.4 l/min or lower and an uncertainty of 5% of the reading above 0.4 l/min.

Film thickness measurements were taken using an optical method (Shedd and Newell, 1995). This optical measurement method involved illuminating the liquid film through the pipe wall by using a small circular light source (such as a light emitting diode, or LED). The liquid film refracted and reflected the light, creating a clearly visible ring of light on the pipe wall. The diameter of the light ring was proportional to the

thickness of the liquid film. Using geometry and the indices of refraction for the pipe wall and the liquid, the film thickness was determined. The average uncertainty of the film thickness measurement was ±0.034 mm.

Particle streak tracking was also used to investigate the flow patterns. Video clips were taken with the aid of a flashing a strobe light and a set of three different colored LED lights. The three different colors indicate flow direction, and the strobe light indicates the size of bubbles and waves. Individual frames of the video can be analyzed for flow behavior and to obtain particle velocities.

Results

For 50.8 mm I.D. Tube

At each oil flow rate, the air flow was decreased from a rate that produced a definite up-flow of oil to a definite down-flow of oil (see Table 4.1). During the period of decreasing air flow, a churning ridge or ring of oil became visible in the test section of the 50.8 mm tube. This churning ring of oil appeared at flow rates near the onset of flow reversal and remained stationary if the air flow was not lowered further. With slight decreases in air flow, the churning oil ring began to recede down the pipe (in the direction of the gravity force). The amount of oil being pushed up through the test section could be visually observed in the clear section of the return pipe after the vertical test section. It is interesting to note that significant oil flow was observed in the return pipe even after the oil ridge (or definite down flow) appeared in the

Table 4.1: Flow conditions used in air/oil experiment in 50.8 mm tube.

Flow Conditions for 50.8 mm Tube	
Oil Flow kg/s	Range of Air Flow kg/s
0.00077	0.0233 - 0.0337
0.00188	0.02196 - 0.0340
0.0036	0.0208 - 0.03198
0.0058	0.01845 - 0.0323

test section for the 50.8 mm tube. It was believed that the oil carryover from the test section is due to oil droplets being entrained in the gas stream.

The pressure drop for the 50.8 mm tube was measured and can be seen in Figure 4.2. The circled data points show the flow reversal point for each liquid flow (occurring at a minimum pressure drop). It is thought that the flow reversal occurred at a minimum pressure drop because the film thickness was increasing as the vapor velocity was being decreased, causing the velocity gradient to decrease rapidly. After flow reversal has occurred the flow transitioned to churn flow, causing the pressure drop to increase again.

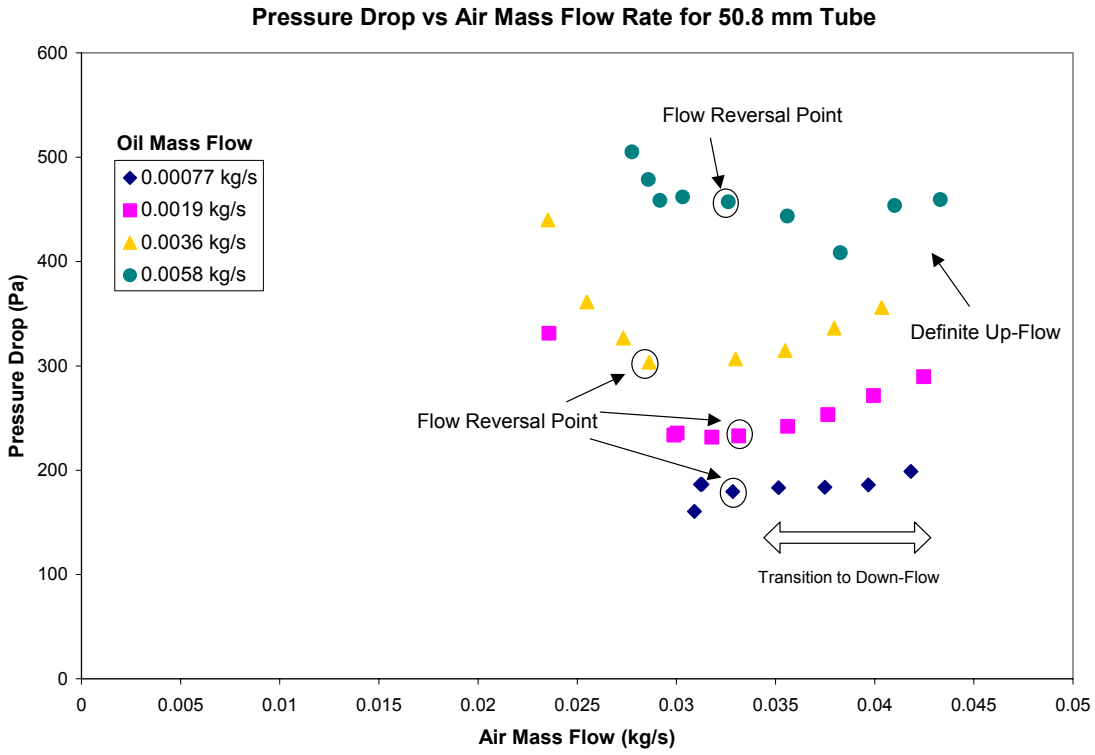

Figure 4.2: Pressure drop data for 50.8 mm tube showing the point of flow reversal.

Film thickness measurements, shown in Figure 4.3, were taken at an approximate height of 1.6 meters at several flow conditions while the flow was being lowered from definite up-flow to definite down-flow. More film thickness measurements were taken

just above, below, and on the churning oil ridge point. The lowest data point for each oil mass flow rate was taken after the churning oil ridge had passed and basically shows a falling film of oil. At this point, the only oil moving upward through the system was entrained in the air flow. The measurement uncertainty for a single data point was included in Figure 4.3 to show the relative size of uncertainty for all data points. The uncertainty for all data points was on the order of ±0.00045 kg/s for the air mass flow rate and ±0.034 mm for the film thickness.

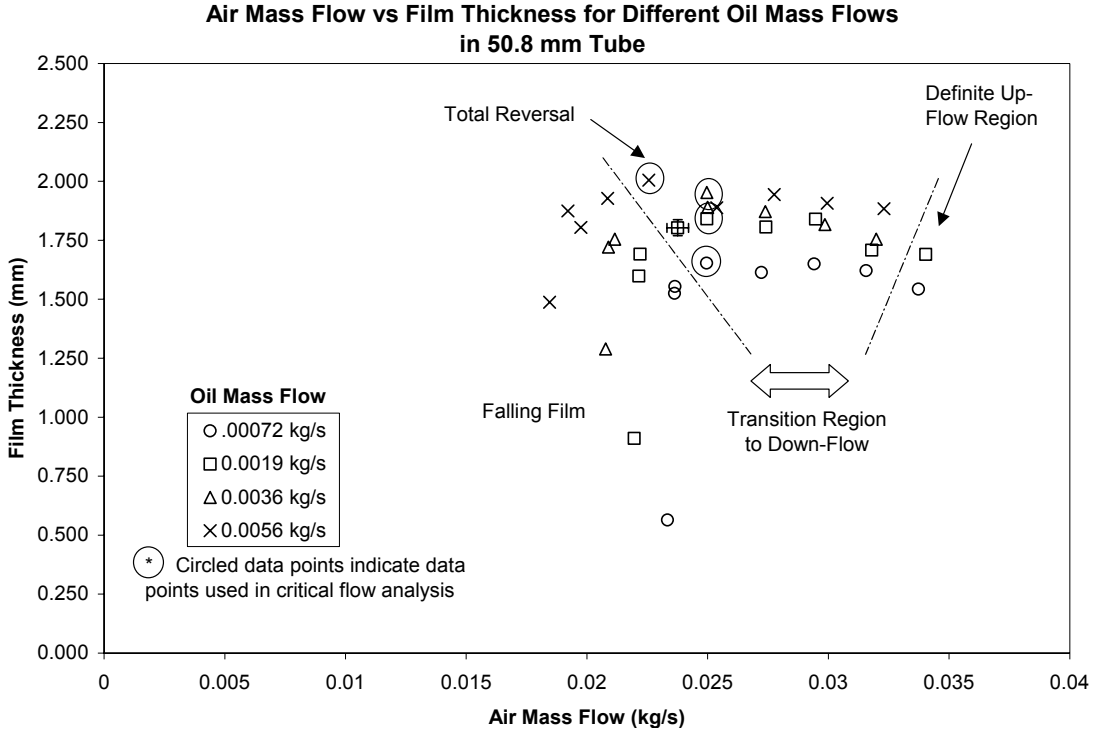

Figure 4.3: Film thickness data for 50.8 mm tube showing point of flow reversal.

This experiment presented an unexpected flow pattern for the vertical flow. The liquid oil film along the pipe wall appeared to be saturated with small vapor bubbles. It was hypothesized that the majority of the bubbles were entrained while introducing oil at the oil inlet located at the riser base. Analyzing video images of the flow revealed that

the bubbles inhabit a layer of fluid close to the wall. There was another layer of fluid between the inner layer and the core air flow in which a wave flow pattern was exhibited. It seemed that the majority of the bubbles appeared to be only in the inner layer of oil. This was significant because the bubbles were observed to be moving downward (in opposition to the wave flow) for nearly all air flow rates studied. This was shown in the characteristic liquid film velocity profile, Figure 4.4. At very high air flow rates, the bubbles (and the inner layer of oil) appeared to be moving very slowly upward, or basically standing still. Waves of oil, like those shown in Figure 4.5, were drawn upward with the air flow. The waves changed the direction of the bubble movement, causing upward flow for an instant as they passed. In between each wave, the bubbles continued to move downward. This can be seen in the particle streak images of Figure 4.6. The waves appeared to be the primary means of large-scale oil mass transport to the top of the pipe in up-flow.

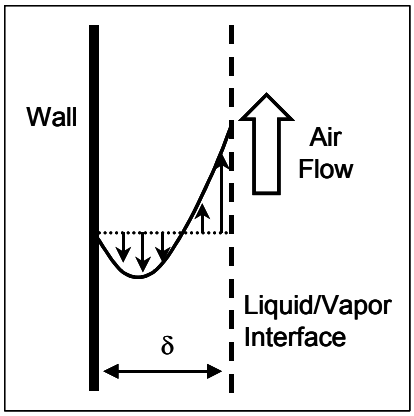

Figure 4.4: Representation of liquid film velocity profile.

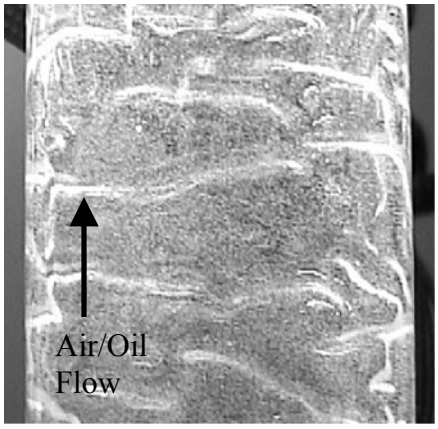

Figure 4.5: Waves in vertical air/oil flow in 50.8 mm tube.

Figure 4.6 shows the use of particle streak tracking to determine the direction of a bubble as a wave passes. A three-color LED strobe light with variable pulse width was used to generate the streak images by using long light pulses with respect to the camera shutter speed. The order of flashing of the LEDs was white, red, blue. Figure 4.6(a) was

taken as a wave passed over, dragging a bubble upward. Figure 4.6(b) was the next frame of the video (33 ms later), after the wave has passed. It can be seen here that the flow was downward for all bubbles in the frame. This demonstrated the flow behavior of the film layer closer to the wall (bubble layer), the layer of oil above this (the wave layer), and the interactions between the two.

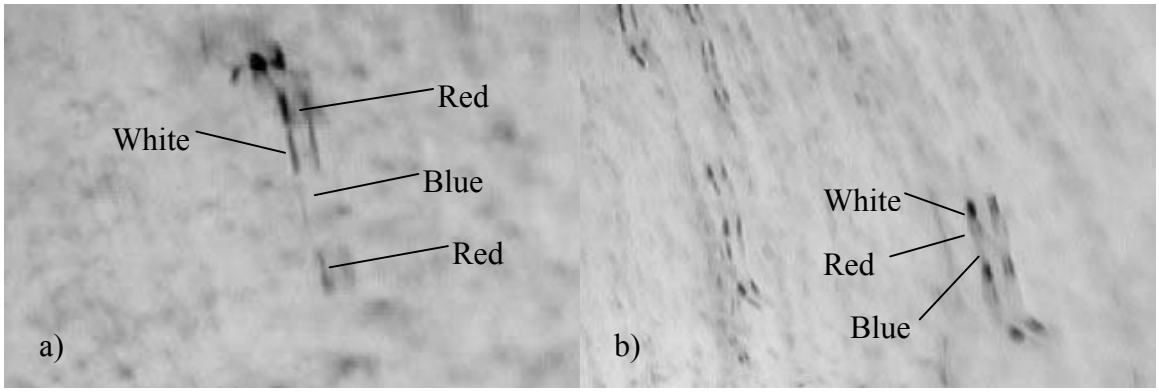

Figure 4.6: (a)Bubble caught by a wave and flowing upward (b)Bubble just after a wave passes, moving downward (taken just after (a)) (direction of flow is white, red, blue)

For 25.4 mm I.D. Tube

At each oil flow rate, the air flow was decreased from a rate that produced a definite up-flow of oil to a definite down-flow of oil in the 25.4 mm diameter tube (see Table 4.2). At the lower oil flow rates of 0.0012 and 0.0003 kg/s a churning oil ridge was visible as in the 50.8 mm tube. For the aforementioned lower oil flow rates, the churning ring of oil appeared at air flow rates close to the onset of flow reversal and would remain stationary if the air flow was not lowered further. With slight decreases in air flow, the churning oil ring began to recede down the pipe

Table 4.2: Flow conditions used in air/oil experiment in 25.4 mm tube.

Flow Conditions for 25.4 mm Tube	
Oil Flow kg/s	**Range of Air Flow kg/s**
0.0003	0.004 - 0.017
0.0012	0.0038 - 0.021
0.0027	0.0041 - 0.021
0.0047	0.0036 - 0.022

(in the direction of the gravity force). At the higher oil flow rates of 0.0047 and 0.0027 kg/s the oil flow became extremely churn-like with definite down-flow conditions and a churning oil ridge was not visible. As the air flow was decreased further, the oil flow became more and more churn-like and it was questionable as to whether there was any oil film to measure.

The amount of oil being pushed up through the test section could be viewed in the clear section of the return pipe after the test section. It was interesting to note that, unlike in the 50.8 mm tube, there was not significant oil flow observed in the clear return pipe after the oil ridge (or definite down flow) appeared in the 25.4 mm test section. There were a few droplets entrained in the air flow that were carried through the return section. However, the lack of oil being sent back to the separator caused a build up of oil in the test section and therefore these flow conditions could not be sustained for extended periods of time.

The pressure drop across the test section was obtained for the 25.4 mm tube in the same manner as for the 50.8 mm tube. The pressure drop measurements can be seen in Figure 4.7. Flow reversal occured at the minimum pressure drop for each oil flow rate (the circled data points). As previously stated, flows could not be maintained after the reversal point due to a build up of liquid, therefore no pressure drop readings were taken after this point.

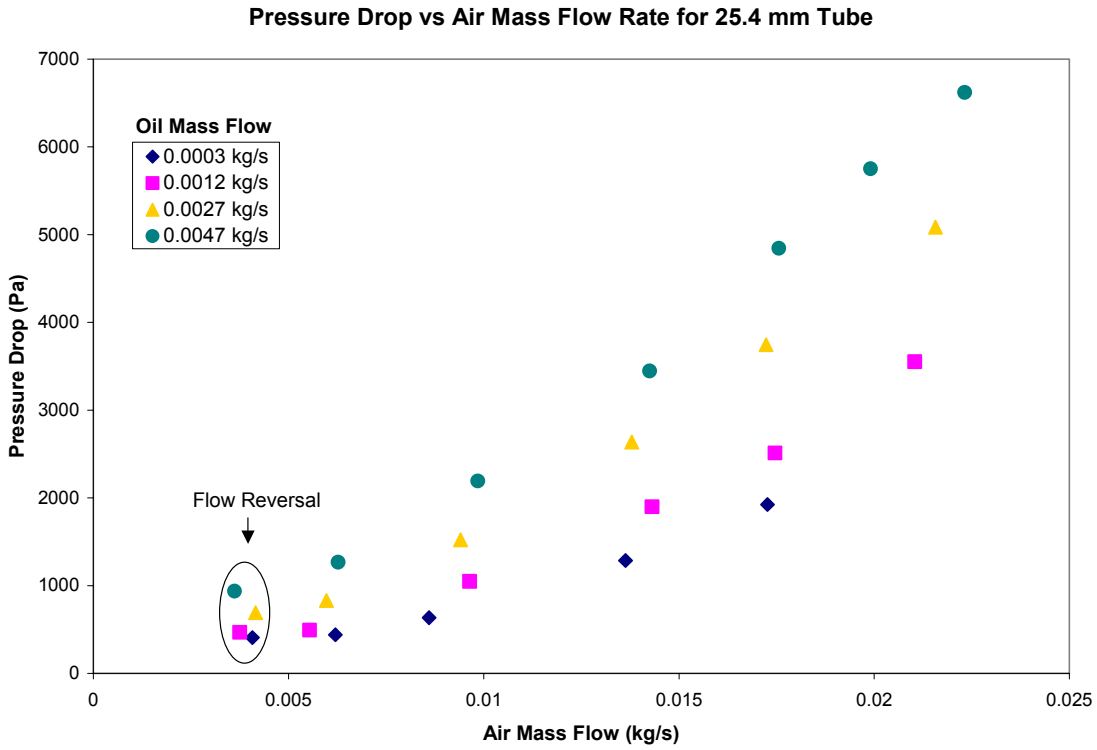

Figure 4.7: Pressure drop data for air/oil experiment in 25.4 mm tube showing the point of flow reversal.

Film thickness measurements, shown in Figure 4.8, were taken at several flow conditions while the flow was being lowered from definite up-flow to a definite down-flow regime. The circled data points on the far left show the onset of flow reversal. As mentioned above, flow conditions after the onset of flow reversal could not be sustained for long periods of time; therefore, this is the last data point taken. The measurement uncertainty for a single data point was included in Figure 4.8 to show the relative size of uncertainty. The uncertainty was of the same order as for the 50.8 mm I.D. tube measurements.

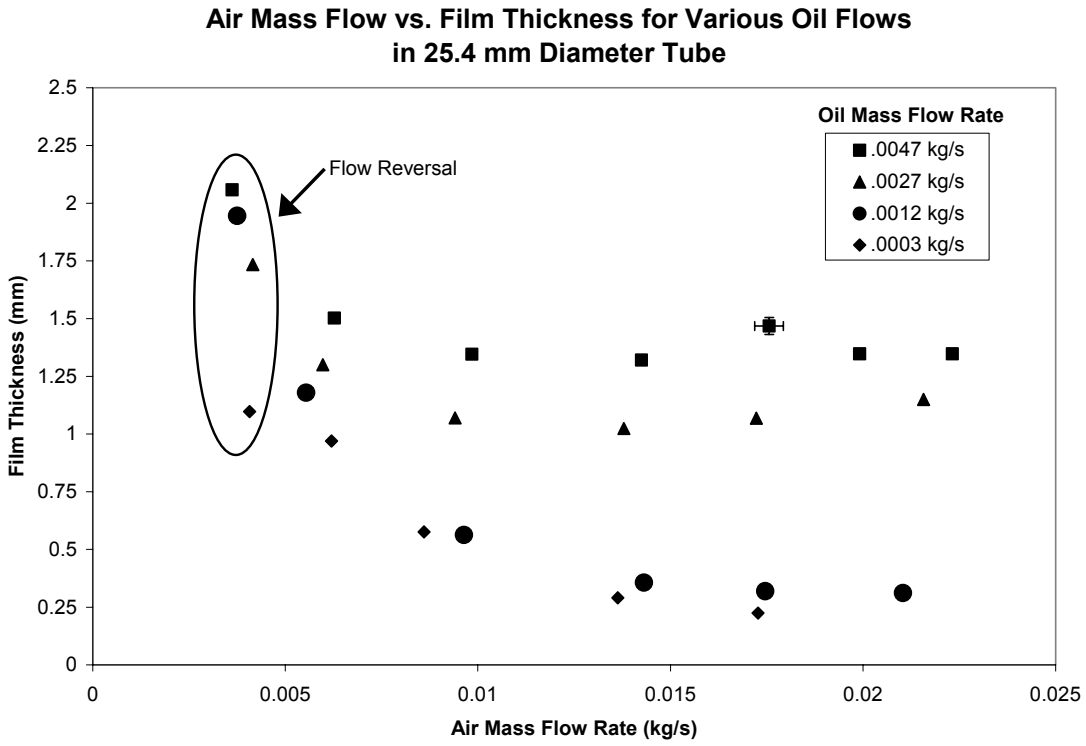

Figure 4.8: Film thickness data for air/oil experiment in 25.4 mm tube showing point of flow reversal.

As in the 50.8 mm tube, there appeared to be a liquid film along the wall that was saturated with very small air bubbles. Just as in the larger tube, this film appeared to move either very slowly upward or downward, depending on the amount of air flow. Also, similar to the 50.8 mm tube there was another layer of fluid between the inner bubble layer and the core air flow in which a wave flow pattern was exhibited. However, this pattern was a ring-type wave pattern in the 25.4 mm tube, which was not the case in the 50.8 mm tube. These waves, shown in Figure 4.9, were drawn upward with the air flow. The waves changed the

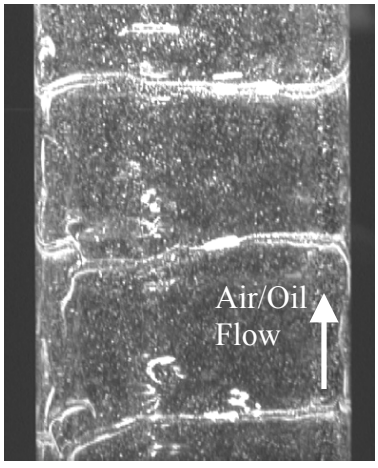

Figure 4.9: Example of ring-type waves in 25.4 mm tube.

direction of the bubble movement, causing the bubble to have upward flow for an instant as the wave passed. In between each wave the bubbles continued to move downward. This can be seen in the particle streak images of Figure 4.10. As in the 50.8 mm tube, the waves appeared to be the primary means of oil mass transport to the top of the pipe in up-flow.

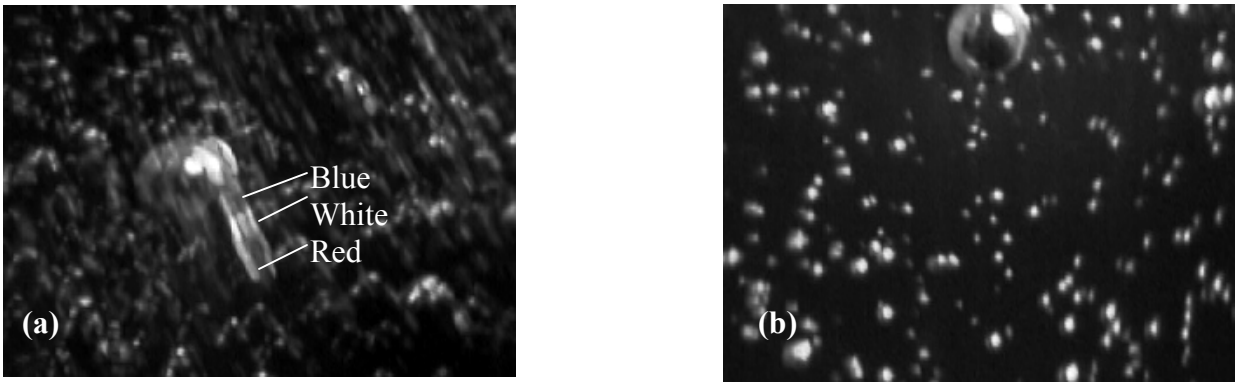

Figure 4.10: (a) Bubble caught by a wave and flowing upward (b) Bubble just after a wave passes, not moving up or down (taken just after (a)) [direction of flow is white, blue, red]

Discussion

Mehendale and Radermacher (2000) created a model for predicting the film thickness and the vapor velocity required to drive a liquid film up the pipe. In their model, they predict that as the film thickness increases, the amount of vapor required for flooding to occur decreases. The film thickness data found in this experiment, shown in Figure 4.3 and Figure 4.8, show a similar trend, albeit a weak one. It was also shown in the aforementioned figures that for a given air flow rate, as the oil mass flow rate increased, generally the oil film thickness increased. By combining these two observations it could be hypothesized that as the oil mass flow rate increases, the air flow rate required for flow reversal to occur decreases. It was also observed that the liquid

was primarily transported by waves. Based on these observations and Schadel and Hanratty's (1989) theory that there is a critical liquid flow needed for waves to form, it was hypothesized that as liquid flow increases, waves will form at lower air flows (which is related to upward flow or flow reversal).

An important observation to note was the wave structure apparent in both tubes. The 25.4 mm tube showed a ring-type wave structure, where the 50.8 mm tube seemed to have a random wave pattern. A similar difference was also noted in the findings of Vijayan et al. (2001). The difference in wave patterns could possibly be due to the difference in the cross-sectional area occupied by the liquid in each tube. The liquid occupied relatively less area in the 50.8 mm tube. There was less oil used in the 50.8 mm tube and therefore this could suggest a critical amount of liquid needed to form ring-type waves in upward flow. Due to the limitations of the experimental set-up, lower oil flow rates were not investigated for the 25.4 mm tube and higher oil flow rates were not investigated on the 50.8 mm tube to test the validity of this theory.

It was observed that at low air flows, the film appeared to become so thick that the interface was unstable, leading to a localized churning motion in both tube sizes. In some cases for the 25.4 mm tube, the entire test section was churning liquid. Above this ring of churning liquid, a smooth, gravity-driven film fell down the pipe for all cases except the two highest oil flow rates in the 25.4 mm tube. Below the churning ring of oil, the waves on the film appeared to be moving upward, while the bubbles in the inner layer maintained a general downward motion. The air flow at which the churning ring moved beyond the top of the test section was considered to be the critical air mass flow rate for upward liquid flow (flow reversal point).

Fukano and Furukawa (1998) proposed a correlation for finding the interfacial friction factor in viscous two-phase flows. This was used to calculate the expected pressure drop for the air/oil mixture and compared with the measured pressure drop. It was found that, for both tube sizes, the correlation under predicted the pressure drop significantly. This correlation was developed using different types of fluids with different viscosities in pure up-flow conditions only. The flow reversal point is of particular interest when designing a system and therefore, it was unfortunate that this correlation did not appear to be useful outside of the pure up-flow conditions.

An attempt was made to fit the flooding data to the Wallis-Hewitt correlation shown in Eqns. (1-3). It was found that this correlation over-predicted the vapor velocity required for flooding. Hewitt (1977) suggested that flooding would occur at a value of $j_g^*=1$ (for air/water), and Jacobs et al. (1976) suggested that $j_g^*=0.72$ (for oil and refrigerant), regardless of the liquid flow (with $m=1.0$ and $C=0.88$ for low flow). The value found for both tube sizes using the Wallis-Hewitt correlation with $m=1.0$ and $C=0.75$ was $j_g^*=0.47$ (see Figure 4.11), nearly half of what was suggested by Hewitt. The superficial gas velocity was calculated using Equation 4.1 and averaged over the entire range of liquid flow data. Then C was found using Equation 4.3, keeping $m=1.0$. It is interesting to note that the value obtained did appear to be a constant superficial vapor velocity as indicated by both Hewitt and Jacobs. The difference in value, however, could be attributed to the fact that the constants used in this correlation (m and C) are dependent on the liquid viscosity and C is also dependent on the way in which the liquid is introduced to the system (Jacobs et al, 1976). Exactly how they are dependent on the

liquid viscosity is not stated, and therefore, the constants could not be adjusted appropriately to correct for the significant differences in viscosity.

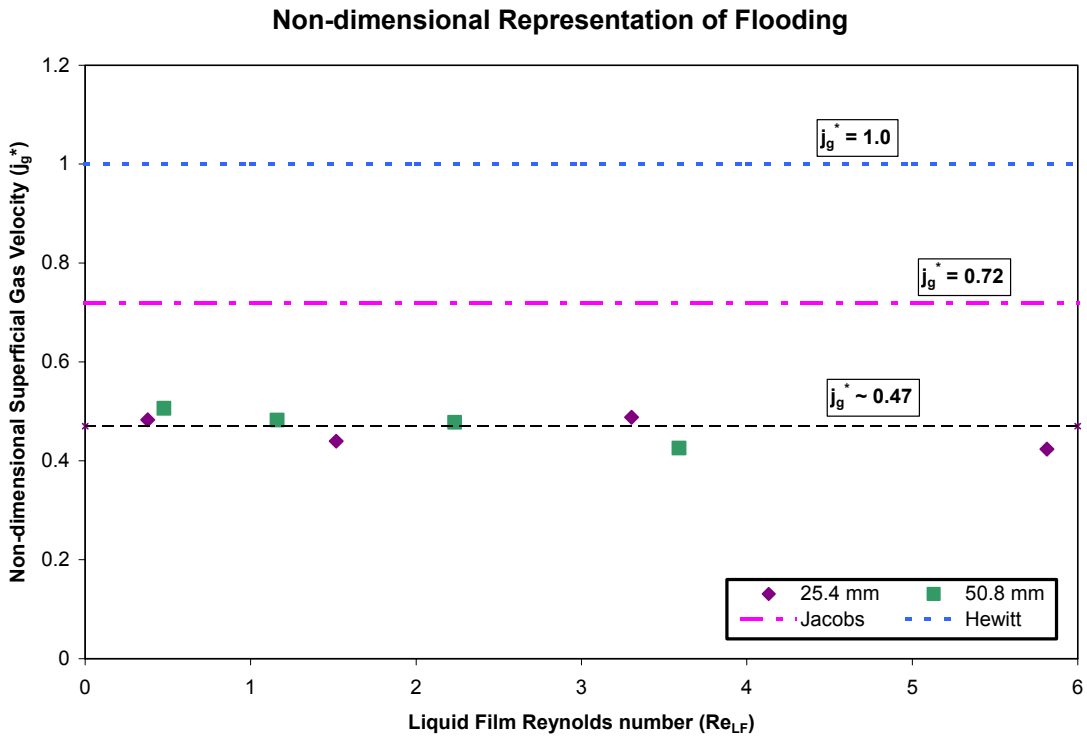

Figure 4.11: Attempt to identify flooding point using a non-dimensional superficial gas velocity suggested by both Hewitt and Jacobs.

Another attempt was made to fit the data to the Kutateladze correlation, Eqns. (4.4) and (4.5), with $C_1=1.0$ and $C_2=1.79$ (Vijayan et al., 2001). This correlation over-predicted the flooding velocity by about 1.23 times for both the 25.4 mm tube and 50.8 mm tube.

The Feind correlation (Vijayan et al., 2001 and 2002) for determining the film thickness was used to predict the flooding film thickness. According to the data found, this correlation under-predicted the film thickness at flooding conditions by a factor of 3, or 65%.

The above-mentioned correlations are the correlations commonly used to predict the characteristic flooding behavior in annular flow. These all proved to be inadequate for use with fluids other than those that the correlations are based on (i.e. air/oil), which was likely due to differences in liquid viscosity and density and differences in the entrance and exit conditions and flow ranges. Caution must be practiced when using any of these correlations with fluids other than those used in the actual experiment.

As was mentioned in a previous section, the pressure drop across each test section was measured. In an effort to find the dimensionless film thickness associated with this experimental flooding data, the pressure drop was used to calculate the interfacial shear stress, $\tau_{i,P}$, by

$$\tau_{i,P} = -\frac{D}{4}\frac{\mathrm{dP}}{\mathrm{dz}} \quad , \tag{4.8}$$

where D is the tube diameter and dP/dz is the pressure drop across the test section. This value found for the shear stress was used to non-dimensionalize the film thickness (δ_τ^+) as shown in Equation (4.9),

$$\delta_\tau^+ = \left(\frac{\delta u_\tau}{\nu_f}\right) \quad \text{with} \quad u_\tau = \sqrt{\tau_{i,p}/\rho_f} \quad , \tag{4.9}$$

where ρ_f is the liquid density, ν_f is the liquid kinematic viscosity, and δ is the measured film thickness. This δ_τ^+ was plotted against the vapor kinetic energy in an effort to collapse the data (see Figure 4.12). The 50.8 mm data appeared to have a somewhat constant dimensionless film thickness for each oil flow. The 25.4 mm data did not appear to have a trend. The flooding point for the 25.4 mm tube appears to be at nearly the same flooding value as the similar oil flow in the 50.8 mm tube.

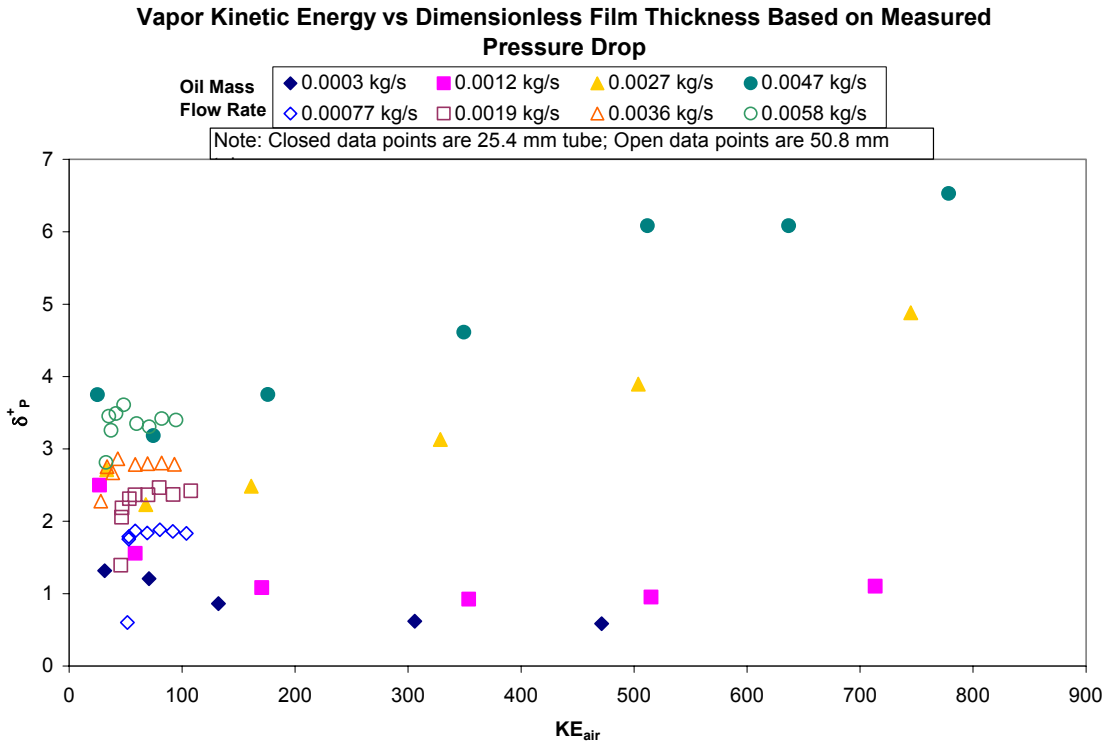

Figure 4.12: Plot of δ^+ found using the measured pressure drop and vapor Reynolds number.

Many experiments use the dimensionless two-phase Lockhart-Martinelli parameter (Whalley, 1987), X_{tt}, to describe the flow behavior observed. In an attempt to compare the data from the different sized tubes the Lockhart-Martinelli parameter (shown in Eqn 4.10), was calculated and plotted versus the two-phase friction factor. The Lockhart-Martinelli parameter is given by

$$X_{tt} = \left(\frac{1-x}{x}\right)^{0.9} \left(\frac{\rho_g}{\rho_f}\right)^{0.5} \left(\frac{\mu_f}{\mu_g}\right)^{0.1} \tag{4.10}$$

where x is the mass quality, ρ_g and ρ_f are the gas and liquid densities, respectively, and μ_f and μ_g are the viscosities of the liquid and the gas respectively (Lockhart and Martinelli, 1949). The mass quality, x, is found by dividing the gas mass flow rate (W_g) over the total mass flow rate of the gas and liquid ($x=W_g/(W_g+W_f)$). The Lockhart-Martinelli

parameter was plotted against the two-phase friction factor for both the 25.4 mm and 50.8 mm tube in Figure 4.13. The trends to note are that all data groups start on one line (f_{tp} = 5.4*X_{tt} + 0.099) and move upward toward the point of reversal (circled data point). The 25.4 mm flooding point data correlates to a line (f_{tp} = 6.5*X_{tt} + 0.24) and the 50.8 mm flooding point data correlates to a different line (f_{tp} = 16.3*X_{tt} + 0.091). Without more data, it would be difficult to make a generalized statement about the flooding behavior in relation to the two-phase friction factor and the Lockhart-Martinelli parameter.

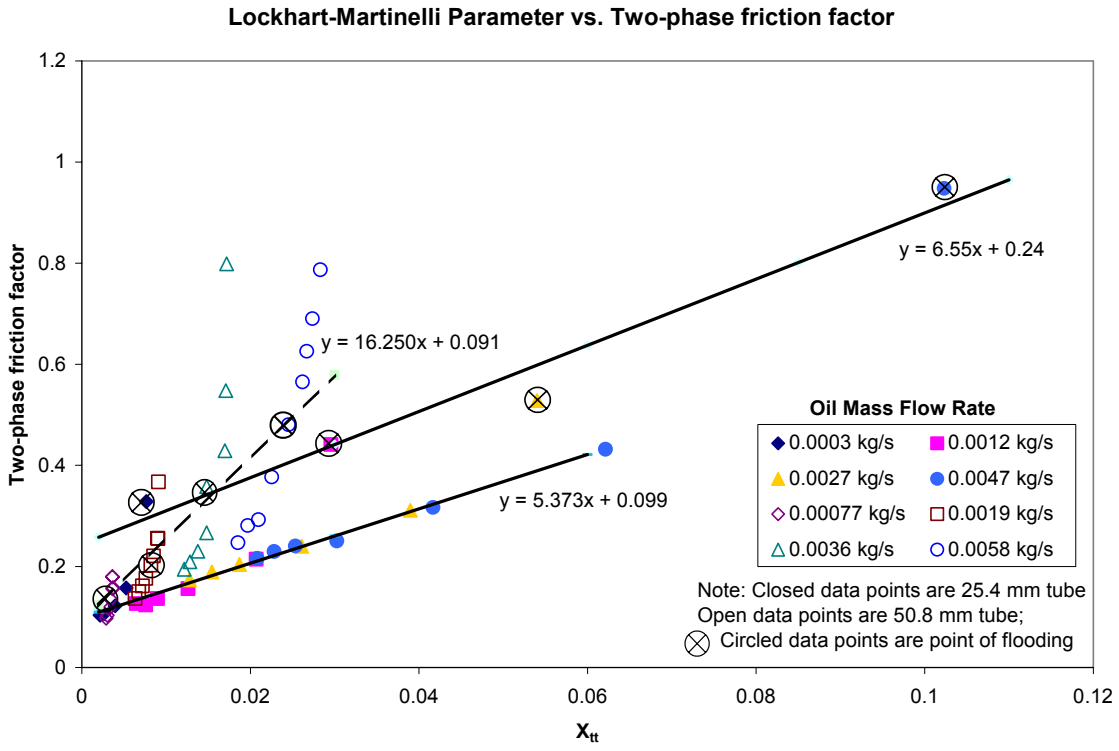

Figure 4.13: Non-dimensional film thickness found using the calculated shear stress plotted vs the dimensionless two-phase Lockhart-Martinelli parameter

A unique observation was that two layers existed in the liquid film, a bubbly layer along the wall and a wavy layer. The inner, bubbly layer appeared to have a downward flow for all air-oil flow combinations studied. The waves appeared to be the main mode of mass transfer for the liquid film before flow reversal has occurred. (There was

significant droplet flow at air velocities below the critical air velocity, and thus some oil still traveled to the top of the pipe.) There appeared to be a difference in how much oil was entrained in the air for each of the different tube sizes. This may be related to the type of waves seen in the flow. The 50.8 mm tube carried much more oil to the top of the tube even after down-flow had occurred. This was likely in the form of droplets entrained in the air, but it appeared that a fair amount of oil would also gush through in waves. The 25.4 mm tube had fewer droplets and no waves gushing through and, therefore, could not sustain the down-flow conditions long, due to the lack of oil being moved through the system.

Conclusions/Recommendations

- From the pressure drop data taken, it appeared that the minimum pressure drop was associated with the point of flooding. Whereas, the maximum film thickness was associated with the flooding point.
- This experiment showed a weak trend in support of the model found by Mehendale and Radermacher (2000), which predicts a decrease in the required vapor flow rate for flooding to occur as the liquid flow increases in a 50.8 mm tube and 25.4 mm tube. The data showed a slight decrease in the required air flow for flooding.
- This experiment showed that care must be taken when employing commonly used correlations, such as the Hewitt-Wallis correlation and the Kutateladze correlation when using different types of fluids than the correlations were intended for.

- The two-phase friction factor was plotted vs. the Lockhart-Martinelli parameter, which revealed a different line fit for the flooding data of the 25.4 mm and the 50.8 mm tube.
- After observing the flow, there appeared to be two separate layers in the liquid film – a bubbly layer along the wall and a wavy layer above this. The waves were thought to be the method of mass transport for the oil upward, whereas bubbles in the inner layer appeared to move downward or remain nearly stationary.

Acknowledgements

The author appreciates the financial support for this project provided by the University of Wisconsin and the National Science Foundation under award number CTS-0134510.

Nomenclature

C – Wallis' empirical constant (Eqn 4.3)	[--]
C_1 – Kutateladze's empirical constant (Eqn 4.4)	[--]
C_2 – Kutateladze's empirical constant (Eqn 4.4)	[--]
D – inner pipe diameter	[m]
dP/dz – pressure drop across test section per unit length	[Pa/m]
e – wall roughness	[--]
f – smooth tube friction factor	[--]
f_i – interfacial friction factor	[--]
Fr_{GO} – gas only Froude number given by $Fr_{GO} = j_g / ((g\,D)^{1/2})$	[--]
g – gravitational constant	[m/s^2]
j_f – liquid superficial velocity	[m/s]
j_f* – dimensionless liquid superficial velocity (Eqn 4.2)	[--]
j_g – gas superficial velocity	[m/s]
j_g* – dimensionless gas superficial velocity (Eqn 4.1)	[--]
Ku_f* – Kutateladze dimensionless liquid superficial velocity (Eqn 4.5)	[--]
Ku_g* – Kutateladze dimensionless gas superficial velocity (Eqn 4.5)	[--]
L – length of pipe (general)	[m]
m – Wallis' empirical constant (Eqn 4.3)	[--]
Re – Reynolds number based on pipe diameter (general)	[--]
Re_g – vapor Reynolds number given by $Re_g = j_g\,D / \nu_g$	[--]
Re_{LF} – liquid film Reynolds number given by $Re_{LF} = (4\,W_f) / (\pi D\,\mu_f)$	[--]
U – velocity (general)	[m/s]
u_g – velocity of gas	[m/s]
u_f – velocity of liquid	[m/s]

u_τ – shear velocity (used for non-dimensionalization) (Eqn 4.9)	[m/s]
W_f – liquid film mass flow rate	[kg/s]
W_g – gas mass flow rate	[kg/s]
x – mass quality given by $x=W_g/(W_g+W_f)$	[--]
X_{tt} – dimensionless two-phase Lockhart-Martinelli parameter (Eqn 4.10)	[--]

Greek Variables

δ – optically measured film thickness	[mm]
δ_τ^+ – non-dimensional film thickness (Eqn 4.9)	[--]
ΔP – pressure drop (general)	[Pa]
μ_f – liquid viscosity	[kg/m-s]
ν_f – liquid kinematic viscosity	[m^2/s]
ν_g – gas kinematic viscosity	[m^2/s]
ν_w – kinematic viscosity of water at 20°C	[m^2/s]
ρ – density (general)	[kg/m^3]
ρ_f – liquid density	[kg/m^3]
ρ_g – gas density	[kg/m^3]
σ – surface tension	[N/m]
$\tau_{i,P}$ – interfacial shear stress (Eqn 4.8)	[Pa]

References

Asali, J.C., T.J. Hanratty, and P. Andreussi, "Interfacial drag and film height for vertical annular flow." *AIChE Journal*, **31**(6): 895-902, 1985.

Colebrook, C. F., "Turbulent Flow in pipes, with particular reference to the transition region between the smooth and the rough pipe laws." *Journal of the Institution of Civil Engineers*, London **11**: 133-156, 1938-39.

F-Chart Software: Engineering Equation Solver (EES). *www.fchart.com*, 2002.

Fukano, T. and T. Furukawa, "Prediction of the effects of liquid viscosity on interfacial shear stress and frictional pressure drop in vertical upward gas-liquid annular flow." *International Journal of Multiphase Flow*, **24**(4): 587-603, 1998.

Henstock, W.H. and T.J. Hanratty, "The interfacial drag and the height of the wall layer in annular flows." *AIChE Journal*, **22**(6): 990-1000, 1976.

Hewitt, G. F, "Two-phase flow patterns and their relationship to two-phase heat transfer." In S. Kakac and F. Mayinger, editors, *Two-phase Flows and Heat Transfer*, **Volume 1** of *NATO Advanced Study Institute on Two-Phase Flows and Heat Transfer*, pages 11-35. Hemisphere Publishing Company, Washington, D.C., 1977.

Hewitt, G. F. and N. S. Hall-Taylor, *Annular Two-phase Flow*. Pergamon Press, Oxford, 274-276, 1970.

Jacobs, M. L., F. C. Scheideman, S. M. Kazem, and N. A. Macken, "Oil transport by refrigerant Vapor." *ASHRAE Transactions*, **82**(2): 318-329, 1976.

Jeong, J. H. and H. C. No, "Experimental study of the effect of pipe length and pipe-end geometry on flooding." *International Journal of Multiphase Flow*, **22**(3): 499-514, 1996.

Lockhart, R. W. and R. C. Martinelli, "Proposed correlation of data for isothermal two-phase two-component flow in pipes." *Chem. Eng. Prog*., **45**: 39, 1949.

Mehendale, S. S. and R. Radermacher, "Experimental and theoretical investigation of annular film flow reversal in a vertical pipe: application to oil return in refrigeration systems." *HVAC&R Research*, **6**(1): 55-74, 2000.

Rush, T. A., T. A. Newell, and A. M. Jacobi, "An experimental study of flow and heat transfer in sinusoidal wavy passages." *International Journal of Heat and Mass Transfer,* **42**: 1541 – 1553, 1999.

Schadel, S.A. and T.J. Hanratty, "Interpretation of atomization rates of the liquid film in gas-liquid annular flow." *International Journal of Multiphase Flow*, **15**(6): 893-900, 1989.

Shedd, T.A. and T.A. Newell, "Automated optical liquid film thickness measurement method." *Review of Scientific Instruments*, **69**(12): 4205-4213, 1998.

Vijayan, M., S. Jayanti, A.R. Balakrishnan, "Effect of pipe diameter on flooding." *International Journal of Multiphase Flow*, **27**: 797-816, 2001.

Vijayan, M., S. Jayanti, A.R. Balakrishnan, "Experimental study of air-water countercurrent annular flow under post-flooding conditions." *International Journal of Multiphase Flow*, **28**: 51-67, 2002.

Wallis, G.B., *One-Dimensional Two-phase Flow*. McGraw-Hill, New York, 1969.

Whalley, P.B., *Boiling, Condensation, and Gas-Liquid Flow*. Clarendon Press, Oxford, 1987.

5. Conclusions/Recommendations

This work described two adiabatic, two-phase flow experiments that compared the behavior of different fluid pairs to the behavior of air and water. The fluid pairs chosen to be compared with air/water data were R-123 liquid/vapor and air/oil. In addition to air/water data collected during the course of the present investigation, additional data were gathered from previously published independent research efforts. The first experiment directly compared air/water and R-123 vapor/liquid to explore the influence of changing vapor properties. However, the results also showed that the slight changes in liquid properties had noticeable effects. The second experiment described is a vertical air/oil experiment in which the data were compared to that of other works that mainly used air/water as the working fluids. This experiment involved keeping the vapor properties relatively constant while the liquid properties were altered. In this manner both variations on the liquid properties and the vapor properties were explored.

These particular fluids (R-123 vapor/liquid and air/oil) were chosen to be studied because of their relevance to design issues of refrigeration systems. The goal of comparing R-123 data with air/water data was to find a method of relating very different fluids with one another. This would allow experiments to be run in simple systems to gain knowledge that could be used to design a system using other fluids, in particular refrigerants. The air/oil experiment allowed the exploration of a particular design problem found in refrigeration systems. The problem centers around the difficulty in designing vertical risers that are capable of entraining and transporting oil in a vertical direction as part of an overall oil management strategy for a refrigeration system.

R-123 and Air/Water Experiment

One of the main findings of the R-123 liquid/vapor and air/water experiments was that, by equating the vapor kinetic energies, several of the aspects of the flows exhibited similar behavior, including the flow regimes, pressure drop, and film thickness. However, the wave behavior of the two flows was still noticeably different. There appeared to be two different mechanisms at work in the flow behavior, one for low quality vapor flows and one for high quality vapor flows. Both vapor kinetic energy and gravity effects appeared to significantly influence flow distribution or liquid film distribution under low quality flow conditions, whereas the behavior of the high quality flows appeared to be best characterized by only the vapor kinetic energy term (or interfacial shear stress effect). The work of Fukano and Ousaka (1989) supports this finding.

The present investigation appeared to have validated a potentially fundamental two-phase behavior of two very different fluids. These fluids have very different vapor and liquid properties, and yet by equating the vapor kinetic energies the flow behavior (pressure drop, film thickness, flow regime, etc.) could be matched. This method even appears to have identified a transition point at which both fluid pairs change from being characterized by both vapor kinetic energy and liquid density to only needing to be characterized by vapor kinetic energy. This transition region appears to be in the same range of vapor kinetic energy for both fluid pairs. This leads to the thought that this will be applicable to many fluids.

Recommendations for the R-123 and air/water experiment

As for using this method of relating data for design purposes, it is recommended that more work be done to determine the ranges of the low and high flow mechanisms, which would require running flows over a larger range. It is also recommended that experiments be performed with different types of fluids and different tube sizes for each fluid pair, thereby, testing its universality. Ideally, the selected working fluid pairs should have properties varying above and below the values of the properties for water to determine if all types of fluids can be related.

Air/Oil Experiment

One of the main findings of the air/oil experiment was that the correlations most commonly used for designing vertical risers in refrigeration systems did not predict the film thickness or pressure drop data taken in this experiment well. For example, previously presented correlations used to predict the point of liquid flow reversal could not be successfully validated in the present experiment. Nearly all of these correlations are dependant on constants that are based on either fluid properties or inlet and exit geometry, or both. This indicated that a method was needed to relate results taken in different fluids to one another to achieve a more general correlation. The flow reversal data taken in this experiment showed a minimum pressure drop and a maximum film thickness at flow reversal. The data obtained appeared to correlate well using the two-phase friction factor and the Lockhart-Martinelli parameter; however, the flooding point followed a different curve for each tube size.

A qualitative observation of the air/oil flow showed two separate layers in the oil film: a bubbly layer along the wall and a wavy layer moving over this. The waves were

hypothesized to be the mechanism responsible for mass transport for the oil upward, whereas bubbles in the inner layer appeared to move downward or remain nearly stationary.

Recommendations for Air/oil Experiment

In order to test the correlation found using the two-phase friction factor and the Lockhart-Martinelli parameter, more data should be taken in different sized tubes. The same experiments should be run in an identical air/water system to be able to make direct comparisons as in Chapter 3. This would give a more complete understanding of the behaviors observed in this experiment.

Extension of Both Experiments

The significance of this work can be seen by applying the results of each study to the practical design of vertical risers. As was stated in the air/oil experiment, the air was used to simulate a refrigerant vapor that would actually be used in a refrigeration system. Therefore in order to predict what the actual refrigerant vapor flow rate would be at the flow reversal point, the methods of Chapter 3 were used. The vapor kinetic energies were equated between air and refrigerant vapor (R-123 as an example) to obtain a good approximation of the vapor flow required for flow reversal to occur. The refrigerant vapor kinetic energy required for flow reversal could be identified by finding the maximum film thickness for a given liquid flow. Therefore, a designer of an R-123 refrigeration system would know the minimum vapor flow required to drag any oil in the system to the top of a long vertical riser and in order to return it to the compressor. The significance of combining both experiments can be seen in Figure 5.1 and Figure 5.2.

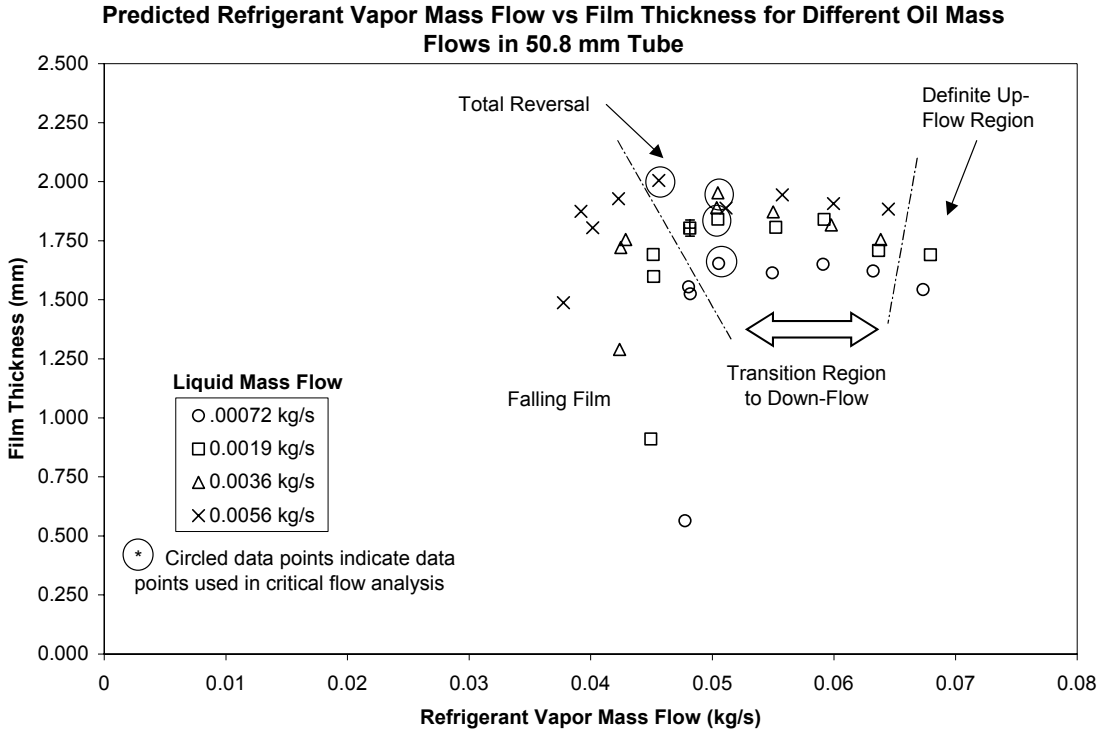

Figure 5.1: Predicted refrigerant vapor flow required for flow reversal to occur in 50.8 mm diameter vertical riser.

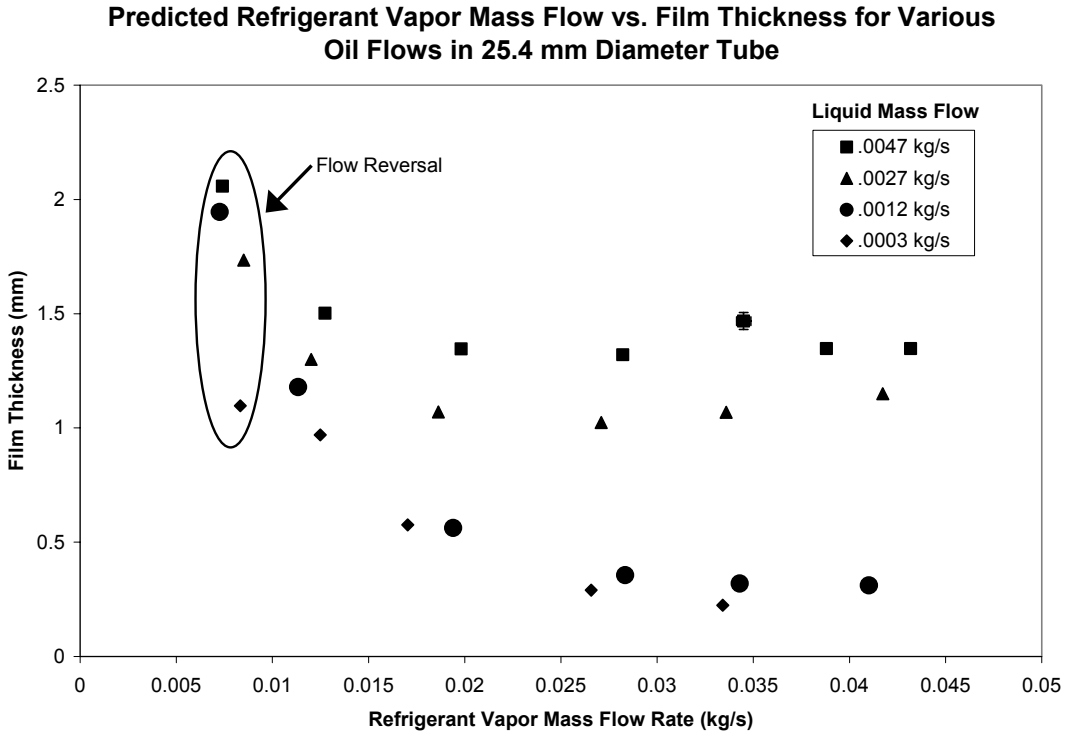

.

Figure 5.2: Predicted refrigerant vapor flow required for flow reversal to occur in 25.4 mm diameter vertical riser.

References

Fukano, T. and A. Ousaka, "Prediction of the circumferential distribution of film thickness in horizontal and near-horizontal gas-liquid annular flows." *International Journal of Multiphase Flow,* **24**(4): 587-603, 1989

A. Compatibility Charts

Shows the compatibility of R-123 with various materials taken from http://www.dupont.com/suva/na/usa/literature/pdf/h42443_4.pdf .

Plastics Compatibility of CFC-11 versus HCFC-123
(Screening Test Conditions: Plastic specimens exposed to liquid in sealed glass tubes at temperatures and exposure times given below.)

Plastic		Compatibility Ratings			
		4 hr at 24°C (75°F)		100 hr at 54°C (130°F)	
Chemical Type	Trade Name	CFC-11	HCFC-123	CFC-11	HCFC-123
ABS	Kralastic	0	4	0	4
Acetal	Delrin®	0	0	0	1
Acrylic	Lucite	0	4	0	4
Fluorocarbon PTFE	Teflon®	0	0	0	1
Polyamide 6/6 nylon	Zytel®	0	0	0	0
Polycarbonate	Lexan	0	4	0	4
Polyethylene-HD	Alathon	0	0	1	1
Polypropylene	Alathon	0	0	2	2
Polystyrene	Styron	0	4	4	4
Polyvinyl Chloride		0	0	1	1

Ratings: 0 = Suitable for use
1 = Probably suitable for use
2 = Probably not suitable for use
3 = Not suitable
4 = Plastic disintegrated or dissolved in liquid

Ratings Based On: Specimen dimensional, weight, and surface changes.

Delrin®, Teflon®, and Zytel® are DuPont registered trademarks.
Alathon is an Oxy Petrochemicals Inc. registered trademark.
Kralastic is a USS Chemicals registered trademark.
Lexan is a General Electric registered trademark.
Lucite is an ICI Americas registered trademark.
Styron is a Dow Chemical registered trademark.

Elastomer Compatibility of CFC-11 versus HCFC-123
(Test Conditions: Exposure to liquid in sealed tubes for 7 days at 54°C (130°F), then ambient air drying for 21 days.)

Elastomer		Length Change at End of Exposure, %		Weight Change After Drying, %	
Chemical Type	Trade Name	CFC-11	HCFC-123	CFC-11	HCFC-123
Butyl Rubber		16	11	–4	–2
Chlorosulfonated Polyethylene (CSM)	Hypalon®	2	12	–2	–5
Fluoroelastomer	Viton® A	2	23	0	5
Hydrocarbon Rubber (EPDM)	Nordel®	12	13	–9	–6
Natural Rubber		31	39	–4	–4
Neoprene		2	10	–8	–9
Nitrile Rubber					
Buna N (NBR)		1	50	0	–4
Buna S (SBR)		13	26	–8	–9
Polysulfide	Thiokol FA	0	7	–1	–2
Silicone		33	28	–2	–2
Urethane	Adiprene C	7	56	–3	–5

Hypalon®, Viton® A, and Nordel® are DuPont registered trademarks.
Thiokol FA is a Morton Thiokol registered trademark.
Adiprene C is a Uniroyal registered trademark.

Stability of HCFC-123 with Steel, Copper, Aluminum, and Heavy Naphthenic Oil

(Test Conditions: Sealed tubes containing 3.0 mL refrigerant + 0.52 mL lubricant; metal specimens: 6.0 cm [2-3/8″] × 6.4 mm [1/4″] × 1.6 mm [1/16″]; exposure: 2.95 days at 151°C [304°F])

Metals: Steel 1010
Copper
Aluminum 1100

Oil: Witco Freezene, heavy white naphthenic mineral oil, 255 SUS (approx. 55 cSt at 38°C [100°F])

		HCFC-123	
Refrigerant	**R-11**	**Sample 1**	**Sample 2**
Visual Ratings			
Liquid	3	0+	2
Steel	1	1+	2
Copper	3	2	2
Aluminum	1	0	0
Decomposition Analyses			
Chloride, wt%	1.7	0.08	0.13
Fluoride, wt%	0.42	0.003	0.004

Visual Ratings: 0 to 5

Rating	**Metal**	**Liquid**
0	Bright, shiny	Clear, colorless
3	Darkening	Clear, brown
5	Severe deposits	Black, coke present

(Ratings of 3 and higher considered unacceptable.)

B. Method of Assembling Thermocouples

The procedure for making thermocouple wires into thermocouples.

1. Strip the ends of both wires to give short exposed ends

- On Thermocouple welding device:

2. Using a pair of needle nose pliers, gently pull the center electrode toward you a **short** distance
3. Insert the leveling tool into the center hole to center this electrode
4. Turn on Argon gas till it shows a pressure reading (2 valves)
5. Turn the power on
6. Purge the system by pressing and holding the purge button for a few seconds
7. Center the wire ends in the holder with a small amount of the tip exposed ($^{1}/_{8}$" to ¼") with the wire ends touching one another and the metal holder (the holder acts as part of the circuit)
8. Place the holder (and wires) in the center hole
9. Hold down the *Arc* button until a bright light appears, you may need to gently twist the holder in the slot to insure good contact at the same time
10. Release the button and remove the holder and the wires from the holder
11. You should now have a small welded bead on the tip of the now-connected wires. If this is not the case you will need to snip off the ends and start over from step 1 (you may not need to re-center the center electrode however).
12. When finished turn off the Argon gas (both valves) and purge the system until the pressure of the tank drops down to zero
13. Turn off the machine

C. Channels Used in LabVIEW Program

Agilent Multiplexor	
Channel Number	**Description**
101	Vapor inlet temperature
102	Liquid inlet temperature
103	Vapor tank temperature
104	Liquid tank temperature
105	Start of test section mixture temperature
106	End of test section mixture temperature
107	Heat Exchanger, R-123 inlet temperature
108	Heat Exchanger, R-123 outlet temperature
109	Heat Exchanger, water inlet temperature
110	Heat Exchanger, water outlet temperature
111	Vapor inlet pressure
112	Liquid inlet pressure
113	Mixture pressure at start of test section
201	Heater voltage reading (Red)
202	Heater voltage reading (Black)
203	Heater voltage reading (Blue)
221	Heater current reading (Black)
222	Heater current reading (Blue)
121	Heater current reading (Red)

PID Parameters	
Proportional gain	500
Integral	0
Derivative	5
Output range	0.8-4.4

National Instruments	
Channel Number	**Description**
DAC 0	Heater voltage output (analog output channel)
0	Vapor volume flow rate
8	Liquid volume flow rate
1	Test section differential pressure
9	Liquid inlet density
2	Heater temperature
10	Reference temperature
3	Pressure in the heat exchanger section

D. LabVIEW Code

Figure D.1: Entire LabView Program

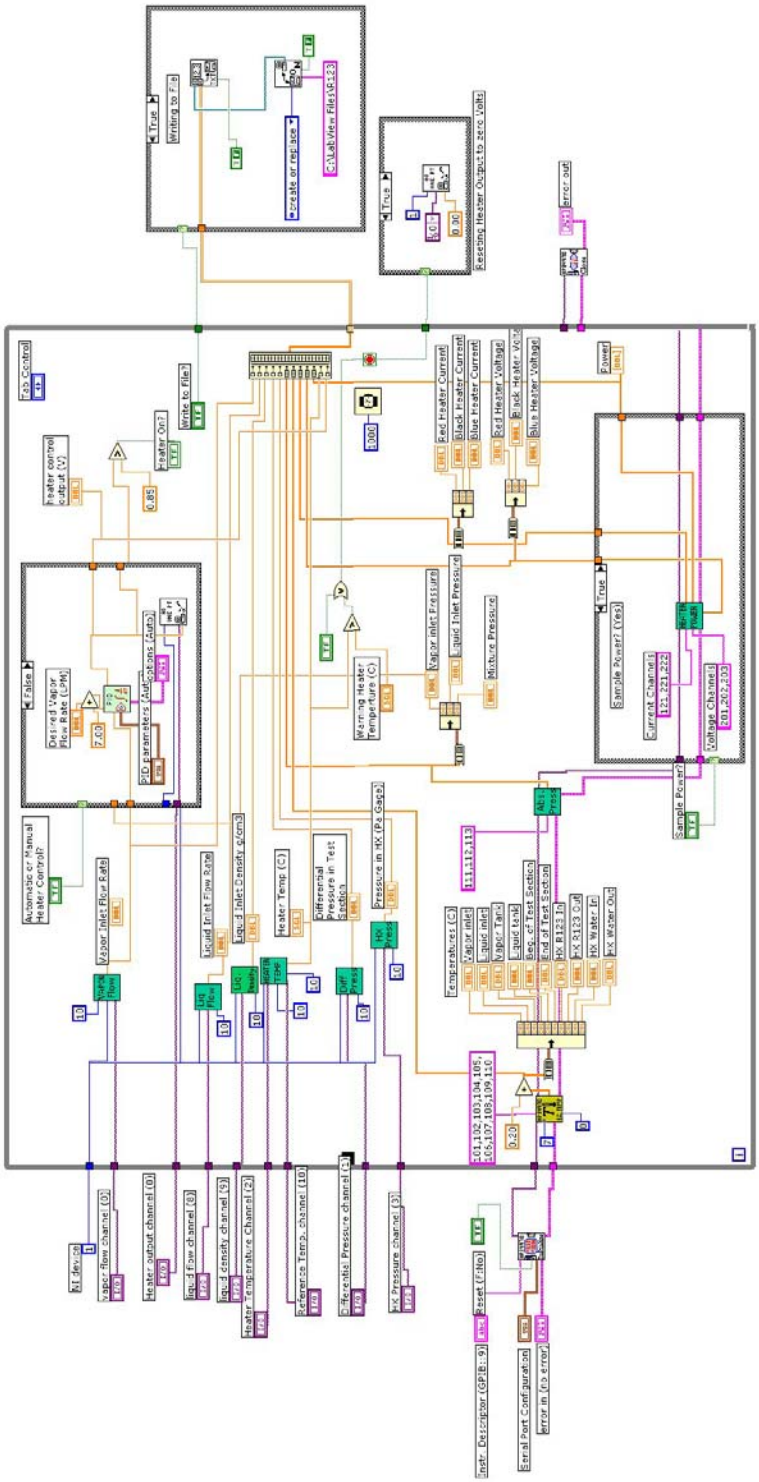

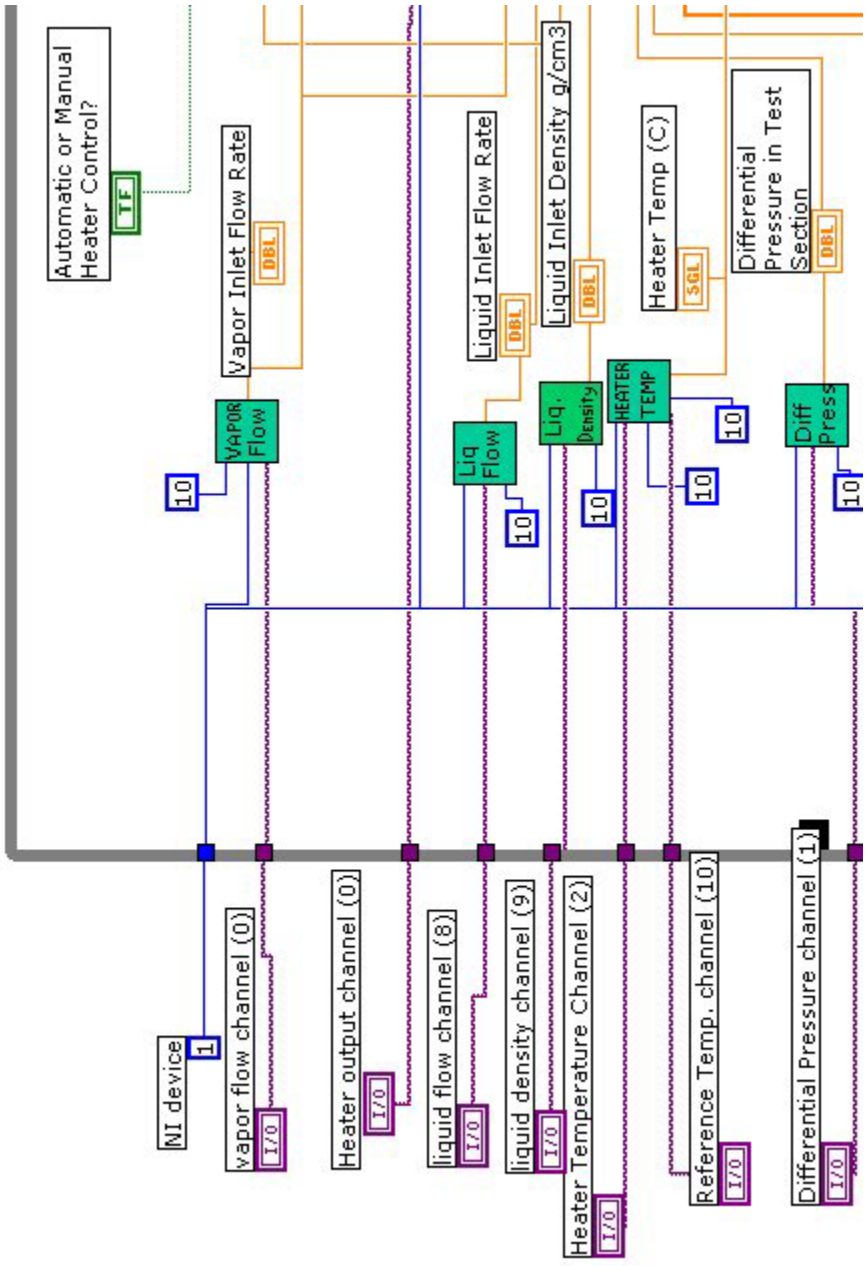

Figure D.2: Enlarged view of upper left section of program.

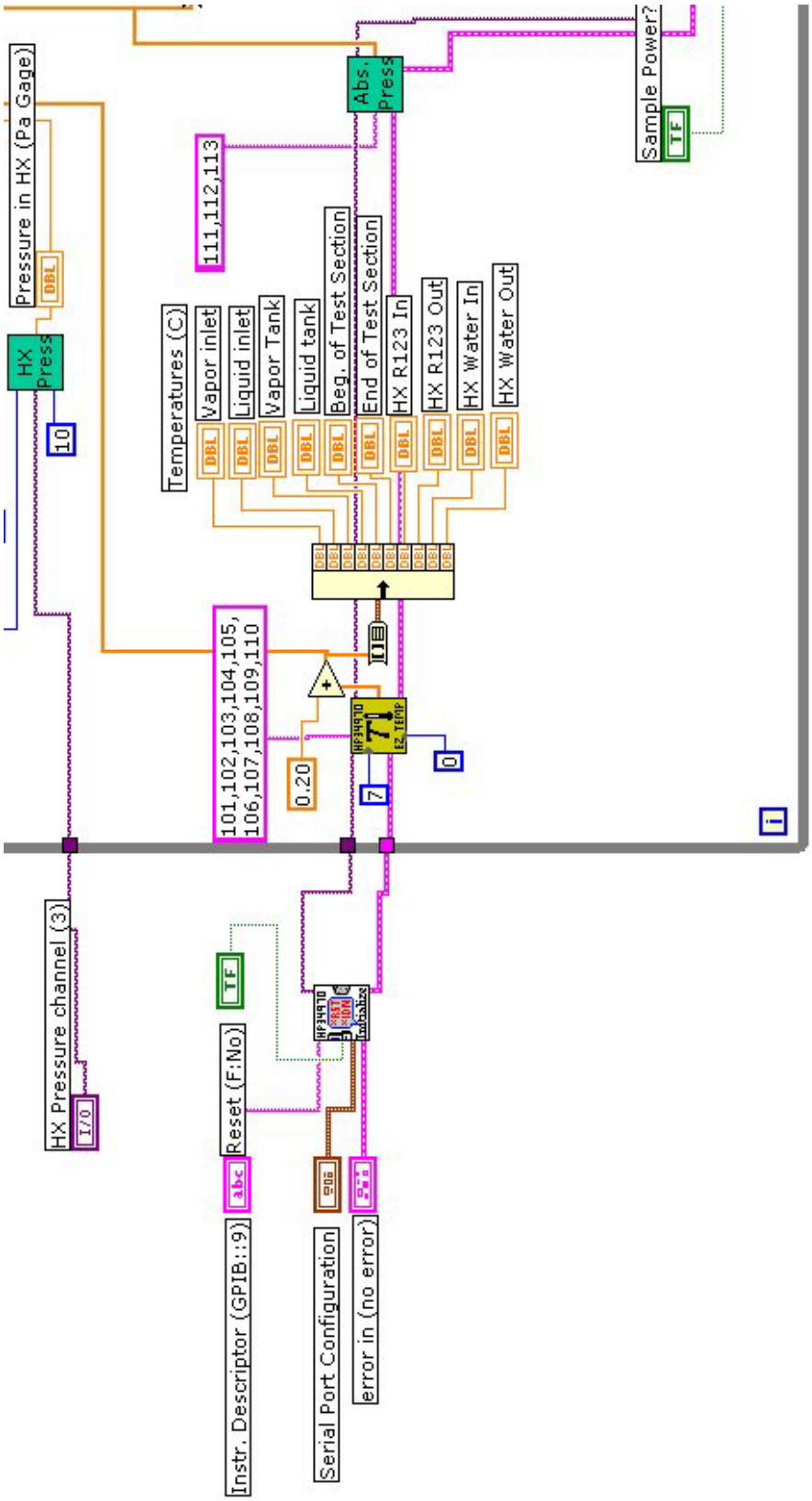

Figure D.3: Enlarged view of lower left section of program.

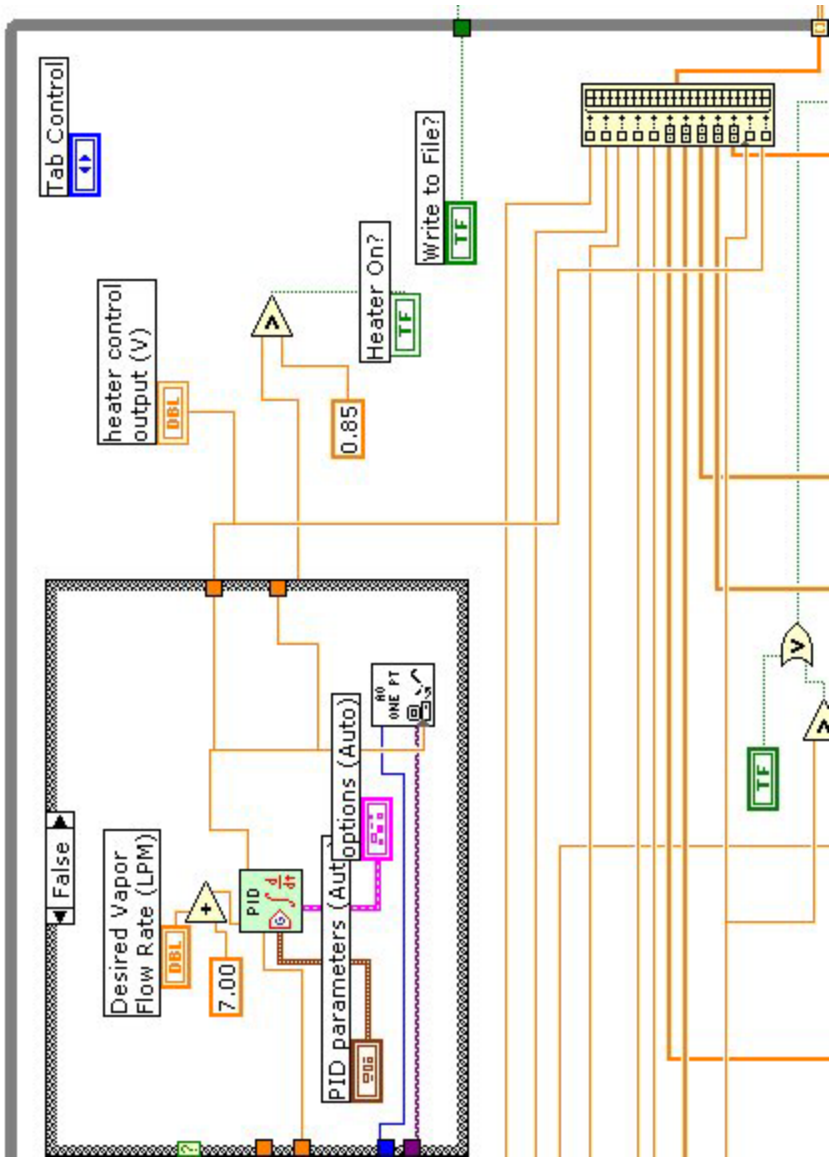

Figure D.4: Enlarged view of upper right portion of program

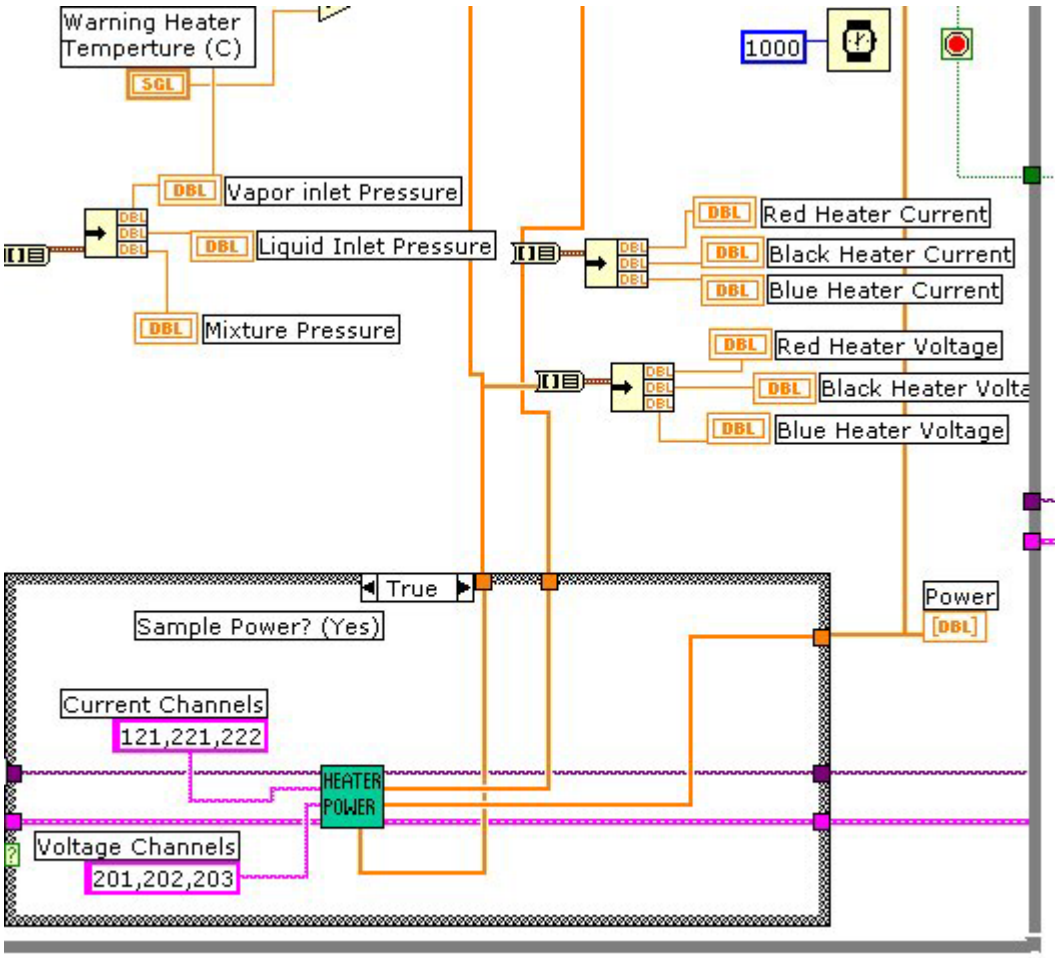

Figure D.5: Enlarged view of lower right section of program.

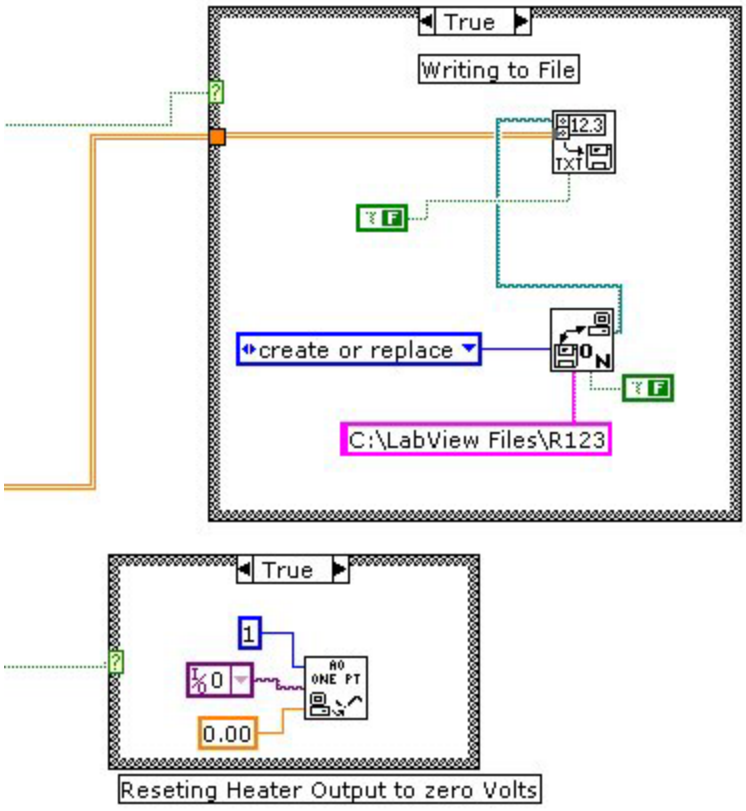

Figure D.6: Enlarged view of far right of program.

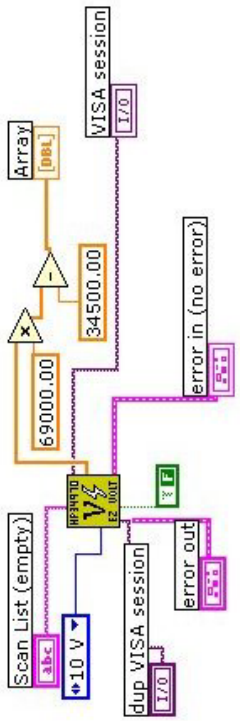

Figure D.7: Sub-program for measuring absolute pressure.

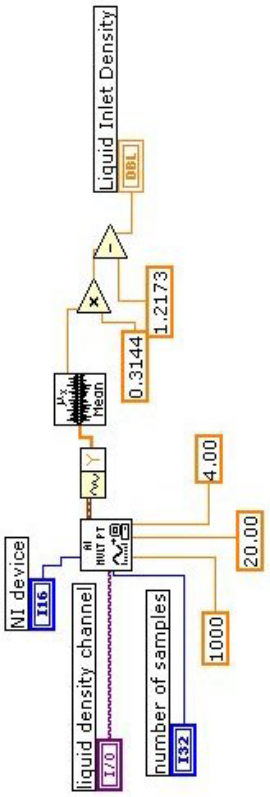

Figure D.8: Sub-program for measuring liquid density.

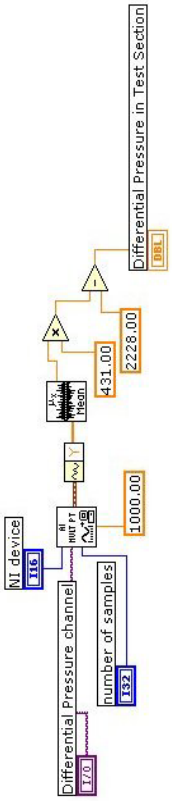

Figure D.9: Sub-program for measuring differential pressure.

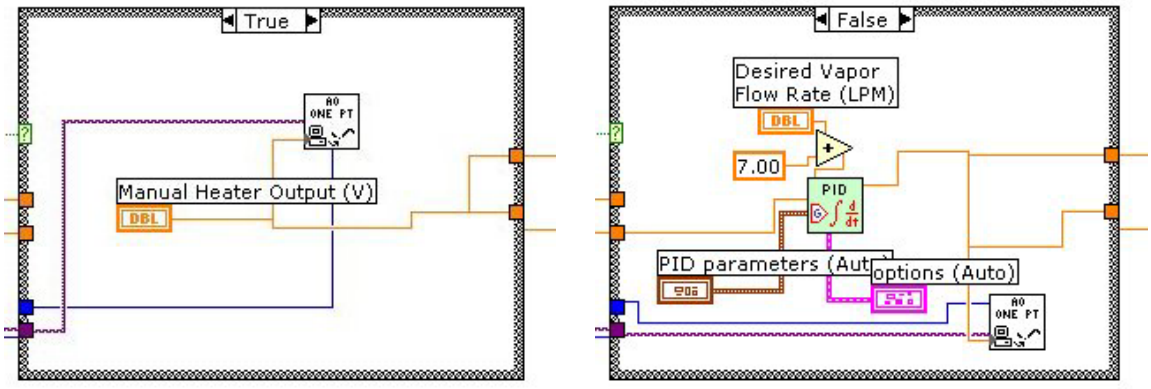

Figure D.10 (a, b): Sub-program used for heater control

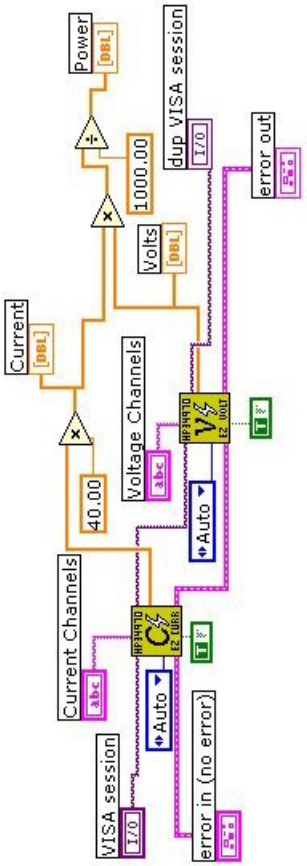

Figure D.11: Sub-program for sampling heater power.

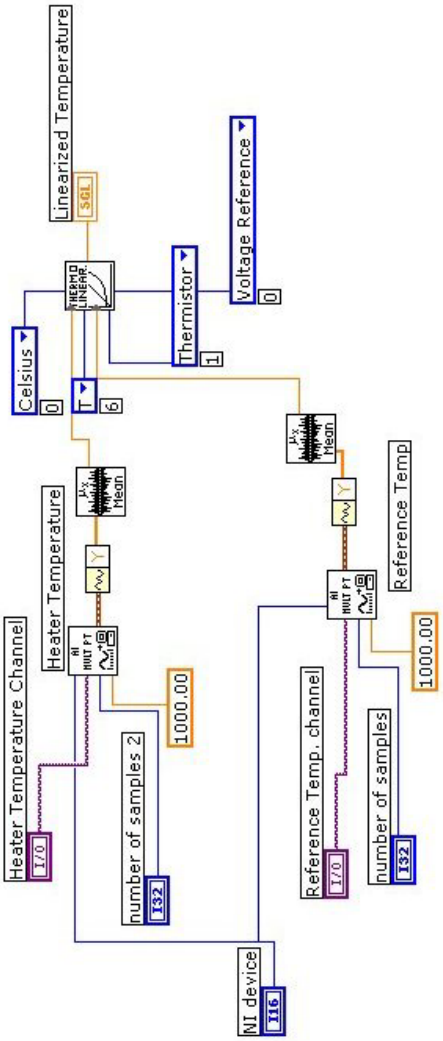

Figure D.12: Sub-program for sampling heater temperature.

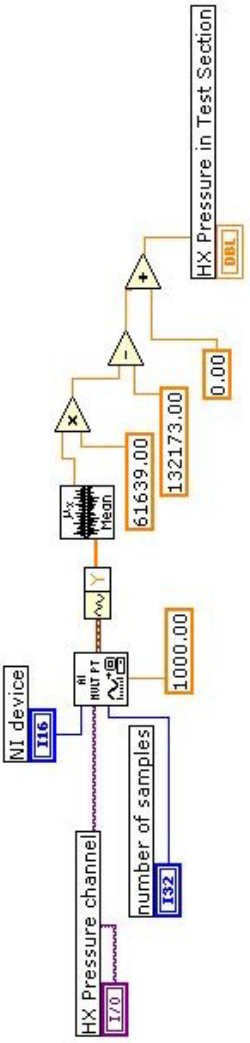

Figure D.13: Sub-program for sampling heat exchanger pressure.

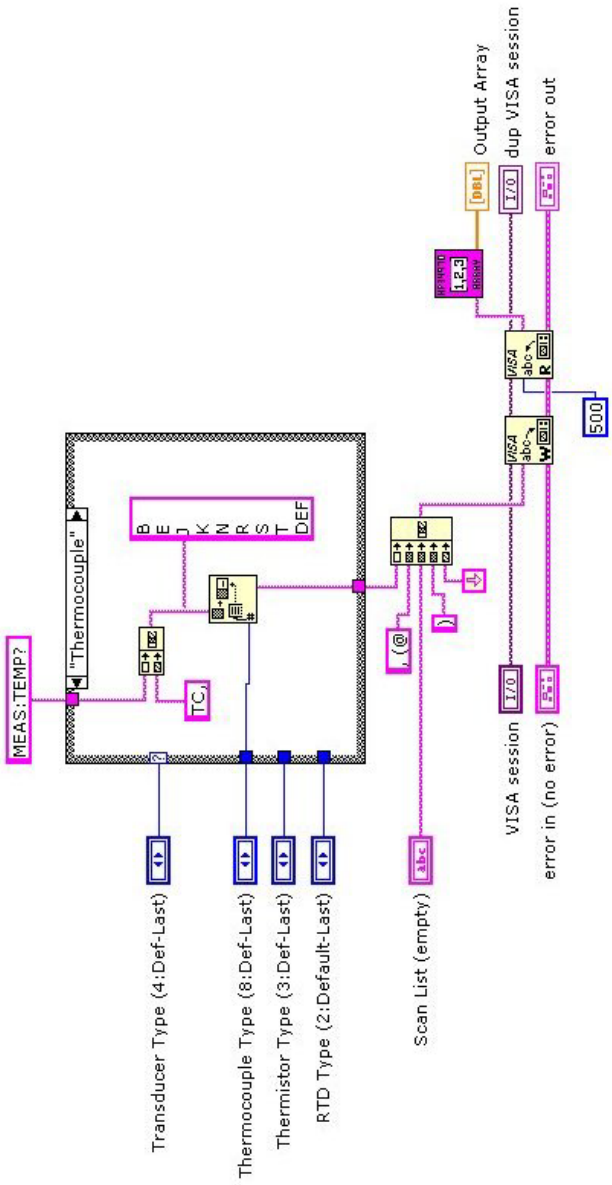

Figure D.14: Sub-program for sampling thermocouples.

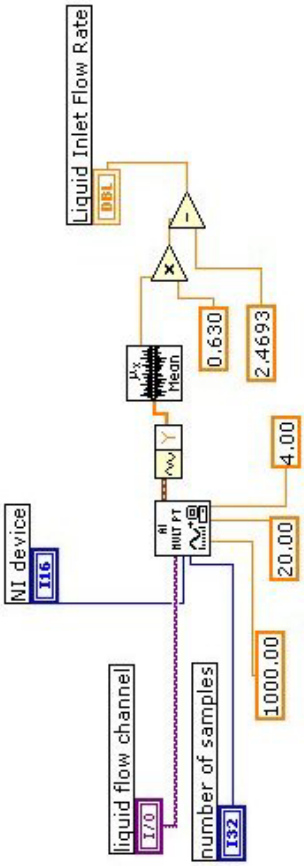

Figure D.15: Sub-program for sampling liquid flow.

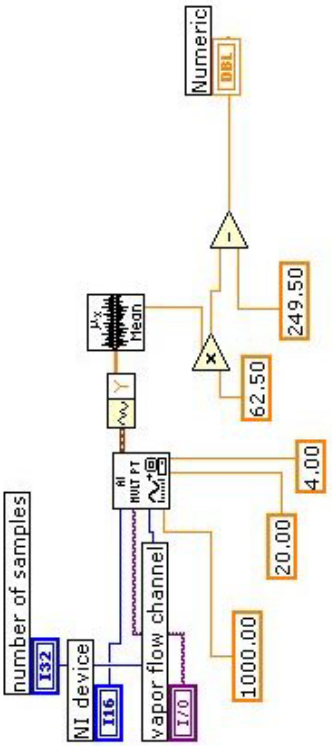

Figure D.16: Sub-program for sampling vapor flow.

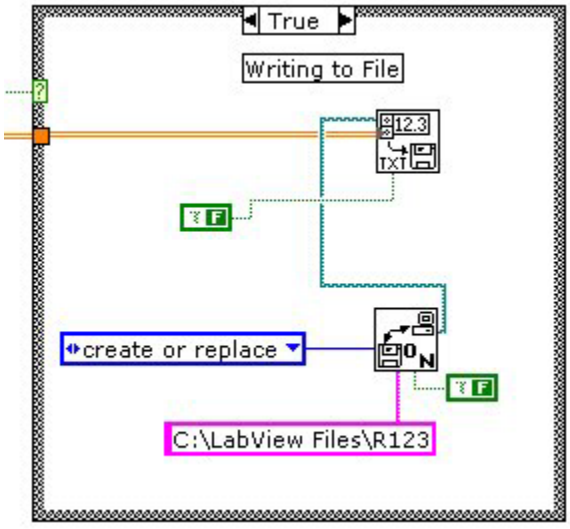

Figure D.17: Sub-program for option to write data to file.

E. Operation of R-123 Test Facility

Start-up

The loop must be primed before running. There are several necessary procedures that must be done to prepare the facility. The main purpose of these procedures is to rid the loop of as much air as possible. If there is air in the system the vapor will either not flow at all or be very difficult to control. Therefore, the data obtained will not be of high quality. One way to be sure that most of the air is out of the system is to check your saturation temperature and pressure in any location with refrigerant vapor to be sure they match. The air will cause the pressure to be higher than it should be.

Vacuum pump set-up

1) **ALWAYS** have the vacuum pump outlet attached to the system exhaust port. This is the port located on the tee-section on the top of the vapor tank that also holds the pressure gauge and safety relief valve. This will exhaust the contents vacuumed from the system to the outdoors and not the room.
2) To minimize any inflow of air and any outflow of R-123, turn on the vacuum pump first, and then connect the inlet port to the desired vacuum port in the system. The main ports being on the underside of the vapor flow section, the upper end of the separator, and near the liquid peristaltic pump.
3) Disconnect from the system first, replacing the vacuum port cap, and then turn off the vacuum pump.

Helpful Hints

- Check the oil level in the vacuum pump. Check the usage log to be sure the oil does not need changing. Use only DVO-12 J/B Fast Vac Vacuum pump oil.
- To extend the length of the inlet tubing, use the manifold gauge set.
- Use the refrigerant tubing with built in Schroeder valves on one end when connecting to the system. This will cut down on refrigerant let into the room when disconnecting and will be safer for those in the surrounding area.
- Always replace valve caps after disconnecting a vacuum hose.
- If the pressure does not seem to dropping in the system when vacuuming, check likely areas where liquid refrigerant would be (i.e. filters, low points in liquid line or vapor return line) to see if they are cold. This indicates that there is liquid in this area that is being vaporized and sucked out of the system and will cause the pressure to stay relatively constant during this process.

Heater set-up

To operate the heaters:

1) Turn three marked circuit breakers to *ON* (blue, black, and red markings).
2) Turn three power switches above circuits to *ON* (also marked blue, black, and red).
3) Be sure the circuit is plugged in (large white transformer).

4) In LabVIEW program, set the type of control desired – *Manual* or *Auto*. (See LabVIEW program set-up.) Start with *Manual* for purging of the system.
5) For Manual control, set the desired voltage output to turn on the heaters. It is recommended to stay under *2.5 volts*, usually set at *1.7 volts*.

   <u>*Helpful Hints*</u>

   - The *Heater On* light will turn on whenever a voltage signal is being sent to the control circuit, meaning that this light will come on even if the power to the heaters is not on. Check the heater temperature to be sure the heaters have come on.
   - **DO NOT** touch any exposed wires leading to or from the heaters. These carry a current of 20 amps and a voltage of 240 volts. **This is very dangerous!**
   - **IMPORTANT**: The LabVIEW program has two safety checks for disengaging the heaters. The first is the heater warning temperature (which can be adjusted) set at 100ºC. The warning temperature is set at 100ºC, because if the refrigerant reaches 150ºC it will begin to break down into hydrochloric and hydrofluoric acid and possibly, carbonyl halides. If the heater temperature ever reaches this temperature, the program will shut down and send a voltage signal of *0.8* volts (or no signal) to the heaters, immediately beginning the cooling process. The second safety point is less obvious. The *STOP* button in the program also closes the program and sends a voltage signal of *0.8* volts (or no signal) to the heaters and therefore should always be used to stop the program. The major reason

for this is if the stop button on the menu bar is used to abort the program the program will continue to send the last voltage signal sent to the heaters. With the program shut off, the first safety check is no longer activated and the heaters could easily overheat the system and cause it to run wild. The pressure release valve on the vapor tank is the only safety check left after this point.

Purging the system

1) Be sure that all valves are in the closed position, especially all inlet and outlet valves on both tanks and the liquid line valves.
2) Open the LabVIEW program and start the program to monitor temperatures and pressures. (Heater control should be on *Manual* and set to *0.8 volts*.)
3) Turn on the cooling water for the vapor tank by turning the small valve leading to the cooling coil. (In order to vacuum out the tank to rid it of air, the refrigerant must be kept cool (in liquid form).)
4) After the vapor tank has cooled and is below atmospheric pressure, turn on the vacuum pump and attach the inlet side to the vacuum port in the vapor flow meter section (underneath side of the 3-inch PVC section). (See Vacuum Pump Set-up.)
5) To vacuum out the air in the vapor tank, open the valve between the vapor tank and the vapor flow meter section for about 2-3 minutes, leaving the cooling water running. **DO NOT** leave this valve open for long – you will vacuum out large amounts of refrigerant, a very costly mistake!
6) Leave the vacuum running and shut the vapor tank outlet valve. Shut off the cooling water for the vapor tank. Vacuum the vapor flow meter section down to

about 30-35 kPa. **DO NOT** go below this point because more air will be sucked in through leaks under low vacuum pressures.

7) While vacuuming out the vapor flow meter section start heating the tank by setting the voltage to about *1.6 V*. (See Heater Operation.) Heat the tank until the pressure in the vapor tank is above the pressure in the vapor flow meter section (about 18ºC).
8) Briefly open the vapor tank outlet valve to release some vapor and any air left in the tank. Close this valve and continue to vacuum down the vapor flow meter section to 30 kPa again.
9) If the system has been unused for a long period of time, you will need to repeat step 8 again.
10) Open the valves on either end of the test section (and, if using liquid, open the liquid lines) and vacuum all areas (except both tanks) down to 30 kPa. The vapor tank should still be at a slightly higher pressure as in step 7.
11) After vacuuming, briefly open the vapor tank outlet valve to fill the system with vapor. Close this valve and vacuum system down to 30 kPa again.
12) Repeat step 11. If the system has not been used in a long period of time, repeat step 11 twice or more if necessary. As stated above, check the pressure in any location with refrigerant vapor and check that the temperature is the saturation temperature at that pressure (or vice versa). This will be an indication that the system is purged of air (no partial pressures involved).
13) Leave the vacuum pump running as you disconnect the hose and cap the vacuum port. Then turn off the vacuum pump.

Running Vapor

1) Heat vapor tank to about 28ºC (try to keep it under 30ºC to prevent the vapor from condensing in the test section). The pressure should be above 0 psig.
2) While heating the tank, turn on the cooling water to the heat exchanger to reduce the pressure at the end of the test section. The valve to turn on the cooling water is located on the 1-inch tube that leads to the inlet side of the heat exchanger, which is at the top and in the center of the metal support structure of the facility.
3) When the vapor tank reaches about 28ºC and the heat exchanger reaches about 14ºC, turn on the vapor gear pump and open the liquid inlet valve to the vapor tank. Then open the vapor outlet valve. There should be vapor flow. If there is not see Troubleshooting Section.
4) Immediately switch to *Auto* heater control in the LabVIEW program and set a desired vapor flow rate. A suggested vapor flow rate is a low flow rate or to match whatever is currently flowing after opening the vapor outlet valve. Check to see how well the PID controller maintains this flow. If the vapor control appears to be inconsistent (large overshoots, etc), see the Troubleshooting Section.
5) If the vapor is flowing and has not condensed in the test section or vapor flow meter section and the vapor control is working smoothly, you will be able to set any vapor flow within the range. You may need to wait a few moments for everything to even out.
    - Be sure to slowly increase the desired vapor flow (move in increments of about 25 LPM) in order to avoid overheating the tank and driving the

pressures above atmospheric. This maintains better vapor flow control as well.

- Check the vapor pump to be sure it is not cavitating. Adjust the speed if necessary.

Running Liquid

1) Be sure that you have vacuumed out the liquid lines while vacuuming out the entire system. If you have not, there is a vacuum port near the liquid peristaltic pump that can be used even while vapor is running in the test section. Be sure the valve on the downstream side of the liquid flow meter is shut and the valve on the upstream side of the filter is open in order to vacuum the entire liquid line. Disconnect when finished vacuuming.
2) In order to zero the liquid flow meter the lines must be filled with stationary liquid (no vapor bubbles).
    a. Open the liquid tank outlet valve (the upper branch of the tee located on the bottom of the liquid tank). The liquid will begin flowing out of the tank.
    b. Place the pump tubing in the liquid pump head and clamp it shut. Keeping the tubing free of sharp bends and twists, because the liquid will cavitate and vaporize in a sharp bend causing the liquid flow to stop. Adjust the occlusion on the pump heads if necessary.
    c. Start the pump at a moderate speed making sure that the valve downstream of the pump is open and the liquid tank inlet valve is open. You may need to slightly open the valve on the downstream side of the liquid flow meter

to allow liquid to fill the lines. When the lines are full, close the valves on either side of the liquid flow meter and immediately turn off the liquid pump.

d. On the liquid flow meter interface, "press" both the select and scroll buttons at the same time until the display changes from flow rate to the menu options. (The buttons are optical sensors; simply place a finger over the sensor to activate the desired button.) Press scroll until the '*Config*' menu appears and press select. Press scroll until the *Zero* selection appears and press select. The indicator light will flash yellow briefly, wait for the display to read '*Zero OK?*' and hit select. After the device is finished zeroing, return to the flow rate display using the scroll and select buttons to find the exit commands for each menu. If the indicator light is still flashing, you will need to check all errors and acknowledge all errors using the same procedures. The errors are displayed in the first set of menus. A list of errors can be found in the flow meter manual. The indicator light should be a constant green light. (See Micromotion, Inc. manual for further questions.)

3) Now you can turn on the liquid pump to a moderate speed, immediately open the valve upstream of the filter, and open the valve downstream of the flow meter. Try to avoid having back flow or no flow, because you will need to perform the '*acknowledge errors*' procedure listed above again.

4) The liquid flow rate is adjusted using the pump speed control and the occlusion adjustment. A higher occlusion means a higher flow rate. For the higher flow rates, the pump tubing can be looped through a second pump head.

Helpful Hints

- The indicator light on the liquid flow meter should be periodically checked, and if it is not a constant green light, the device has experienced some errors that must be checked and acknowledged using the procedure in step 2(d).
- When running liquid, the vapor flow will be dampened slightly. In order to maintain the target vapor flow rate, set the desired vapor flow rate a few liters per minute over the target flow. Experiment until the target flow is the average reading.
- The pump tubing should only be used for short periods of time to avoid breaking the tubing and causing a leak. Keep moving the pump head to a new location on the tubing and if necessary a complete replacement may be needed.

Shut-down

1) If running liquid flow, turn off liquid pump and turn pump on in reverse. This will drain the liquid from the lines and keep in storage in the liquid tank. Try to get as much liquid back in the tank as possible, then close the liquid tank outlet valve and shut off the liquid pump. Close the valve downstream of the liquid flow meter and the valve upstream of the filter. Leave the inlet valve to the liquid tank open until all liquid is through the test section, and then close this valve.

2) When all liquid is through the system, turn off the heaters. This can be done by setting the desired vapor flow to *Zero* or by switching to *Manual* control and having the voltage output set to *0.8 volts*.
3) Shut off the heater switches and breakers.
4) When the vapor flow reaches zero, turn on the cooling water for the vapor tank. After a few minutes, turn off the cooling water for the heat exchanger. Leave the vapor pump running until the condensed vapor stops flowing out of the heat exchanger.
5) Open all valves (including the liquid line valves) except the liquid tank inlet and outlet. This will allow all excess liquid to vaporize and move toward the vapor tank for storage as the vapor tank cools.
6) It is recommended to leave the cooling water on and all valves open for about 1 hour to recapture most of the R-123 in the vapor tank. If the system will not be used for an extended period of time, the cooling process should be as long as 2 hours. Check obvious areas for remaining liquid before shutting the vapor tank inlet and outlet valve and turning off the vapor tank cooling water. These areas include the vapor and liquid pump tubing, both filters (if still vaporizing these will feel cold), and the liquid tank inlet line (if still vaporizing it will feel cold). The LabVIEW program can be stopped at this time by pressing the large, red *STOP* button in the program. (This insures that the program will send no signal to the heaters after the program is stopped.)

7) Be sure to close **ALL** valves after cooling is completed, including the valves at either end of the test section and both liquid line valves. Both tanks should still be closed off. In the event of a leak, this will prevent all areas venting to the room.
8) You can now shut the program and turn off the power to the Agilent data acquisition and the power supply for the pressure transducers.

Maintenance

The system must be charged with R-123 before any experiments can be run. In order to do this, the purchased drum of R-123 must be opened and 'tapped', using the device shown in Figure E.1. While wearing a mask, gloves, and goggles, and after taking the drum to a well-ventilated area (preferably outside), **quickly** open the larger of the two fittings on the top of the drum and **immediately** slide the filling device (with all valves closed) into the hole and tighten it. Check to be sure the drum is not leaking before bringing it back inside. Fix any leaks using Teflon tape or glue if necessary. Before

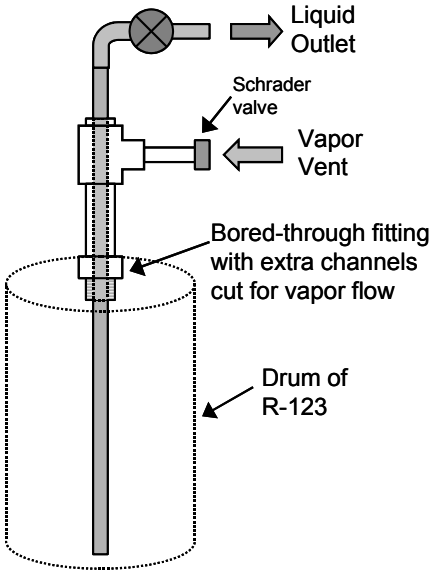

Figure E.1: Schematic of device used to charge system with R-123.

filling, the vapor tank should have all valves shut and be vacuumed down. The vapor return tube (vapor vent) of the filling device should be attached to the small outlet valve on the top of the vapor tank, while the liquid outlet tube of the filling device should be attached to the vapor tank at the valve located on the bottom of the tank. Pump tubing should be used to continue pumping the R-123 into the tank after the initial pressure driven flow has stopped. The amount of liquid pumped into the tank can be seen in the sight glass on the side of the tank. The liquid tank can be filled by evacuating the tank and connecting the liquid outlet of the filling device to the valve on the underside of the liquid tank. The liquid tank does not need to be very full. The filling device should be removed from the drum (in the same manner as installing it) when filling is completed. The drum should be properly capped and stored after the filling process is completed. The system can be drained of fluid in a similar manner when necessary.

After using the test facility, the system should be shut down properly such that nearly all the refrigerant is stored in both the liquid and vapor tanks. The procedure outlined in the shutdown procedures should be followed to accomplish this. In the event that the system would need to be drained of all fluid, the liquid tank valves (and liquid line valves) would be left open while the vapor tank is open and being cooled (with the cooling coil). This would cause most of the refrigerant to migrate to the vapor tank. There is also a redistribution line that is attached to the valves on the bottom of each tank that uses a peristaltic pump. The liquid tank can be drained or filled using this line from the vapor tank.

Trouble Shooting

Why is the vacuum pump making a funny noise?

If the vacuum pump suddenly becomes louder or sounds different than normal check the oil level. If the wrong type of oil is used the refrigerant being pumped from the tank will mix with the oil and cause the oil level to rise. The pump will start forcing the mixture out the exhaust port, causing the pump to overheat (which is escalated by the change in properties of the oil mixture now being used in the engine.) The pump should be disconnected (carefully) and turned off immediately. The oil will need to be drained and the proper oil added before using again. Follow the instructions in the manual for draining and refilling procedures.

Why is the vapor flow reading so high?

If the flow meter reading suddenly starts to climb to very high rates for no apparent reason and the vapor does not appear to be flowing at all, the vapor has likely condensed in the vapor flow meter section. The liquid covering the flow meter probe has a different conductivity than the vapor and would therefore cause the flow meter to show a higher flow rate than is actually occurring. In the event that condensation occurs, either wait for the liquid to evaporate and the system to stabilize or turn on the heater tape that is wrapped around the vapor flow meter section to speed up the process.

Why won't the vapor flow?

If the vapor does not appear to be flowing and is condensing in the test section (and other places as well) there are several things as the cause of this.

- Check that the heat exchanger cooling water is on. If it is not, turn it on to lower the pressure at the end of the test section and give the system time to stabilize.
- Check that the vapor pump is on and not cavitating. If the pump is not on, turn it on to lower the pressure at the end of the test section. If the pump is cavitating adjust the speed appropriately. Also check to see that the liquid inlet valve to the vapor tank is open. The system will need time to stabilize after any adjustments are made.
- If all appears to be properly set up, the system may simply need time to stabilize. Therefore, after re-checking all possible causes of a no-flow condition, give the system some time to achieve a balance. (The vapor line filter often needs to become saturated with liquid before allowing the flow to run properly.)
- If all else fails to get the flow started, there is always the possibility that there is too much air in the system and it is interfering with the flow. Therefore the system must be shut down and vacuumed out at least one more time.

Why is the vapor flow control wildly overshooting the target flow?

If the flow control seems to be out of control by overshooting the target flow by a great deal (30 LPM or higher), the system still contains a lot of air. The system will have to be shut down and vacuumed out several times before running again.

Why is the liquid flow intermittent or hard to control?

If the liquid flow is becoming intermittent or hard to control there are several possible reasons. The first being that there is no longer a sufficient amount of liquid in

the tank, and therefore some must be pumped from the vapor tank to the liquid tank. The second reason may be that the pump tubing needs to be changed and the tubing is becoming too malleable. Another possible reason for intermittent liquid flow is that the flow is cavitating as it leaves the copper tubing and flows into the pump tubing. To avoid this, keep the pump tubing as flat as possible with no sharp bends.

What is this white powdery residue?

The white residue currently found in parts of the test facility was due to a mistake in material selection. A saddle-tee used on the vapor flow meter section was made of ABS plastic instead of PVC. The R-123 started to break down the ABS and caused the system to become saturated with a white residue. The ABS fitting has been removed and the production of powder has stopped.

What do I do if a leak occurs?

If a leak occurs, immediately turn on the vapor tank cooling valves and shut off the heaters to begin drawing the refrigerant into the tank. Put on a mask and try to isolate the affected section if there is only vapor present. Attempt to temporarily fix or cover the leak while the system is cooling. While doing this, the room should be well ventilated. If the leak is extremely large, vacate the area and be sure no one is allowed into the area until it is safe.